

AN ABSTRACT OF THE THESIS OF

Tara L. O'Donnell for the degree of Master of Science in
Water Resources Engineering presented on March 9, 2012.

Title: Evaluation of Stream Temperature Spatial Variation Using
Distributed Temperature Sensing

Abstract approved: _____

John S. Selker

Water temperature in rivers and streams is an important factor for aquatic ecosystem health. Measurement of stream temperature has traditionally been accomplished by point temperature measurements, continuous point temperature loggers, and more recently, airborne remote sensing techniques such as Forward-Looking Infrared Radar (FLIR) or Thermal Infrared Radiometry. While each of these measurement techniques has certain advantages, none allows for the combined spatial and temporal information provided by Distributed Temperature Sensing (DTS). DTS employs fiber optic signals to measure temperature and is a relatively new temperature measurement technology for hydrologic sensing applications.

Nine DTS stream temperature datasets were collected in the Middle Fork John Day River (MFJDR) as part of a basin-wide stream monitoring effort. The datasets encompassed five 1-3 kilometer long reaches, some monitored over three summers

(2009-2011). In contrast to existing stream temperature measurement technologies, DTS can provide stream temperature data in both the spatial and temporal domains. Techniques and challenges of interpreting DTS stream temperature data were documented, and three applications of the technology to stream temperature monitoring were explored.

Cold water patches, potentially used by fish as thermal refugia during stream temperature maximums, were located using DTS. No identified cold patch exceeded 2.31°C cooler than ambient stream temperature. Tributary inflows provided some of the most temperature-differentiated cold patches. These findings provide a reference for the degree of thermal heterogeneity in the MFJDR system and beg the question of whether fish respond to small (<3°C) spatial temperature variations. Theoretical predictions of stream mixing potential (Richardson number and cavity flow mixing predictions) suggested that increasing stream thermal heterogeneity would require channel modification to decrease stream flow velocity in select areas.

The combined spatial and temporal coverage of a DTS stream temperature dataset on the Oxbow Conservation Area allowed diagnosis of a 2°C longitudinal stream temperature decrease observed in multiple Thermal Infrared Radiometry (TIR) and Forward-Looking Infrared Radiometry (FLIR) datasets collected on that reach. Advection velocity and channel depth, rather than groundwater or tributary inflows, were the main cause of the decrease, and the magnitude of the decrease peaked in the early afternoon, disappearing completely by evening. This finding suggests caution for interpretation of FLIR and TIR stream temperature datasets, which represent snapshot temperature measurements. For these datasets, knowledge of flow conditions (velocity

and depth) may help avoid misinterpretation of temporally-transient temperature anomalies.

Diurnal slope periodicity was observed in linear-like spatial trends in four DTS datasets, and an analysis was made to examine this subtle spatially and temporally varying phenomenon. The phase of the diurnal slope variation differed between river reaches, suggesting that propagation of larger-scale thermal waves might be one driving mechanism. Temporally-constant offsets between slope magnitudes within reaches suggested some intra-reach differences in heat fluxes.

©Copyright by Tara L. O'Donnell
March 9, 2012
All Rights Reserved

Evaluation of Stream Temperature Spatial Variation Using Distributed
Temperature Sensing

by

Tara L. O'Donnell

A THESIS

submitted to

Oregon State University

in partial fulfillment of
the requirements for the
degree of

Master of Science

Presented March 9, 2012
Commencement June 2012

Master of Science thesis of Tara L. O'Donnell presented on March 9, 2012.

APPROVED:

Major Professor, representing Water Resources Engineering

Director of the Water Resources Graduate Program

Dean of the Graduate School

I understand that my thesis will become part of the permanent collection of Oregon State University libraries. My signature below authorizes release of my thesis to any reader upon request.

Tara L. O'Donnell, Author

ACKNOWLEDGEMENTS

This work was made possible by the collaboration of the Confederated Tribes of the Warm Springs Reservation of Oregon (CTWSRO). Most of the data described herein were collected on CTWSRO property, and all field workers were housed within the CTWSRO research station at the Oxbow Conservation Area. A great debt of thanks is due to CTWSRO employees Stephane Charette, Amy Charette, Dennis Molt, Brian Cochrain, and Martin Eisenbraun for their support, assistance with data and equipment, and invaluable field knowledge. This project was funded by the National Oceanographic and Atmospheric Administration (NOAA), the Oregon Watershed Enhancement Board (OWEB), The Freshwater Trust (TFT), and the U.S. Bureau of Reclamation (BOR). Helpful incite was gained through discussions with the Intensively Monitored Watershed team of the MFJDR. Cyrus Curry is particularly thanked for the time he took to assist with data management.

My academic adviser, Dr. John Selker, contributed his vision, guidance, and inspirational intellect to this project. I would never have come to OSU had it not been for the direction and inspiration of Dr. Gordon Grant, who may not know how much helpful guidance I gained through our sporadic meetings. Also, great thanks to Dr. Patricia McDowell, who inspired me as a researcher and as a person, and whose level-headed presence at the CTWSRO research station guided me and a multitude of other young researchers.

Julie Huff and Aida Arik preceded me as student coordinators of OSU's stream temperature monitoring program on the MFJDR, and I have used field methods and data analysis techniques that they developed. Aida went beyond the call of duty by assisting me with temperature modeling and thesis preparation. Her calm presence and intellect have been an inspiration to me, and she and Estefania Elorriaga were the best office mates I could have hoped for. Many field workers, including Julie Huff, Aida Arik, Daniel Bailey, Landon Gryczkowski, Michael Collier, Estefania Elorriaga, Chadi Sayde, Matthieu Mollet, Khalil Yaker, Michael Summers, Greg Nagle, Marie Perennes, Baptiste Déjean, Chloé Paré, and Javier Benitez have been integral in data collection work. James Wagner designed the solar trailers that made this data collection possible, and he provided invaluable support on power system operation and weather monitoring equipment.

I am grateful to my family for their support over the years, and to friends in Oregon who have become my family away from home. Finally, to my future husband Scott Meininger, thank you for helping me discover new happinesses every day.

CONTRIBUTION OF AUTHORS

Aida Arik taught me DTS field set-up and dataset calibration. She provided me with invaluable calibration, stream temperature modeling, and thesis writing files and guidance. Dr. John Selker is sincerely thanked for his excellent direction, guidance, and advice for the completion of this work.

TABLE OF CONTENTS

	<u>Page</u>
1 Introduction	1
1.1 Scope of Study	6
2 Cold Patch Survey	7
2.1 Introduction	7
2.2 Site Description	9
2.3 Methods	13
2.3.1 DTS Installation	16
2.3.2 Dataset Analysis	16
2.3.3 Vertical Temperature Measurements	27
2.4 Results	29
2.4.1 DTS Dataset Visual Assessment	29
2.4.2 DTS Analysis Results	30
2.4.3 Vertical Temperature Measurement Results	33
2.4.4 Stream Mixing Potential	36
2.5 Discussion	46
3 Interpretation of Remotely Sensed Temperature Datasets	53
3.1 Introduction	53
3.2 Anomaly in TIR and FLIR datasets	56
3.3 Methods	59
3.4 Results	59
3.4.1 Comparison of TIR and FLIR with DTS	59
3.4.2 Synoptic Discharge Measurements	65
3.4.3 Visual Channel Condition Observations	68
3.4.4 Simple Stream Temperature Model	69
3.5 Conclusions	73
4 Data Artifacts in DTS Stream Temperature Measurements	75
4.1 Introduction	75
4.2 DTS Deployment in Fluvial Systems	76
4.3 Data Artifacts in DTS Stream Temperature Measurements	80

TABLE OF CONTENTS (Continued)

	<u>Page</u>
4.3.1 Streambed influence on DTS measurements	80
4.3.2 Influence of solar radiative heating on DTS measurements	83
4.4 Conclusions	89
5 DTS Analysis of Longitudinal Stream Temperature Patterns	91
5.1 Introduction	91
5.2 Longitudinal Stream Temperature Trends	94
5.3 Potential Drivers of Temperature Slopes	100
5.3.1 Tributary Inflows	100
5.3.2 Groundwater Inflows	102
5.3.3 Thermal and Hydrodynamic Waves	103
5.3.4 Heat Flux Variation	105
5.4 Conclusions	109
6 Conclusion	111
Bibliography	115
Appendices	121

LIST OF FIGURES

<u>Figure</u>		<u>Page</u>
1.1	Stream heat transfer processes	3
1.2	Longitudinal stream temperature, John Day River basin	4
2.1	Map of the MFJDR watershed	10
2.2	Photos of the study reaches	11
2.3	Conceptual model of cold patch causation	19
2.4	Diurnal stream temperature signal, Forrest 2011	21
2.5	Daily Maximum Profiles, Forrest 2011	23
2.6	Daily Maximum Profile from the hottest day in each of nine DTS datasets	25
2.7	Vertical temperature profile time series, Pool1	35
2.8	Richardson number computation locations	38
2.9	Conceptual model of cavity with skimming overflow	43
2.10	Tailings pond diurnal temperature signal	51
3.1	Longitudinal stream temperature, John Day River basin	54
3.2	TIR and FLIR datasets from the MFJDR	57
3.3	Oxbow3 and Oxbow2 daytime longitudinal stream temperature profiles	60
3.4	Oxbow3 and Oxbow2 nighttime longitudinal stream temperature profiles	61
3.5	Oxbow2 diurnal stream temperature signal	63
3.6	Synoptic discharge measurement locations, Oxbow2 and Oxbow3	66
3.7	Oxbow2 simple stream temperature model	71
4.1	Milfoil bed, MFJDR	81
4.2	DTS stream measurements impacted by streambed temperature	82
4.3	Diurnal temperature signal within and above a soft silt streambed	84
4.4	DTS stream temperature measurement exhibit	85

LIST OF FIGURES (Continued)

<u>Figure</u>		<u>Page</u>
4.5	Photograph of the RPB reach	88
5.1	Longitudinal profiles and segment slopes, Forrest Reach 2010	96
5.2	Longitudinal profiles and segment slopes, Forrest Reach 2011	97
5.3	Longitudinal profiles and segment slopes, Oxbow3 Reach	98
5.4	Longitudinal profiles and segment slopes, Oxbow1 Reach	99
5.5	Net heat flux, Forrest reach 2011	107

LIST OF TABLES

<u>Table</u>		<u>Page</u>
2.1	Summary of DTS installations on the MFJDR	15
2.2	Maximum subsurface water-fed cold patch magnitudes	32
2.3	Maximum tributary-fed cold patch magnitudes	34
2.4	Vertical temperature measurements, Pool1 and Pool2	36
2.5	Richardson number computation	42
3.1	Synoptic discharge measurements, Oxbow2 and Oxbow3	67
5.1	DTS installation summary	93

LIST OF APPENDICES

	<u>Page</u>
A Air temperature data summary, 2009-2011	122
B Large-scale versions of the graphs in Figure 2.6	127
C Oxbow2 HEC-RAS hydraulic model	137
D Groundwater temperature data summary, June-August, 2011	141

Chapter 1 – Introduction

Water temperature in rivers and streams is an important factor for aquatic ecosystem health. Following passage of the Clean Water Act in 1972, stream temperature in United States water bodies has come under increasing regulation. Section 303 of the Clean Water Act requires states to define water temperature standards. In the Pacific Northwest states, these temperature standards are often defined by fish health criteria. This focus is motivated by the temperature sensitivity of aquatic habitat, relative to other water body uses, and by the protection of certain Pacific Northwest fish populations under the federal Endangered Species Act (ESA). Stream temperature standards and river-specific Total Maximum Daily Load (TMDL) levels developed by states provide the basis for state regulatory action on thermal pollution. The development of these programs entails extensive stream temperature measurement and modeling, and achievement of regulatory goals and aquatic habitat benchmarks depends on a robust understanding of stream temperature dynamics.

Stream temperature varies in both time and space. Temporal variation occurs on the scale of seasons, weeks, and days; diurnal temperature cycles can be large, over 15°C in some systems (Brown and Krygier, 1970; Constantz et al., 1994). Spatial stream temperature variation is generally more subtle, though one researcher identified temperature differences of up to 9°C over distances of meters (Nielsen et al., 1994). Given the turbulent conditions typical within most rivers and streams, mixing prevents strong

spatial temperature gradients. For most fluvial systems, one-dimensional (longitudinal) advection-dispersion models with large distance steps (50-100 meters) are considered adequate for modeling temperature for habitat appraisal (ORDEQ, 2012).

Though gradients are rarely strong, spatial variation in stream temperature can still be significant for temperature-sensitive aquatic species, and spatially-discrete cold patches are frequently cited as significant habitat features (Torgersen et al., 1999; Ebersole et al., 2003; RDG, 2007; BOR, 2008). Additionally, understanding the causes of spatial temperature variation is useful for temperature model design and improvement. Researchers have examined spatial variation in stream temperature at the watershed-level of kilometers (Torgersen, 1997; Caissie et al., 2007; Johnson and Jones, 2000), at the reach-level of hundreds of meters (Torgersen et al., 1999; Loheide and Gorelick, 2006; Schmidt et al., 2006; Lowry et al., 2007), and at the microscale of meters (Nielsen et al., 1994; Ebersole et al., 2003).

Variation at all scales derives from water flow conditions and from variation in heat fluxes, each of which depends on a number of meteorological, hydraulic, and landscape parameters. Water flow conditions include flow volume and velocity, as well as inflows, which may include tributaries, groundwater, and hyporheic water inflows. An understanding of the heat flux terms can start from the equation for total stream thermal energy

$$\Phi_{stream} = \Phi_{radiation} + \Phi_{conduction} + \Phi_{latent} + \Phi_{sensible} \quad (1.1)$$

where the energy of the stream (Φ_{stream}) is the sum of longwave and shortwave radiation

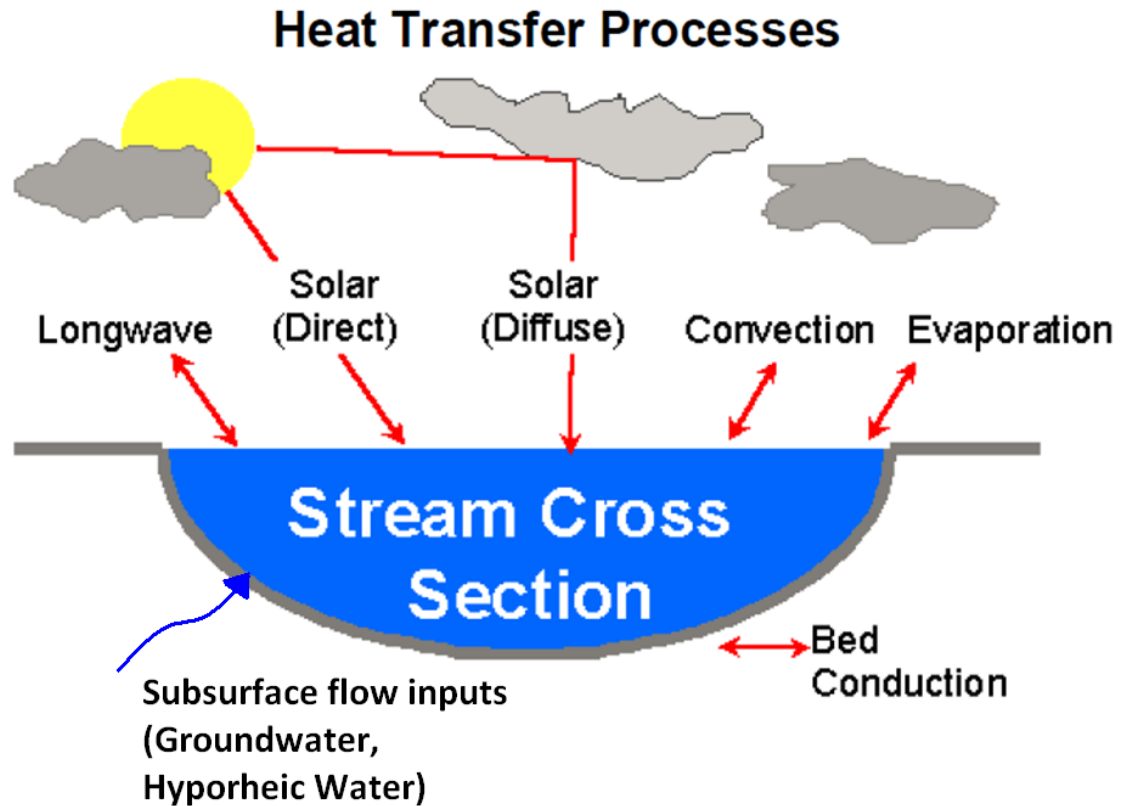


Figure 1.1: Stream heat transfer processes (Boyd and Kasper, 2004)

($\Phi_{radiation}$), streambed conduction from the temperature gradient between the substrate and water interface ($\Phi_{conduction}$), latent heat from evaporation (Φ_{latent}), and sensible heat from the air temperature ($\Phi_{sensible}$) (Boyd and Kasper, 2004). These energy components are summarized in Figure 1.1.

Stream headwaters tend to exhibit the temperature of local groundwater, with temperature evolving in a downstream direction due to net energy fluxes. A longitudinal stream temperature profile at the watershed scale was demonstrated by FLIR data collected between 14:30 and 16:00 in the John Day Basin in August 1994. (Figure 1.2).

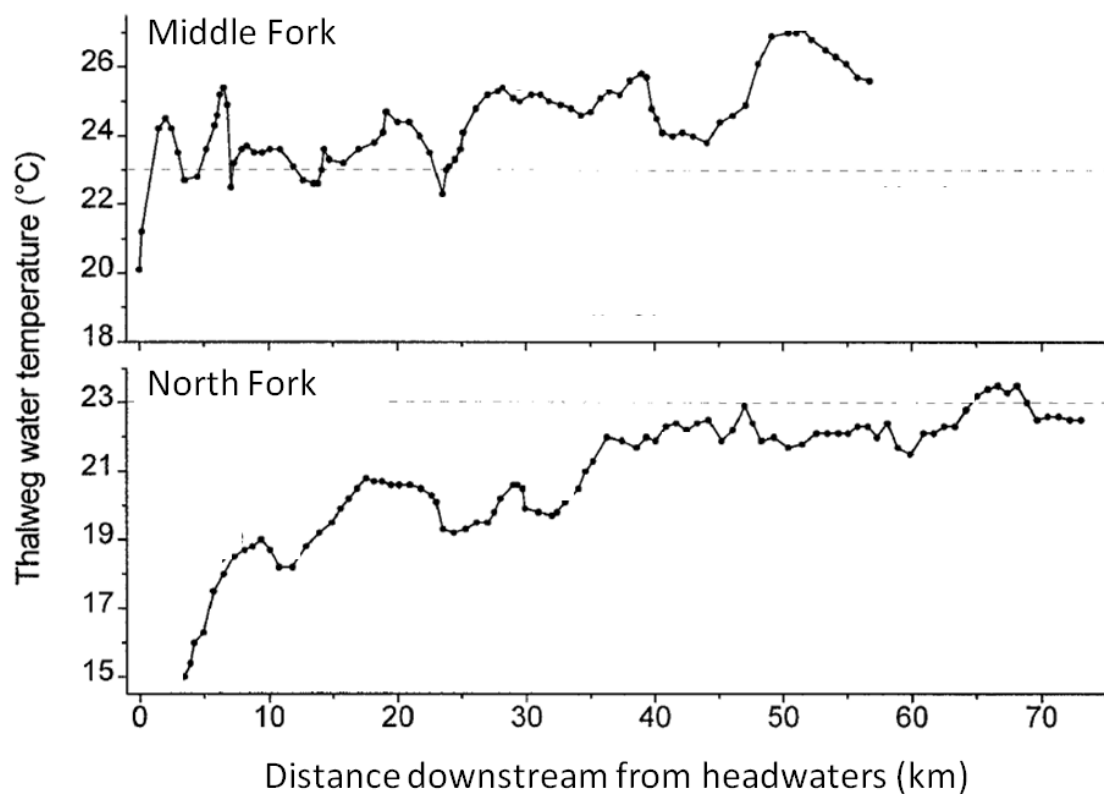


Figure 1.2: Longitudinal stream temperature in the Middle Fork John Day River (top) and the North Fork John Day River (bottom), as measured by Forward-Looking Infrared Radar during 14:30-16:00 August 5 and 8, 1994 (Torgersen et al., 1999)

At the watershed scale, stream temperatures increased in a downstream direction. This pattern reflects stream heating due to solar heat fluxes during daytime hours. At the reach scale, temperature trends exhibited more heterogeneity, increasing in some reaches and decreasing in others. These inter-reach variations are often attributed to differences in channel shading, width-to-depth ratio, tributary inflows, and different rates of groundwater/ hyporheic water inflow (Torgersen et al., 1999; Poole and Berman, 2001). At the scale of meters, a smaller scale than that displayed in Figure 1.2, thermal heterogeneity may also be present, and has been reported by a number of researchers (Nielsen et al., 1994; Ebersole et al., 2001, 2003; Huff, 2009). Temperature variations at this small scale have been attributed to groundwater seeps, unmixed tributary inflows, temperature stratification in pools, the hyporheic exchange processes associated with riffles, among other causes (Nielsen et al., 1994; Ebersole et al., 2003; Storey et al., 2003; Huff, 2009).

Measurement of stream temperature has traditionally been accomplished by point temperature measurements (Baltz et al., 1987; Nielsen et al., 1994; Ebersole et al., 2003), continuous point temperature loggers (Sinokrot and Stefan, 1993; Johnson and Jones, 2000; Bayley and Li, 2008), and more recently, airborne remote sensing techniques such as Forward-Looking Infrared Radar (FLIR) (Figure 1.2) (Torgersen et al., 1995, 1999; Loheide and Gorelick, 2006) or Thermal Infrared Radiometry (TIR) (Torgersen et al., 2001). While each of these measurement techniques has certain advantages, none allows for the combined spatial and temporal information provided by Distributed Temperature Sensing (DTS). DTS employs fiber optic signals to measure temperature and is a relatively new temperature measurement technology for hydrologic sensing ap-

plications (Selker et al., 2006b). Commonly-available DTS systems can measure temperature to a resolution of 0.1°C at 1 meter spatial intervals and 1 minute time intervals, over a cable length of 5 kilometers (van de Giesen et al., 2012).

1.1 Scope of Study

The goal of this research is to explore the spatial and temporal patterns of stream temperature variation, and to describe the use of DTS for monitoring and analyzing those patterns. Chapter 2 evaluates the presence and importance of cold water patches within the Middle Fork John Day River (MFJDR) and evaluates theoretical mixing potential to assess the validity of cold patch measurements. Chapter 3 applies DTS data to investigate a temperature anomaly observed in TIR and FLIR datasets collected on the MFJDR. The diagnosed cause of the anomaly provides an important lesson for TIR and FLIR dataset interpretation. Chapter 4 explores techniques and challenges of DTS deployment in streams. Two types of potential data artifacts in stream temperature DTS measurements are discussed. Chapter 5 employs DTS data in both the temporal and spatial domains to assess longitudinal stream temperature trends. Potential causes of those trends are assessed.

Chapter 2 – Cold Patch Survey

2.1 Introduction

Stream temperatures exceeding certain lethal limits pose a hazard to fishery health (Brett, 1956); however, some researchers have shown that fish are capable of behavioral thermoregulation, identifying and holding in sections of stream that are relatively cooler than others (Kaya et al., 1977; Nielsen et al., 1994; Torgersen, 1997). These cold water patches may serve as “thermal refugia” for fish, allowing them to thrive or survive under ambient thermal conditions that are stressful or lethal (Ebersole et al., 2001, 2003).

Cold water patches in streams, alternately referred to as “cold pools”, “cool water areas”, and “stratified pools” (Ebersole et al., 2003), have been studied by multiple researchers (Bilby, 1984; Ozaki, 1988; Keller et al., 1990; Nielsen et al., 1994; Ebersole et al., 2001, 2003). They are generally defined as spatially-distinct stream areas (i.e. constrained to a single stream pool or limited to one channel width in length) with temperatures cooler than nearby stream areas (i.e. within a 10-meter radius or located upstream of the pool of interest). The temperature of the nearby stream areas has typically been referred to as “ambient” temperature.

Cold patches at least 3°C cooler than ambient stream temperature were reported in three northwestern California streams (Nielsen et al., 1994) and in nine northeastern

Oregon creeks in the Snake River basin (Ebersole et al., 2001, 2003). These studies used a combination of point temperature measurements and temperature loggers, and two of the studies found a positive correlation of fish presence with cold water patches, suggesting that fish were using the patches as thermal refugia. Ebersole et al. (2003) surveyed 16 kilometers of creeks (third-order or larger streams in the Grande Ronde portion of the Snake River basin) and located 57 cold water patches at least 3°C cooler than ambient stream temperatures. Many of the patches identified were attributed to groundwater or tributary inflows. Nielsen et al. (1994) identified thermal stratification in stream pools, and pool-bottom temperatures as much as 9°C lower than ambient stream temperatures. These pools all possessed unique physical characteristics to which Nielsen et al. (1994) attributed the extreme stratification measured: some were channel backwater areas with cool water inflows, some were partially separated from mainstem flow by gravel bars and fed by tributaries, and some had long pool residence times (2.5-9.3 hours).

The Middle Fork John Day River in northeastern Oregon is a fourth to sixth (6+) order stream harboring runs of ESA-listed spring Chinook salmon and steelhead. Torgersen et al. (1995, 1999) proposed that cold water areas were associated with fish presence in this system. The 1995 study found that spring Chinook salmon were consistently located in cold water patches 1°C - 3°C cooler than ambient stream temperatures, and asserted that cold water patches were most often found in pools. However, the 1999 study found no evidence of thermal stratification in deep pools of the MFDJR. That study found that spring Chinook salmon were likely to be located in MFJDR reaches with relatively cool daytime temperatures, but no association was found with microscale cold patch features. River restoration planners have speculated that disturbances to the

channel have reduced the number of off-channel and in-channel thermal refugia in the MFJDR system and have suggested that corrective actions may be possible (RDG, 2007; BOR, 2008).

The objective of this chapter is to assess whether cold patches are significant thermal features in the current MFDJR system and to test whether thermal stratification aids in their development. During the summers of 2009-2011, Distributed Temperature Sensing (DTS) datasets were collected over five reaches of the Middle Fork John Day River in northeastern Oregon. These datasets provided stream temperature information at ten-minute time intervals and one-meter spatial intervals over each reach, and were ideally suited to cold patch detection. The cold patch survey covered a total of 7.2 kilometers of stream distance, with some reaches surveyed on both right and left river banks and/or over multiple years. Additionally, vertical temperature profiles were collected to measure the current degree of thermal stratification in the MFJDR system. The results of these DTS and vertical temperature measurements were then discussed in light of theoretical computations for thermal mixing potential.

2.2 Site Description

The Middle Fork John Day River is a 117-kilometer long stream in northeastern Oregon (Figure 2.1). It extends from headwaters near Austin, OR (1300 meters elevation) to confluence with the North Fork John Day River near Ritter, OR (670 meters elevation). It is classified as a fourth to sixth (6+) order stream (BOR, 2010). Monthly average streamflow peaks in April, with an average discharge of 21.2 cubic meters per second

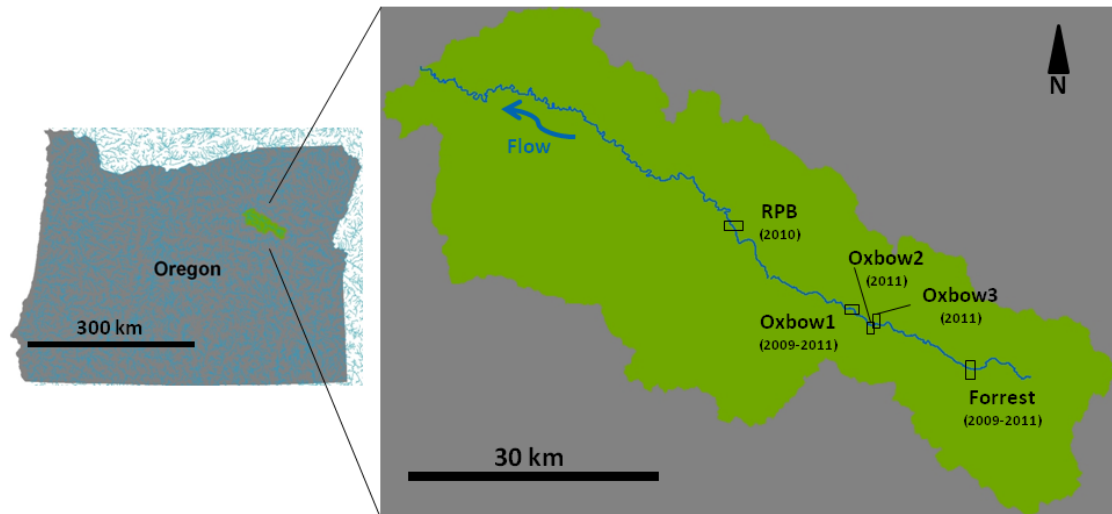


Figure 2.1: Map of the Middle Fork John Day River subbasin in northeastern Oregon. Five reaches monitored for stream temperature are identified.

$\frac{m^3}{s}$ measured at the United States Geological Survey (USGS) gauging station in Ritter, OR from 1930-2010. Monthly average streamflow is lowest in September, with $0.91 \frac{m^3}{s}$ average discharge (USGS, 2012). Daily average air temperature has a maximum monthly average, 18.8°C , in July, and a minimum monthly average, -0.9°C , in December (Agrimet, 2012). During the summer field season (July-September), diurnal fluctuations in air temperature are typically between 5°C and 30°C (Appendix A).

The study site consists of five 1-3 kilometer-long reaches of the MFJDR, named Forrest, Oxbow1, Oxbow2, Oxbow3, and RPB (Figure 2.1). With the exception of the upstream end of Oxbow3, all monitored reaches flow through wide, alluvial meadows (Figure 2.2 and Figure 2.2). Streamside vegetation consists of sedges and grasses, with scattered taller shrubs and trees. The upstream end of Oxbow3 flows through an alluvial canyon and is shaded by a relatively greater density of shrubs and trees (Figure 2.2).



Forrest reach at $118^{\circ}31'33.82\text{W}$, $44^{\circ}35'53.11''\text{N}$, facing northwest and downstream



Oxbow1 reach at $118^{\circ}40'48.67\text{W}$, $44^{\circ}39'16.91''\text{N}$, facing north and downstream



Oxbow3 reach at $118^{\circ}38'10.76\text{W}$, $44^{\circ}38'35.74''\text{N}$, facing southwest and downstream

Figure 2.2: Photos of the study reaches

Over the entire MFJDR basin, 80% of floodplain area contains low vegetation or open areas, 14% contains small trees and shrubs, and 6% contains large trees (BOR, 2008). Landuse immediately adjacent to the study reaches consists primarily of ungrazed grassland. The Oxbow Conservation Area and the Forrest Conservation Area, in which four of the five monitored reaches are located, have been managed for riparian habitat by the Confederated Tribes of the Warm Springs Reservation of Oregon (CTWSRO) since 2001-2002. This management includes elimination of cattle grazing from 50-150 meter-wide riparian corridors. Outside these corridors, cattle grazing is permitted but restricted in intensity. Upland areas in the vicinity of the MFJDR are primarily managed by the United States Forest Service (USFS) for logging, with ponderosa pine (*pinus ponderosa*) constituting the dominant tree species.

Historical landuse in the MFJDR basin, since the entrance of European explorers and settlers in the early 1800s, has mostly consisted of beaver trapping, gold mining, logging, homesteading, cattle grazing, and railroad and road construction. The first beaver trappers were reported to have entered the area in 1811, and beaver populations were largely eliminated by 1847 (McAllister, 2008). Gold mining began in the basin in the 1860's, with the most intense and mechanized mining activity occurring between 1939 and 1942 (McDowell, 2000). Permanent settlement began in the 1880's (McAllister, 2008), with cattle grazing likely following settlement. A railroad was constructed in the alluvial valley in 1910, and was operated until about 1930 (McDowell, 2000). Throughout the 20th century, settlers accommodated cattle grazing by removing shrubs and trees from the alluvial valley and by performing channel straightening and modifications, both for improvement of grazing land and for grass irrigation (McDowell, 2000).

In 2001-02, the properties encompassing the two largest alluvial valleys in the upper MFJDR was acquired by CTWSRO, and the elimination of cattle grazing from riparian corridors on those properties soon followed. Anecdotal evidence suggests that vegetation height adjacent to the stream has increased since the elimination of streamside grazing.

2.3 Methods

Five reaches (Figure 2.1, Section 2.2) of the MFJDR were monitored for stream temperature using DTS technology. The Forrest and Oxbow1 reaches were monitored during three consecutive summer field seasons (2009-2011). The Oxbow2 and Oxbow3 reaches were monitored during the 2011 field season, and the RPB reach was monitored during the 2010 field season.

Table 2.1 displays monitoring dates, length, and dataset properties for each of the nine installations. Some DTS installations were made with one cable in the channel thalweg, and some were made with two cables, each located within 1.5 meters of the stream banks (right bank/left bank). Flow rates were measured at the upstream and downstream ends of each installation with a Marsh-McBirney flow meter. Where a range of flow rates are listed, two measurements were made within the monitoring period. It should be noted that an error of approximately 5% of the flow rate applies to all measurements. For the Oxbow2 reach, the listed downstream flow rate represents the loss of approximately 25% of the stream flow volume to the Oxbow Conservation Area South Channel at river kilometer 95.20. River kilometer values are based on DEQ (2010)

and are presented as location references only. The "full reach length" indicated for each installation is measured at a higher spatial resolution and is a more accurate measure of stream distance. The Oxbow2 installation ends in the North Channel of the Oxbow Conservation Area, at that channel's confluence with Granite Boulder Creek. Because the North Channel was excluded from the stream kilometer accounting system used by DEQ (2010), an estimated river kilometer (River Km: "94.55") was listed for the confluence of Granite Boulder Creek with the North Channel.

The monitored reaches were chosen based on access permission and relevance to ongoing stream restoration projects and planning. Forrest1 was located within the portion of MFJDR classified as a fourth order stream. Oxbow1, Oxbow2, and Oxbow3 were located within a portion classified as a fifth order stream. RPB was located within an unclassified portion of the MFJDR that was downstream of a sixth order stream (BOR, 2010).

Table 2.1: Summary of DTS installations on the MFJDR.

<p>Forrest Reach, 2011 <i>Monitoring Period: Jul26-Aug4, Aug6-Aug8</i> Thalweg installation Full Reach Length: 1643 meters Upstream Coord.: 44°35'45.15"N, 118°31'21.95"W River Km: 109.85 – 108.56 Upstream Flow Rate: 0.50 – 0.41 cms Downstream Flow Rate: 0.90 – 0.56 cms Dataset accuracy: 0.11 °C</p>	<p>Oxbow1 Reach, 2011 <i>Monitoring Period: Jul30-Aug1, Aug4-Aug9</i> Thalweg installation Full Reach Length: 2168 meters Upstream Coord.: 44°38'55.39"N, 118°40'0.11"W River Km: 92.15 – 91.84 Upstream Flow Rate: 1.55 – 1.04 cms Downstream Flow Rate: 1.69 – 1.08 cms Dataset accuracy: 0.06 °C</p>	<p>Oxbow2 Reach, 2011 <i>Monitoring Period: Aug12-Aug24</i> Thalweg installation Full Reach Length: 1086 meters Upstream Coord.: 44°38'30.03"N, 118°38'45.87"W River Km: 95.55 – "94.55" (North Channel) Upstream Flow Rate: 0.69 – 0.63 cms Downstream Flow Rate: 0.51 – 0.47 cms Dataset accuracy: 0.11 °C</p>
<p>Forrest Reach, 2010 <i>Monitoring Period: Aug19-Aug24</i> Thalweg installation Full Reach Length: 1719 meters Upstream Coord.: 44°35'45.15"N, 118°31'21.95"W River Km: 109.85 – 108.48 Upstream Flow Rate: 0.39 – 0.33 cms Downstream Flow Rate: 0.48 – 0.41 cms Dataset accuracy: 0.08 °C</p>	<p>Oxbow1 Reach, 2010 <i>Monitoring Period: Aug5-Aug9</i> Left Bank/ Right Bank installation Full Reach Length: 1848/ 1856 meters Upstream Coord.: 44°38'56.39"N, 118°40'2.25"W River Km: 92.10 – 91.88 Upstream Flow Rate: 0.73 cms Downstream Flow Rate: 0.76 cms Dataset accuracy: 0.36/ 0.26 °C</p>	<p>Oxbow3 Reach, 2011 <i>Monitoring Period: Aug11-Aug21, Aug23-Aug24</i> Thalweg installation Full Reach Length: 1384 meters Upstream Coord.: 44°38'37.43"N, 118°38'5.76"W River Km: 96.85 – 95.55 Upstream Flow Rate: 0.67 – 0.63 cms Downstream Flow Rate: 0.69 – 0.63 cms Dataset accuracy: 0.04 °C</p>
<p>Forrest Reach, 2009 <i>Monitoring Period: Jul21-Jul25</i> Left Bank/ Right Bank installation Full Reach Length: 1590/ 1586 meters Upstream Coord.: 44°35'45.15"N, 118°31'21.95"W River Km: 109.85 – 108.58 Upstream Flow Rate: 0.31 cms Downstream Flow Rate: 0.59 cms Dataset accuracy: 0.21/ 0.17 °C</p>	<p>Oxbow1 Reach, 2009 <i>Monitoring Period: Sept4-Sept12</i> Left Bank/ Right Bank installation Full Reach Length: 1827/ 1818 meters Upstream Coord.: 44°38'59.51"N, 118°40'8.51"W River Km: 92.00 – 91.78 Upstream Flow Rate: 0.59 cms Downstream Flow Rate: 0.46 cms Dataset accuracy: 0.18/ 0.30 °C</p>	<p>RPB Reach, 2010 <i>Monitoring Period: Sept19-Sept21, Sept 23</i> Left Bank/ Right Bank installation Full Reach Length: 855/ 825 meters Upstream Coord.: 44°44'33.66"N, 118°51'4.63"W River Km: 69.32 – 68.52 Upstream Flow Rate: 0.81 – 0.57 cms Downstream Flow Rate: 0.81 – 0.57 cms Dataset accuracy: 0.09/ 0.14 °C</p>

2.3.1 DTS Installation

The nine DTS installations employed a fiber optic cable manufactured by AFL Telecommunications, consisting of two Giga-Link 600 multimode fibers protected by a stainless steel loose tube, a resin-stabilized fiberglass sheath, and a meter-marked polyurethane jacket, completing the cable to a 2.5 millimeter diameter. The cable was installed either in the stream channel thalweg or, for channel edge temperature measurement, within 1.5 meters of the channel banks. The cable was observed to sink in all water conditions except the most turbulent, and alluvial rocks were placed to secure the cable where the risk of cable movement was high. Four different DTS instruments were used for data collection: an Agilent N4386A, two SensorTran Gemini instruments, and an AP Sensing Linear Pro Series instrument. The installations were powered by custom-designed solar trailers. The DTS temperature readings were calibrated to at least three point temperature measurements collected by Onset HOBO Water Temp Pro v2 dataloggers. One or two of these logger measurements were made within 0°C ice baths, co-located with 25-50 meters of cable, and two to eight of the measurements were made within the stream itself, co-located with 2-25 meters of cable.

2.3.2 Dataset Analysis

The nine DTS datasets employed in this study each consisted of four to thirteen days and between one and three kilometers of stream temperature data, collected at ten-minute time intervals and one-meter distance intervals. This spatial resolution constrained the measurement to detection of cold patches that were at least one meter in longitudinal

length.

The value of cold patches for fish habitat is greatest when stream temperature is warmest, so the datapoints collected during the hottest hours of the day were the points of interest for detection and measurement of cold patches.

Previous studies have suggested that cold patches are often associated with cool water inflows. During the time of day when stream temperature peaks (typically late afternoon), tributary water, groundwater, and hyporheic water inflows have the potential to be cooler than mainstem stream water. The conceptual model in Figure 2.3 displays these three types of inflows, the expected diurnal temperature variation of the inflows relative to the mainstem stream temperature, and the location of a thalweg fiber optic cable installation.

The "temperature differentiation" of cold patches refers to how much cooler the patch is than surrounding water temperatures. High differentiation occurs when the temperature of the cool water inflow is much lower than ambient stream temperature and when the inflow quantity is large relative to the rate at which the inflow mixes with mainstem water. Therefore, the two factors affecting cold patch temperature differentiation are the difference between inflow temperature and mainstem temperature and the quantity of cool water inflow. Over the timescale of hours, the quantity of groundwater, hyporheic water, and tributary water inflows is not expected to vary significantly. Groundwater and hyporheic water inflows (henceforth referred to as "subsurface inflows") are expected to have temperatures that are relatively constant in time, relative to mainstem temperature diurnal variation (Figure 2.3). During the hours of peak mainstem water temperature, the difference between mainstem and subsurface inflow tempera-

tures is expected to vary little, relative to the magnitude of the difference. Therefore, the temperature differentiation of subsurface water-fed cold patches has little time-variance during the late afternoon period. On the other hand, tributary water temperatures vary significantly throughout the day and may approach or exceed mainstem water temperatures during the hottest parts of the day (Figure 2.3). The difference between tributary water temperature and mainstem temperature has the potential to vary significantly in time, relative to its magnitude. Because of this variation, the temperature differentiation of cold water patches fed by tributaries has the potential to be time-dependent during the hours of peak stream temperature. To facilitate cold patch detection, cold patches fed by subsurface inflows were tallied differently than patches fed by tributary inflows.

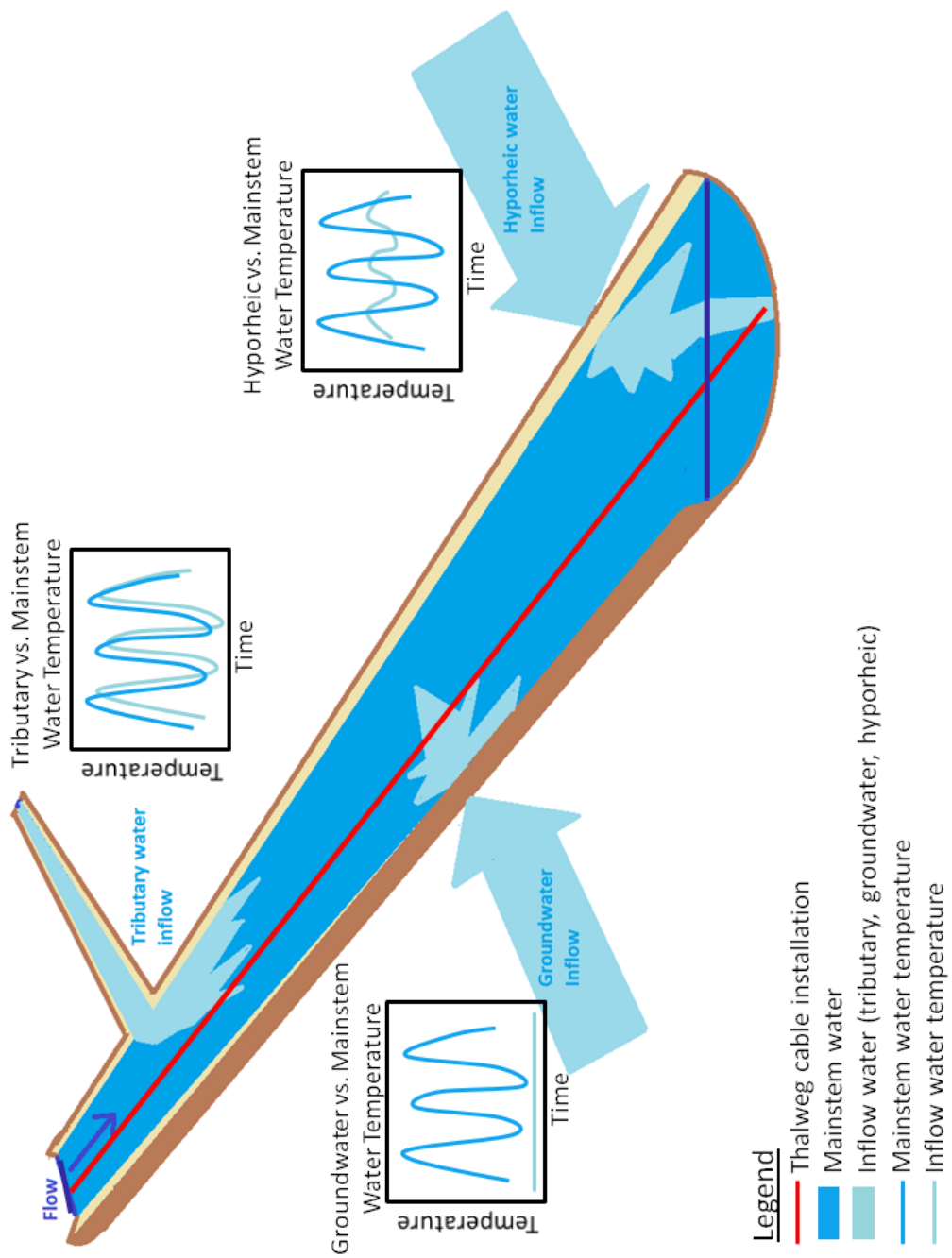


Figure 2.3: Conceptual model of cold patch causation and cable installation.

2.3.2.1 Cold Patches Fed by Subsurface Inflows

DTS data from the period of each day when mainstem temperature was hottest were identified. To adequately capture the daily temperature maximums, a dataset-specific four-hour period was selected. For example, in the RPB dataset, the hours of 15:10 - 19:10 were well-centered around the daily stream temperature maximum, while for the Forrest 2011 dataset the hours of 14:30-18:30 encompassed the maximum (Figure 2.4). For consistency of presentation, the same four-hour period was applied to every day within the dataset. This simplification was determined to have no significant impact on the dataset analysis, as the temporal shifting of maximum stream temperatures was minimal within each dataset.

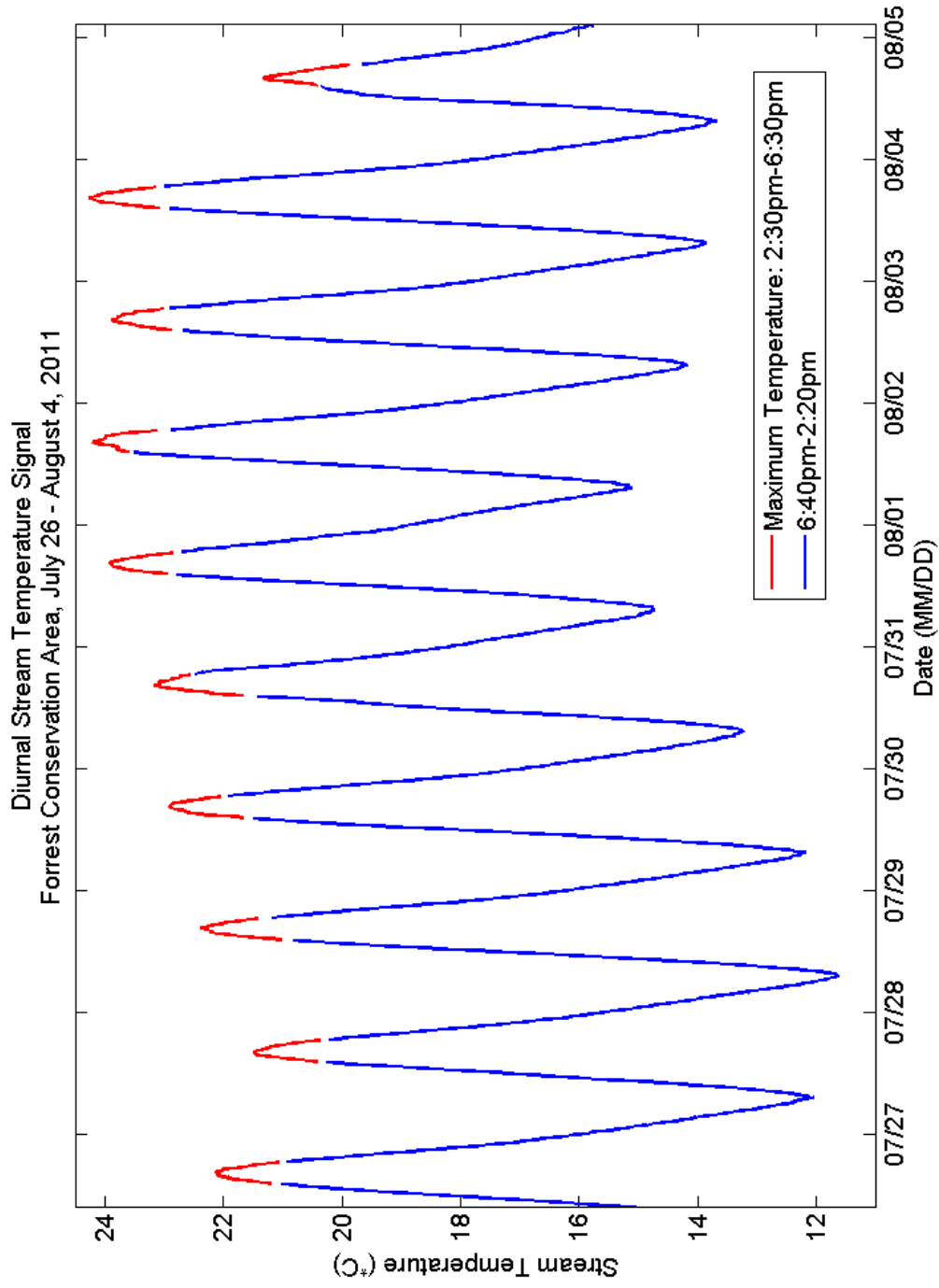


Figure 2.4: Typical diurnal stream temperature signal from the Forrest 2011 reach, with periods of maximum stream temperature highlighted.

Each four-hour period was time-averaged. Because subsurface water-fed cold patches have little time variance during the late afternoon period, the time-averaging process reduced dataset noise without affecting the detected temperature differentiation of cold patches. The time-averaging resulted in one daily maximum longitudinal stream temperature profile (“Daily Maximum Profile”) based on the hottest four hours of each day of monitoring (Figure 2.5).

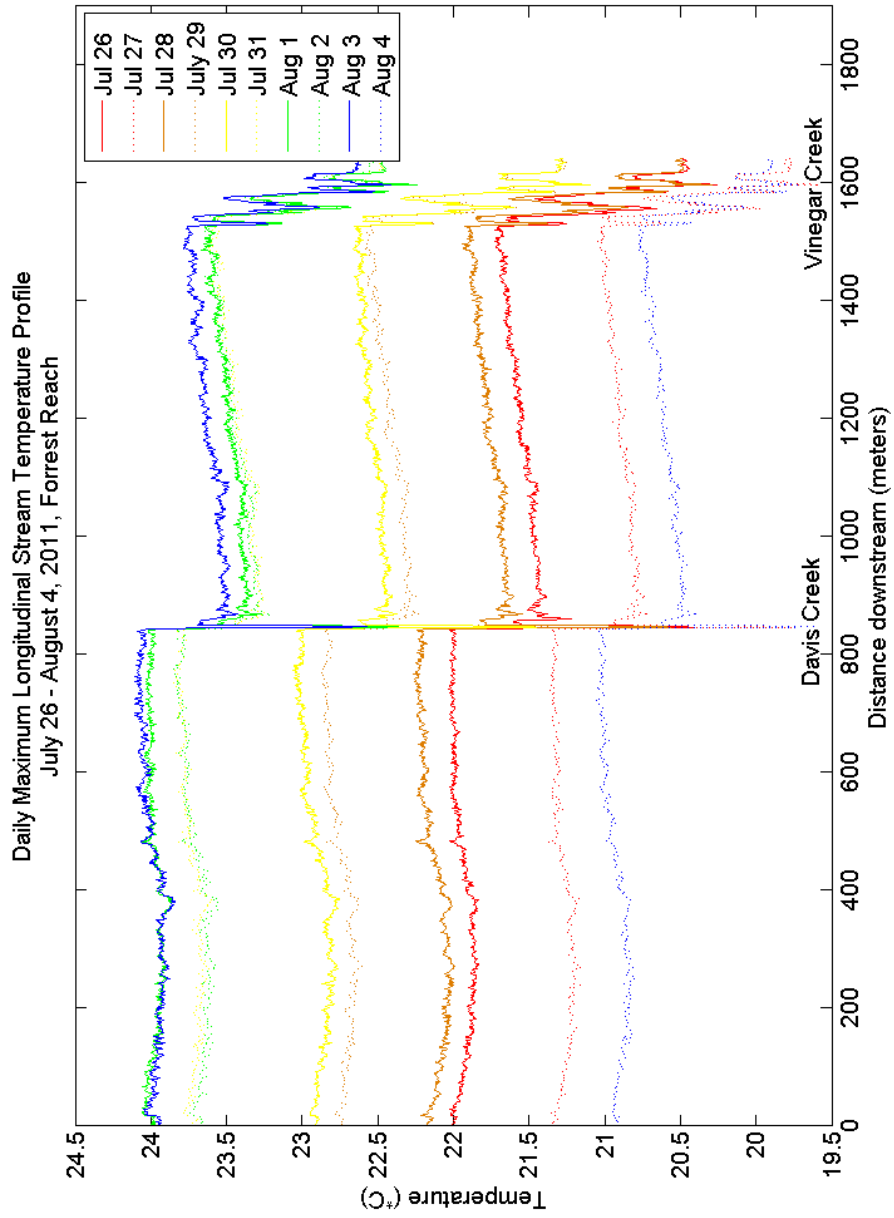


Figure 2.5: Some of the daily maximum longitudinal stream temperature profiles (“Daily Maximum Profiles”) from the Forrest 2011 dataset. Davis Creek flows into the mainstem at 840 meters downstream distance and Vinegar Creek joins at 1520 meters. Air temperature data from this monitoring period is displayed in *Appendix A*.

Daily Maximum Profiles were then split into between three and eight segments based on the locations of linear slope breaks. The number of segments was dataset-specific and the segment locations remained constant over each monitoring period. A linear regression line was then fit to each segment, with a unique slope and intercept value generated for each Daily Maximum Profile. Portions of the Daily Maximum Profiles immediately impacted by known surface water tributary inflows (prior to complete mixing of tributary and mainstem water) were not included in the regression line fitting. Figure 2.6 displays the Daily Maximum Profile, with regression lines, from the hottest day of each dataset. This figure is discussed further in Section 2.4.2.

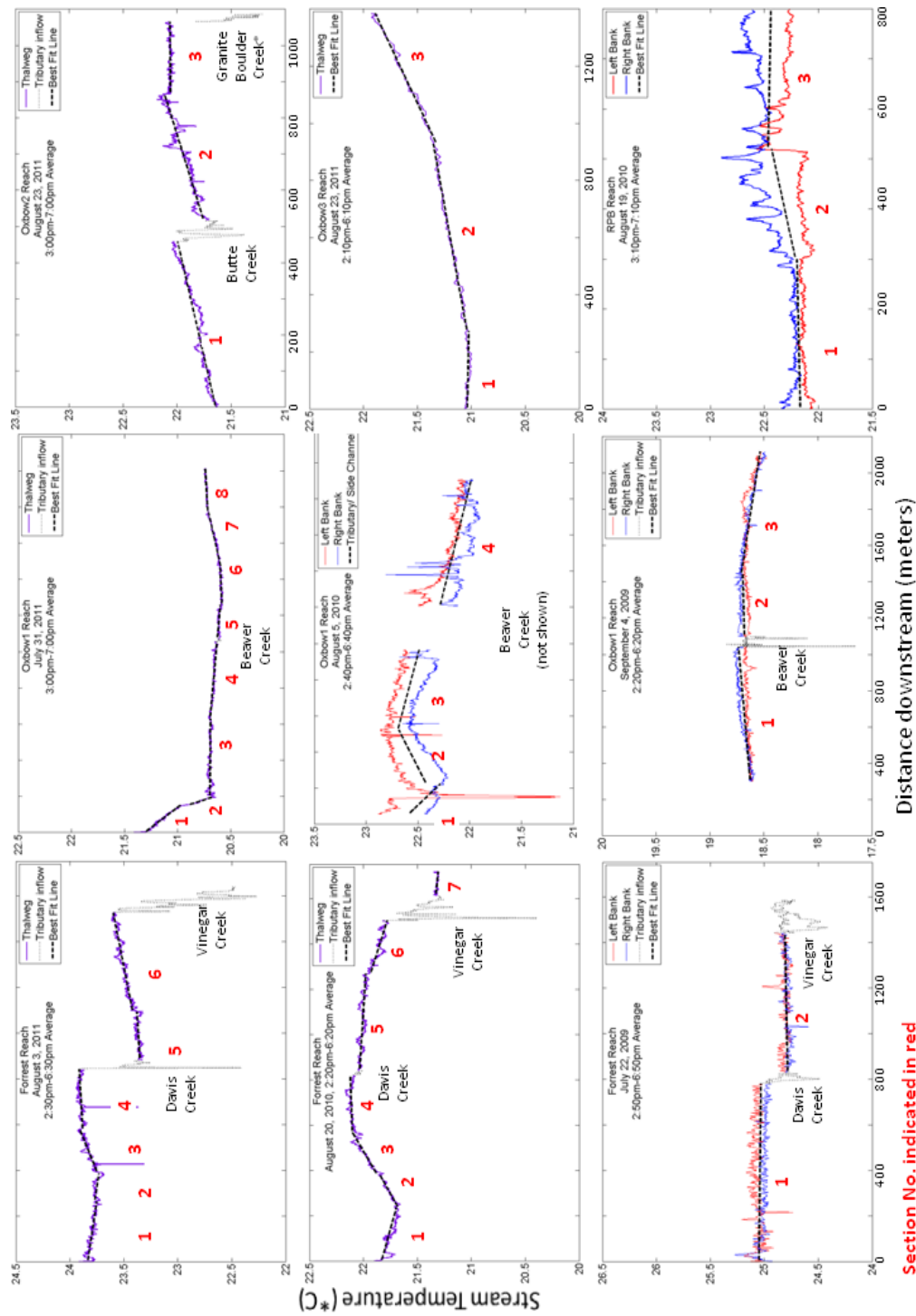


Figure 2.6: Daily Maximum Profiles for the hottest day within each DTS dataset. For dataset accuracy, refer to Table 2.1. Larger versions of each of these graphs are included in *Appendix B*

Because the regression lines were based on a longitudinal series of stream temperature samples, they closely fitted the observed linear stream temperature patterns. The regression lines were taken to represent "ambient" mainstem stream temperature at each location. Thus, a negative deviation of the Maximum Daily Profile from the regression line could be viewed as a cold patch (either groundwater-fed or hyporheic water-fed). The Maximum Daily Profiles retained the one-meter spatial resolution of the raw DTS data, so cold patches that were at least one meter in longitudinal length would be detected.

The maximum temperature differentiation of subsurface water-fed cold patches, equivalent to the maximum negative deviation of the Maximum Daily Profile from the regression line, was computed for each segment of each reach.

2.3.2.2 Cold Patches Fed by Tributary Inflows

Tributary-fed cold patches were evaluated at each ten-minute interval over the hottest four hour period of each day. Computing tributary-fed cold patch magnitude at ten-minute intervals, as opposed to over daily four-hour averages, allowed for more accurate estimation of maximum magnitude, since temperature differentiation of tributary-fed cold patches had the potential to change rapidly. Cold water patches at tributary confluences were assessed by comparing the DTS-measured stream temperature upstream of the tributary to the minimum DTS temperature measurement due to the tributary. Within each dataset, the maximum difference between these two temperatures was recorded. A total of five creeks (Davis Creek, Vinegar Creek, Butte Creek, Vinegar Creek, and Gran-

ite Boulder Creek) were evaluated, some over multiple years.

In addition to the tributary-fed cold patches, one subsurface water-fed cold patch was evaluated at ten-minute intervals. This cold patch had the highest temperature differentiation of all the subsurface water-fed cold patches detected (1.28°C cooler than ambient stream temperature) and is discussed further in Section 2.4.2. The evaluation of this subsurface inflow at a higher temporal resolution was justified as a check on the subsurface water-fed cold patch measurement method (described above), providing an upper limit of cold patch magnitude due to subsurface inflows.

2.3.3 Vertical Temperature Measurements

Thermal profile measurements were made in two 1.5-meter deep pools, referred to as Pool1 in Oxbow1 and Pool2 in Oxbow2. These pools represented the slowest-flowing and deepest sections within the study reaches, and were known to be used by spring Chinook salmon for late-summer holding. Measurements were made in Pool1 on September 7-11, 2009 and in both Pool1 and Pool2 on August 19, 2011. The 2011 measurements were made with a Fluke 1524 thermometer that had a precision of $\pm 0.002^\circ\text{C}$. Four depth measurements were made at a few locations within each pool, in both the morning and late afternoon. The 2009 measurements were made using two Onset HOBO Water Temp Pro v2 temperature loggers, installed at depths of 0.15, 0.85, and 1.45 meters below the water surface, and protected from direct sunlight by PVC tubing. A photograph of the installation is included in Figure 2.7. This measurement set-up was repeated at three locations within Pool1, and only data from the top (0.15 meter depth) and bottom (1.45

meter depth) temperature loggers were included in the final analysis. Because the precision of the loggers was $\pm 0.2^{\circ}\text{C}$, a calibration was required to detect the subtle vertical temperature differences present in the pool. Nighttime temperature measurements were used for this purpose, under the assumption that, without insolation, nighttime vertical temperatures of slow-moving, relatively shallow water bodies tend to become uniform (Nielsen et al., 1994; Bormans and Condie, 1997). Thus, the difference between the top and bottom logger temperatures during the hours of 3:00 and 5:00 was viewed as a 0°C difference datum.

2.4 Results

2.4.1 DTS Dataset Visual Assessment

The nine DTS datasets displayed in Figure 2.6 represent late afternoon stream temperature data from five MFJDR reaches, some monitored over three summers. Several features are worthy of note. First, spatial variation over the 800 to 2200 meter-long datasets was limited to less than 2.5°C in magnitude. This visual observation jibes with the results of the cold patch analysis discussed below. Second, tributary junctions caused step-like decreases in stream temperature in many cases, suggesting that tributaries provide thermal heterogeneity in this system. Synoptic discharge measurements made during the course of this study generally indicated that flow accumulation in those reaches was primarily gained at tributary junctions. Third, linear-like longitudinal slopes were visible in most segments of most datasets. The properties of these sloped segments are discussed further in Section 5. Fourth, there are significant differences between right bank and left bank temperatures in some, but not all, datasets. These differences may relate to dataset accuracy (Table 2.1) or to other factors, such as differences in solar radiation received on the measurement cable (Section 2.1).

2.4.2 DTS Analysis Results

2.4.2.1 Cold Patches Fed by Subsurface Water Inflows

Table 2.2 displays the maximum negative deviations (Section 2.3.2) detected in each segment of each reach, as computed over the full monitoring period of that reach. Highlighted values are significant, exceeding the dataset noise of two standard deviations (Table 2.1). Over the 79 total monitoring days, or a total monitored length of 7.2 unduplicated kilometers (some of those monitored over three seasons or with two-bank monitoring focus), no DTS temperature measurement exceeded 1.28°C degrees lower than the regression lines fitted to the Maximum Daily Profiles.

The coldest detected patch, located on the left bank of Oxbow1 during the 2010 installation, corresponds to a location suspected to have significant subsurface inflow from two tributaries (Ruby Creek and the Oxbow South Channel irrigation ditch). These tributaries intersect each other at a location 120 meters upgradient from the mainstem. From this intersection, a channel carries a portion of the mixed tributary water northward towards the mainstem through a channel bordered by coarse mine tailings on both its right and left banks. The remaining portion of the flow is directed from the intersection westward through the irrigation ditch. In August 2011, flow in that ditch was observed to taper off and end a few hundred meters downstream. Any flow lost from the ditch would be expected to flow downgradient (northward) towards the mainstem. The hydraulic gradient between the Oxbow South Channel irrigation ditch and the mainstem is 0.03 meters per meter (estimated from LiDAR), and the intervening floodplain consists of mine tailings, a typically coarse soil material likely to have high hydraulic conductivity.

2.4.2.2 Cold Patches Fed by Tributary Water Inflows

Maximum stream temperature decreases due to tributary inflows ranged between 0.03°C and 2.31°C (Table 2.3). The subsurface inflow detected on the left bank of Oxbow1 during the 2010 installation was additionally measured at ten-minute intervals. At this temporal resolution and measurement accuracy, the maximum stream temperature decrease caused by this inflow was 1.94°C.

Table 2.2: Maximum cold patch magnitudes, as estimated by the maximum negative deviation of DTS measurements from segment-specific regression lines. Highlighted values are significant, exceeding the dataset noise of two standard deviations.

Forrest Reach, 2011 Segment 1: -0.09°C Segment 2: -0.07 Segment 3: -0.54 Segment 4: -0.56 Segment 5: -0.06 Segment 6: -0.39	Oxbow1 Reach, 2011 Segment 1: -0.05°C Segment 2: -0.15 Segment 3: -0.09 Segment 4: -0.11 Segment 5: -0.11 Segment 6: -0.03 Segment 7: -0.03 Segment 8: -0.02	Oxbow2 Reach, 2011 Segment 1: -0.09°C Segment 2: -0.20 Segment 3: -0.08
Forrest Reach, 2010 Segment 1: -0.13°C Segment 2: -0.06 Segment 3: -0.12 Segment 4: -0.06 Segment 5: -0.07 Segment 6: -0.10 Segment 7: -0.04	Oxbow1 Reach, 2010 Segment 1: -1.28°C Segment 2: -0.41 Segment 3: -0.38 Segment 4: -0.21	Oxbow3 Reach, 2011 Segment 1: -0.04°C Segment 2: -0.05 Segment 3: -0.06
Forrest Reach, 2009 Segment 1: -0.50°C Segment 2: -0.66	Oxbow1 Reach, 2009 Segment 1: -0.44°C Segment 2: -0.19 Segment 3: -0.31	RPB Reach, 2010 Segment 1: -0.16°C Segment 2: -0.33 Segment 3: -0.22

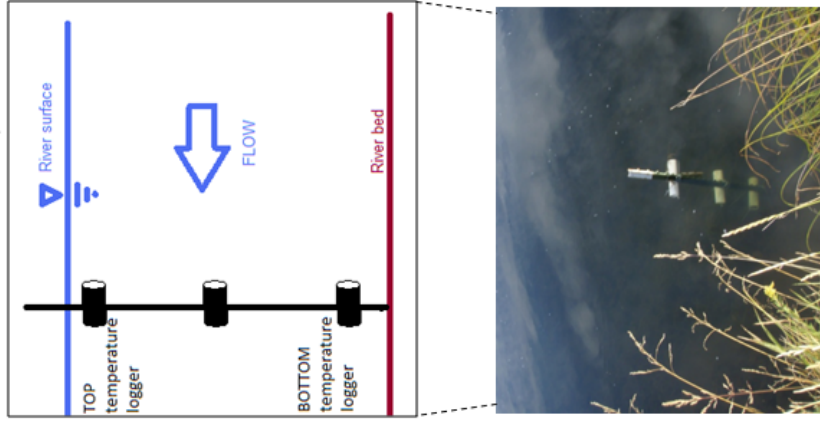
2.4.3 Vertical Temperature Measurement Results

Figure 2.7 displays timeseries of vertical temperature profiles measured in Pool1 on September 7-11, 2009. Table 2.4 displays the vertical temperature profile point measurements made on August 19, 2011 in Pool1 and in Pool2.

Table 2.3: The maximum magnitudes of cold patches associated with tributary inflows, computed as the greatest difference between ambient mainstem temperature and tributary-impacted temperature during the four-hour period with warmest mainstem temperatures. The temperature impact of Granite Boulder Creek, at the downstream end of Oxbow2, is not fully represented, as the cable installation captured just a small portion of that tributary's inflow.

Creek Name	Monitoring Reach, Year	Greatest stream temperature drop due to tributary inflow (°C)
Davis Creek	Forrest Reach, 2009	-0.88
Davis Creek	Forrest Reach, 2010	-0.20
Davis Creek	Forrest Reach, 2011	-1.97
Vinegar Creek	Forrest Reach, 2009	-0.65
Vinegar Creek	Forrest Reach, 2010	-1.75
Vinegar Creek	Forrest Reach, 2011	-1.71
Butte Creek	Oxbow2 Reach, 2011	-0.79
Granite Boulder Creek	Oxbow2 Reach, 2011	-1.07
Beaver Creek	Oxbow1 Reach, 2009	-2.09
Beaver Creek	Oxbow1 Reach, 2010	-2.31
Hyporheic Inflow, Left Bank	Oxbow1 Reach, 2010	-1.95
Beaver Creek	Oxbow1 Reach, 2011	-0.03
Hyporheic Inflow, Left Bank	Oxbow1 Reach, 2011	-1.10

Measurement Set-up:



Temperature Difference, Top – Bottom, Pool1, Three Locations

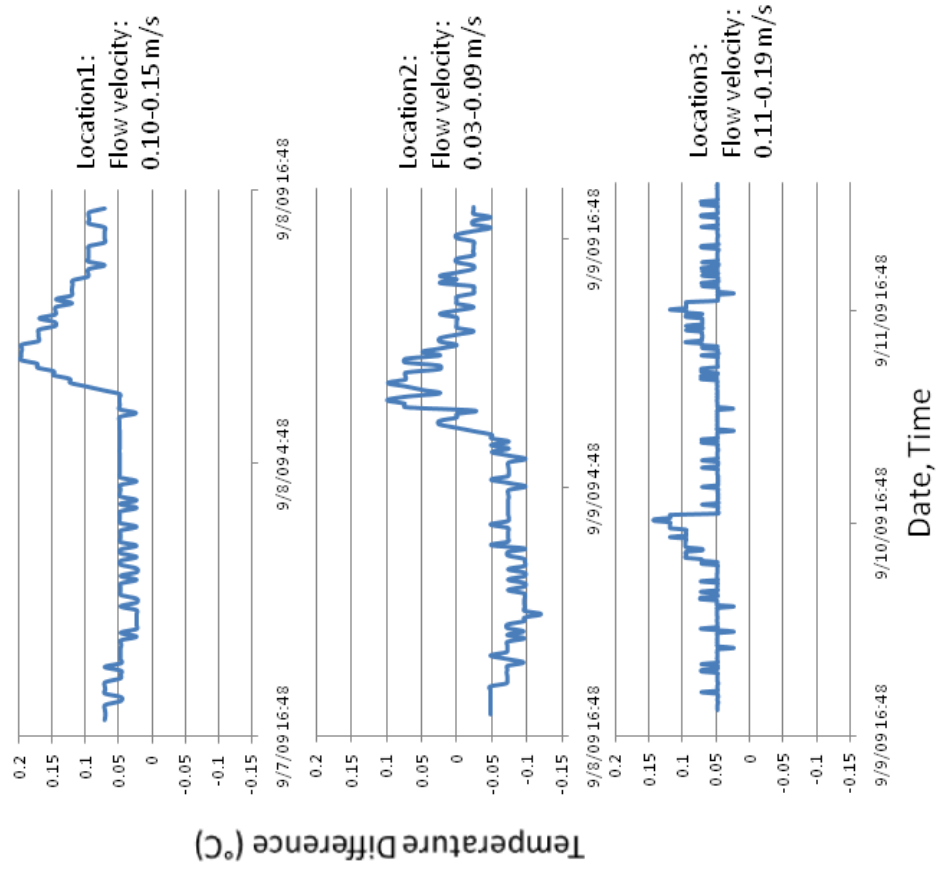


Figure 2.7: Timeseries of the vertical temperature profiles measured in Pool1, Oxbow1, on September 7-11, 2009. Measurements were made with point temperature loggers of accuracy $\pm 0.2^{\circ}\text{C}$.

Table 2.4: Vertical temperature measurements made in Pool1 and Pool2, August 19, 2011. Measurements were made with a thermometer of accuracy $\pm 0.002^{\circ}\text{C}$.

	Pool1				Pool2	
Approximate Coordinates	44°39'3.25"N, 118°40'21.18"W				44°38'33.90"N, 118°39'15.40"W	
Approximate Pool Depth (meters)	1.5				1.5	
Date/Time	August 19, 2011 9:00	August 19, 2011 16:00	August 19, 2011 16:04	August 19, 2011 16:08	August 19, 2011 8:20	August 19, 2011 16:40
Temperature, Top ($^{\circ}\text{C}$) (Approx. 0.15 m depth)	12.128	18.560	18.604	18.707	12.014	20.041
Temperature, Mid-Top ($^{\circ}\text{C}$) (Approx. 0.5 m depth)	12.104	18.527	18.579	18.691	11.987	20.009
Temperature, Mid-Bottom ($^{\circ}\text{C}$) (Approx. 1.0 m depth)	12.103	18.512	18.565	18.687	11.987	20.007
Temperature, Bottom ($^{\circ}\text{C}$) (Approx. 1.45 m depth)	12.101	18.494	18.545	18.692	11.986	20.007

2.4.4 Stream Mixing Potential

Cold water patch formation requires both cool water supply (tributary inflow, groundwater or hyporheic water inflows) and kinetic conditions that prevent mixing. Poole and Berman (2001) suggested that stream temperature patterns can be explained by combining factors external to the stream system (heat fluxes, inflows) and factors internal to the stream (flow velocity, depth). To explore the feasibility of cold patch formation in the MFJDR, the results of DTS and vertical temperature measurements have been used to inform and serve as a reference point for theoretical estimates of stream mixing/stratification potential.

2.4.4.1 Richardson Number

The Richardson number, a dimensionless ratio of potential to kinetic energy, has been used in the fields of aviation and oceanography to assess the importance of potential energy effects (such as density stratification) and kinetic energy effects (such as turbulent mixing) in the media of air and water. Nielsen et al. (1994) created a river-specific Richardson number equation, based on bulk channel characteristics, to assess the degree of thermal stratification and turbulent mixing in stream pools. Thermal stratification is likely at Richardson numbers greater than one.

A version of the Richardson number based on channel-averaged hydraulic parameters is

$$Ri = \frac{\frac{\Delta\rho}{\rho} * g * Q}{W * U^3} \quad (2.1)$$

where the Richardson number (Ri) is a function of gravity (g), stream discharge (Q), stream width (W), channel-averaged flow velocity (U), and the normalized density difference ratio ($\frac{\Delta\rho}{\rho}$) between the cool, pool-bottom water and the bulk stream water at ambient temperature (Nielsen et al., 1994).

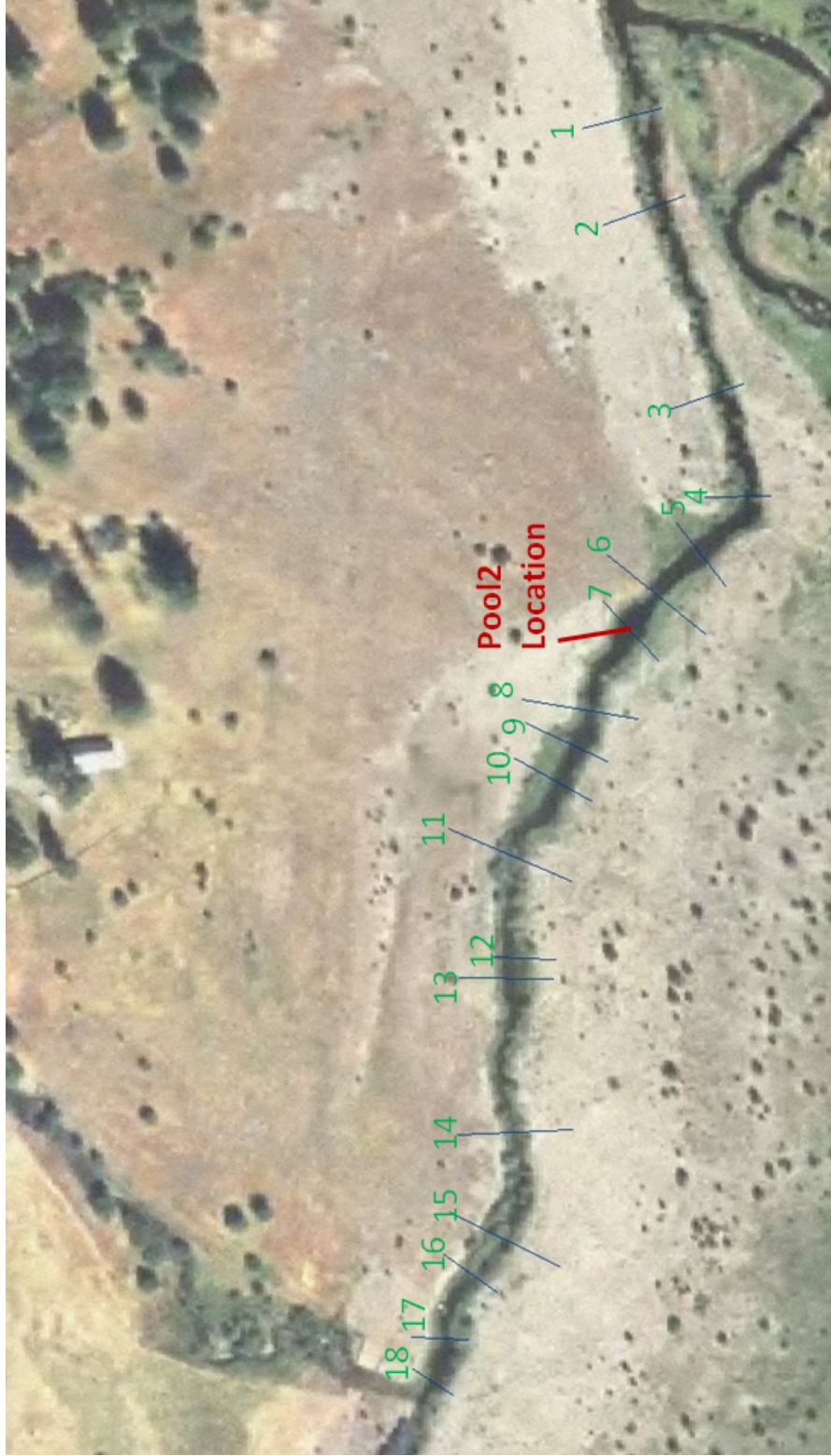


Figure 2.8: Oxbow2 stream cross section locations for which Richardson numbers were computed. Pool2 corresponds to the Cross Section No. 7 indicated in the figure.

To assess the mixing potential of pools in the MFJDR, the equation above was applied to the downstream end of the Oxbow2 reach, an area known to contain many deep, slowly-flowing pools. Hydraulic parameters required for the Richardson number computation included stream discharge, channel width, and average velocity. On August 13, 2011, measurements of these parameters were made at two locations in that reach, corresponding to just upstream of Cross Section 1 and to Cross Section 18 (Figure 2.8). In order to compute the Richardson number at more locations within the reach, a HEC-RAS hydraulic model was constructed to estimate channel velocities at eighteen cross sections along the reach. The model was based on a LiDAR DEM (WSI, 2008), on field estimates of water depth made in August 2011, and on an upstream flow rate, $0.52 \frac{m^3}{s}$ measured in the North Channel just downstream of the South Channel divergence. The discharge measurement was made with a Marsh McBirney flow meter on August 13, 2011. Model-computed velocity values at Cross Section 1 and Cross Section 18 were compared to measured values. At Cross Section 1, which was five meters downstream of the actual measurement location, the model-computed velocity was $0.18 \frac{m}{s}$, as compared to a measured value of $0.24 \frac{m}{s}$. At Cross Section 18, the model-computed velocity was $0.31 \frac{m}{s}$, as compared to a measured value of $0.23 \frac{m}{s}$. Details of the model are included in *Appendix C*.

Thermal parameters required for the fluvial Richardson number computation include cool, pool-bottom temperature and ambient stream temperature. For this analysis, two sets of thermal parameters were used. The first set of parameters was based on vertical stream temperature profile measurements (Section 2.4.3), and represented a “field measurement” scenario. The second set of parameters represented a “hypothetical sce-

nario” of maximum thermal stratification, which provided a theoretical upper bound on stratification potential.

The field measurement scenario consisted of a Richardson number based on the maximum vertical temperature difference observed during the 2009 and 2011 thermal profile measurements. That maximum difference, 0.2°C, was observed in Pool1 on September 9, 2009 between 9:00 and 10:00 (Figure 2.7). Although this difference was measured in Pool1, rather than in Pool2, it was based on temporally continuous stratification measurements and was considered to represent a conservative upper bound on thermal stratification in both pools. The 9:00 DTS temperature measurement from August 13, 2011 at the bottom of Pool2, 14.0°C, was defined as the pool-bottom temperature, and 0.2°C was added to that pool-bottom value to estimate an ambient stream temperature of 14.2 °C.

For the hypothetical scenario, a large, cold groundwater inflow was assumed. Specifically, the coldest reasonable value for groundwater temperature, generally considered to be the average annual air temperature, was used as pool-bottom temperature. In this part of the MFJDR, the average annual air temperature is 8°C (Agrimet, 2012). Ambient stream temperature was defined as the maximum stream temperature measured within Oxbow2 on August 13, 2011, 21.5°C.

Table 2.5 displays the field measurement scenario and hypothetical scenario Richardson numbers computed for eighteen locations within Oxbow2 (Figure 2.8). The hydraulic parameters used to make the computation are also displayed. The slowest channel-averaged streamflow velocity ($0.03 \frac{m}{s}$) was computed at Cross Section No. 7, which corresponded to the location of Pool2. As a cross-check, this channel-averaged

velocity is at the lower end of the range of velocities measured in Pool1 in September 2009 ($0.03 \frac{m}{s}$ - $0.19 \frac{m}{s}$). The thermal parameters used in the computation are discussed above. The field measurement scenario Richardson numbers were all less than one, as expected given the minimal thermal stratification measured. Under the hypothetical scenario, several exceedences of unity occurred (highlighted values in Table 2.5), and the maximum value was 29.7, computed in Pool2. These exceedences suggest that thermal stratification is possible in those locations if very cool pool-bottom temperatures existed. In Pool2, a vertical differential as low as 0.3°C , the difference between 21.5°C and 21.2°C , is sufficient to produce a Richardson number exceeding unity. However, the hypothetical scenario results demonstrate that the hydraulic conditions in Oxbow2 are much less conducive to thermal stratification than were those reported by Nielsen et al. (1994). They reported Richardson numbers greater than 500,000 resulting from pool top-to-bottom temperature differences of only $3-9^{\circ}\text{C}$ or less. It was noted that Pool2 had a residence time of 0.3 hours, while the pools reported by Nielsen et al. (1994) had residence times of 2.5 to 9.3 hours, the longer residence times corresponding to larger pool volume-to-discharge ratios.

Table 2.5: Richardson numbers, as computed for eighteen stream cross sections at the downstream end of Oxbow2, based on data from August 13, 2011

Cross Section No.	Field Measurement Scenario: Richardson Number, based on 14°C pool bottom, 14.2°C ambient		Hypothetical Scenario: Richardson Number, based on 8°C pool bottom, 21.5°C ambient		Q _i (cms)	W (m)	U (m/s)
1	0.00	0.29	0.52	6.00	0.18		
2	0.06	4.23	0.52	6.92	0.07		
3	0.01	0.60	0.52	4.92	0.15		
4	0.04	2.68	0.52	5.13	0.09		
5	0.10	6.89	0.52	11.65	0.05		
6	0.03	1.79	0.52	7.69	0.09		
7	0.42	<u>29.72</u>	0.52	12.51	0.03		
8	0.00	0.19	0.52	10.60	0.17		
9	0.15	10.54	0.52	14.88	0.04		
10	0.00	0.01	0.52	11.61	0.45		
11	0.00	0.00	0.52	5.54	1.04		
12	0.00	0.16	0.52	5.20	0.23		
13	0.03	2.12	0.52	6.50	0.09		
14	0.00	0.02	0.52	3.18	0.58		
15	0.00	0.00	0.52	5.16	1.03		
16	0.00	0.05	0.52	5.61	0.33		
17	0.02	1.15	0.52	3.99	0.13		
18	0.00	0.07	0.52	4.68	0.31		

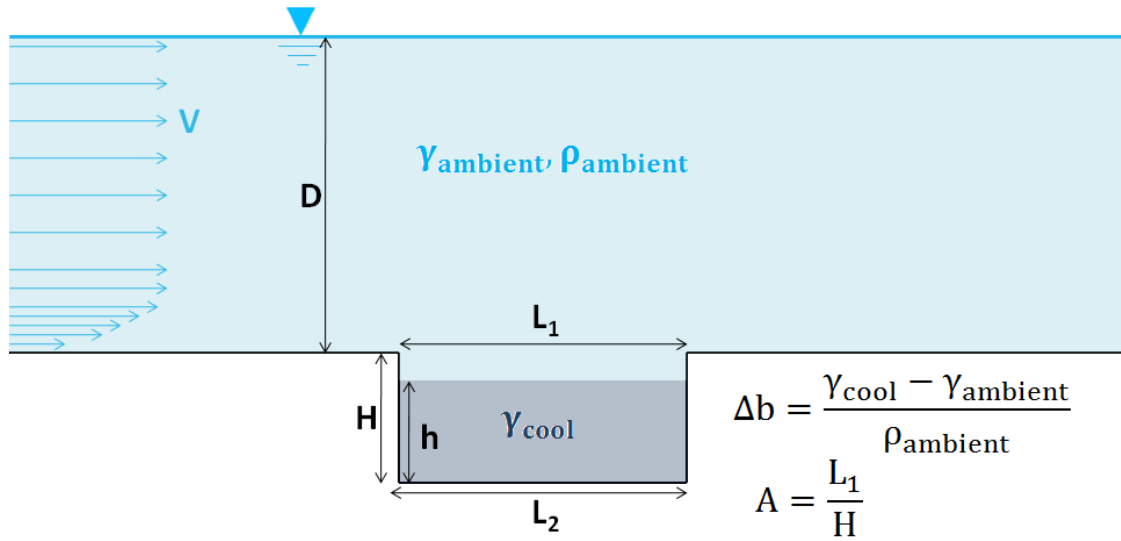


Figure 2.9: Simple conceptual model depicting a streambed cavity with skimming overflow.

2.4.4.2 Cavity Purging by Channel Overflow

While the Richardson number computations described above apply to channel-averaged flow conditions, an alternative conceptualization of thermal stratification incorporates longitudinal variation in channel morphology. A dense fluid partially protected within a recessed cavity from the main channel flow is depicted in Figure 2.9. A fluid of specific weight $\gamma_{ambient}$ and density $\rho_{ambient}$ flows at a free stream velocity V and depth D over a cavity filled with fluid of specific weight γ_{cool} . Geometric parameters are specified as D , the depth of channel flow, H , the height of the cavity, h , the depth of cool water within the cavity, and L_1 and L_2 , cavity length parameters.

Purging of dense fluids from cavities due to skimming channel overflow is a fluid mechanics problem that has been addressed by researchers for a variety of applications

(Briggs et al., 1990; Armfield and Debler, 1993; Debler, 1996; Strang and Fernando, 2004). Debler (1996) showed by experimental data that rectangular cavities ($L_1=L_2$) are rapidly purged of dense liquid for densimetric Froude numbers greater than 1.5-2. Debler and Armfield (1997) applied the principle that the work done to remove dense fluid from the cavity must be equal to the flux of turbulent kinetic energy into the cavity, and developed a non-dimensional equation for the purging rate of dense fluid from the cavity.

Results from these studies were applied to MFJDR data in an attempt to test and explain the DTS measurement results. The cavity could represent any streambed structure containing relatively dense water. For this example, it was likened to an in-stream pool. The depth of the channel upstream of the pool was taken to be D , the depth of the pool below the upstream channel bed was taken to be H , and the length of the pool was taken to be L . It was proposed that ambient stream temperature in the channel was warmer than pool-bottom temperature, causing the specific weight of the pool bottom water γ_{cool} , to be lower than that of the overflowing fluid. The geomorphic or hydraulic likelihood of this scenario was not tested here.

To apply the results of Debler (1996) to this flow situation, the densimetric Froude number was computed for the MFJDR pool "cavity". The Froude number was defined as $Fr = \frac{V}{\sqrt{\Delta b * H}}$, the ratio of free stream velocity (V) to the square root of scaled fluid buoyancy difference $\Delta b = \frac{\gamma_{cool} - \gamma_{ambient}}{\rho_{ambient}}$ multiplied by cavity depth (H). Typical free stream velocity in an MFJDR pool was taken to be $0.1 \frac{m}{s}$, pool depth below upstream channel bed level or "cavity" depth (H) was taken to be 0.75 meters, and the buoyancy difference was taken to be 0.62%, equivalent to the difference between fresh

water at 22°C and at 19°C. These values produce a Froude number of 1.46, a borderline value that suggests the system could barely sustain a cavity filled with water 3°C cooler than ambient. Additionally, as has been discussed above, vertical temperature differences of 3°C magnitude were not detected in the MFJDR system during this study.

To apply the results of Debler and Armfield (1997), the MFJDR variables were used in their equation for cavity purge rate. To simplify the computation, the assumption was made that the depth of dense fluid (h) was steadily equal to half of the cavity height (H), resulting in the equation:

$$Q = \frac{2 * K_{ET} * D * V * Fr^2}{\left(\left(1 + \frac{H}{D}\right) - \frac{H}{2 * D}\right)^2} \quad (2.2)$$

where the purge rate for the whole cavity, Q , is a function of channel depth (D), free stream velocity (V), densimetric Froude number ($Fr = \frac{V}{\sqrt{\Delta b * H}}$), the cavity depth (H), and an efficiency coefficient (K_{ET}), for which Debler and Armfield (1997) proposed some empirical values.

To apply the equation above to the MFJDR system, the following parameter values were selected: $D=1$ meter, $V=0.1$ meter per second, $\Delta b=0.62\%$, based on a 22°C ambient temperature and a 19°C cool temperature, $H=0.75$, $Fr=1.46$, $L_1=8$ meters, $L_2=5$ meters, and $K_{ET}=0.001$, a value which Debler and Armfield (1997) proposed for aspect ratio ($A = \frac{L_1}{H}$) values around 10. Based on those values, Q , the rate at which cool fluid is removed from the cavity, was $2.3 \times 10^{-4} \frac{m^3}{s}$, or $2.8 \times 10^{-5} \frac{m^3}{s}$ per meter of stream length. This value was within the range of groundwater flux rates to the MFJDR estimated by Hopson (1997), based on field measurements of hydraulic gradient and

soil conductivity. This range of flux rates, computed for a location within the Forrest Conservation Area, had an upper bound of $5.1 \times 10^{-4} \frac{m^3}{s}$, per meter of stream length. Even a purge rate computed using only a 1°C temperature difference ($\Delta b=0.22\%$) was within the range of groundwater flux values that Hopson measured. This equivalency between estimated cavity purge rate and field measurements suggests that portions of the MFJDR receive groundwater flux adequate to sustain a cold water “cavity” in the streambed. However, it is important to note that actual flow conditions in the MFJDR may differ significantly from the laboratory conditions upon which the Debler and Armfield (1997) study was based. In particular, the value for K_{ET} is likely to be sensitive to channel and cavity geometry that is not captured by the aspect ratio.

2.5 Discussion

The cold water patches with which Nielsen et al. (1994) and Ebersole et al. (2003) found correlations with fish presence were at least 3°C cooler than ambient stream temperatures. No cold patch measured in the MFJDR during this study exceeded 2.31°C cooler than ambient stream temperature. The present study covered 7.2 kilometers of the MFJDR. It is possible that cold patches with greater temperature differentiation are present in other, unmeasured, portions of the river. However, the results of this study suggest that the MFJDR has a lower density of cold water patches, defined as patches at least 3°C cooler than ambient temperatures, than were observed in some creeks of the Snake River basin Ebersole et al. (2003). The maximum vertical temperature difference (bottom to top of a pool) that was measured in this study was approximately 0.2°C , well

beneath the 3-9°C vertical differences measured by Nielsen et al. (1994).

Differences between this study and those earlier works should be emphasized. This study focused rigorously on the hours of maximum stream temperature for cold patch detection. The other two studies collected temperature measurements throughout the day or throughout the afternoon (12:00 to 18:00). The four-hour averaging procedure employed for subsurface water-fed cold patch detection in this study may have slightly reduced estimates of patch magnitude. However, the most differentiated cold patch identified from that analysis was additionally measured over ten-minute intervals, so an upper bound for subsurface-fed cold patch magnitude was determined.

The results of this study provide an estimate for spatial thermal heterogeneity in the current MFJDR system and provide a baseline against which river restoration planners might make comparison for projects that aim to create thermal refugia in the MFJDR system. The results also provide a context for asking whether historical thermal heterogeneity in the historical MFJDR system was higher.

Torgersen et al. (1995) concluded that fish in the Middle Fork John Day River were responding to cold water patches 1°C - 3°C cooler than habitat within a 10 meter radius. However, other fish behavior studies have focused on temperature differences greater than 3°C. Anecdotal evidence suggests that, during late summer, many MFJDR salmon hold in one of three pools, Pool1 in Oxbow1, Pool2 in Oxbow2, and a pool in Forrest a few hundred meters upstream of Vinegar Creek. These locations were not identified during this study to contain significant cold patches. Two of these locations (Pool2 and the Forrest pool) were located within a few hundred meters upstream of cold creeks, but fish were not observed to be holding closer to creek mouths. Further research

would be needed to assess whether fish respond to spatial temperature differences less than 3°C, such as those observed in the MFJDR system.

Results from the DTS datasets reported here suggest that tributaries are an important source of summertime temperature heterogeneity in the MFJDR. Cold water patches were observed at tributary confluences, and some tributary inflows caused a step-like decrease in the ambient stream temperature, potentially significant for downstream temperature potentials. Given this importance of tributaries in the MFJDR system, the consideration of tributary condition, including the condition of tributary fans and the tributary-mainstem junctions, may be a useful exercise for restoration planning. Most tributaries of the MFJDR flow through forested watersheds and a tributary fan before joining the mainstem. Some tributary fans are highly vegetated, providing stream shading, but also possibly reducing streamflow by evapotranspiration effects. Some tributaries flow through unshaded fans, and some break into multiple smaller stream channels over the fan. At tributary-mainstem junctions, flow conditions are often highly turbulent, facilitating quick mixing of tributary water with the mainstem, but failing to provide spatially sustained cooler temperatures or hydraulic conditions conducive to fish holding. Gravel bars are evident downstream of Granite Boulder Creek and Big Boulder Creek, two of the largest tributaries in the upper mainstem MFJDR, but significant gravel bars are not apparent at other tributary confluences. Large woody debris at tributary-mainstem junctions might have the effect of slowing streamflow or creating pools.

The difference in cold patch magnitude between the MFJDR and the northwestern California creeks reported by Nielsen et al. (1994) or some Snake River basin creeks

reported by Ebersole et al. (2001) and Ebersole et al. (2003) suggests a fundamental difference in processes between these systems. Physical differences between the MFJDR and the California creeks are immediately evident. Pools in the California creeks were located in channel backwaters, were partially separated from the mainstem flow by gravel bars and fed by tributaries, or had long pool residence times of 2.5 to 9.3 hours, as compared to residence times of <0.3 hours in the MFJDR pools that were evaluated. Differences between the MFJDR and the Snake River basin streams were not pinpointed as part of this research, but likely relate to stream size and morphology.

Results of Richardson number and cavity purging computations supported the lack of observed stratified pools seen in the temperature data collected during this study. The combination of hydraulic conditions (flow volume, velocity, depth) and thermal conditions (cool tributary/ groundwater/ hyporheic water inflow rates and temperature) are predicted to be non-conductive, or barely conductive, to vertical temperature stratification. This result is consistent with the finding of Torgersen et al. (1999) that deep pools in the MFJDR were not thermally stratified. The lack of thermal stratification in the MFJDR is significant for FLIR and TIR image data processing, suggesting that the surface temperatures measured by those images are consistent with temperatures throughout the water column. The estimation of cavity purging rate, possibly applicable to transport from a cool water pool in the MFJDR, resulted in a purge rate lower than available estimates of groundwater flux to the MFJDR, suggesting that portions of the MFJDR receive groundwater influx adequate to sustain a cold water “cavity” in the streambed. However, it is possible that the experimental conditions upon which the cavity purge rate equation was based do not match natural flow conditions, resulting in

an underestimate of actual stream mixing processes.

There is evidence to suggest that constructing a deep, cool, backwater pool, similar to those encountered by Nielsen et al. (1994), may be possible within the Oxbow1 reach. From July 30-August 11, 2011, temperature measurements were made within an off-channel mine tailings pond that was separated from the mainstem by a 2-5 meter thick man-made gravel bar. The diurnal temperature signal in the pond was significantly dampened compared to the MFJDR temperature signal, fluctuating just 2°C on a diurnal cycle, and remaining 4°C below the ambient stream temperature during the hottest times of the day (Figure 2.10). This data suggests that the temperature conditions for a cooler backwater area may be present at this location, if the pool were connected to the channel at its downstream end. However, the pond was observed to be covered with a layer of aquatic plant material during the summer months, and it is unknown whether the dissolved oxygen conditions within the pond would be suitable for fish.

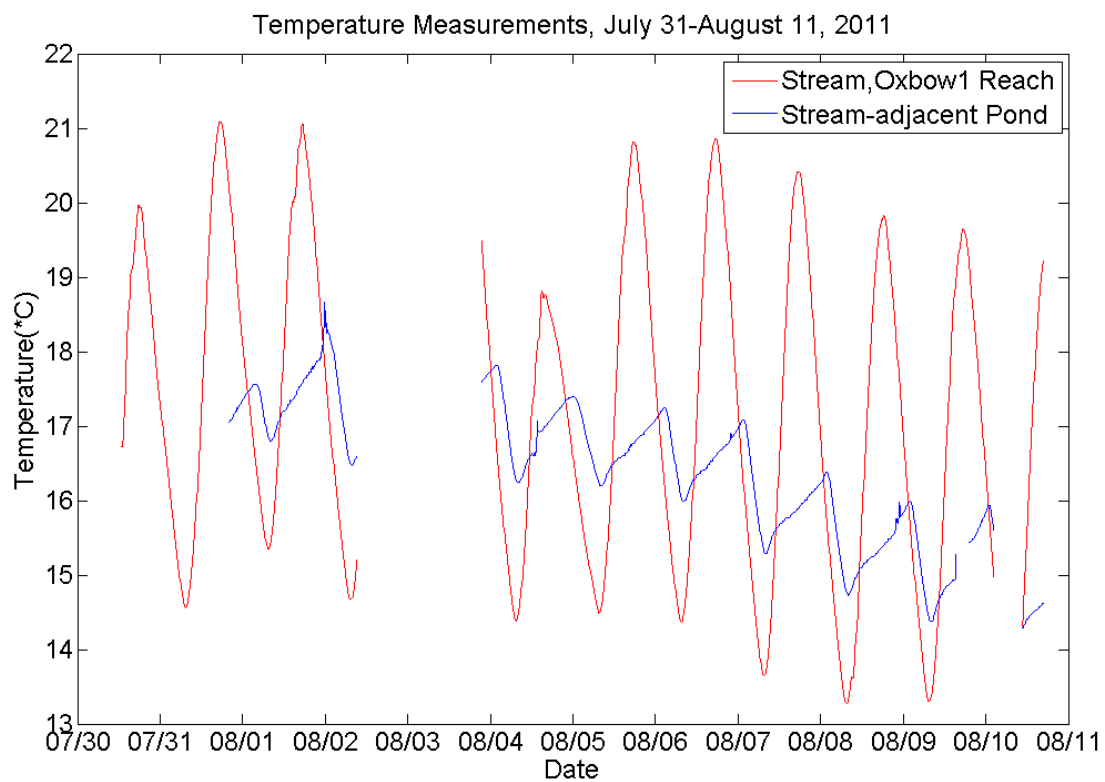


Figure 2.10: A pond adjacent to the MFJDR Oxbow1 reach has a dampened diurnal temperature signal, as compared to the mainstem temperature.

With regard to constructed features that provide thermal heterogeneity, separation from mainstem flow conditions seems to be key to cool patch development (Nielsen et al., 1994). In this study, the slowest predicted channel-averaged streamflow velocity in the mainstem MFJDR (in Pool2) was $0.03 \frac{m}{s}$. The slowest measured streamflow velocities (in Pool1) were $0.03 \frac{m}{s}$ - $0.19 \frac{m}{s}$. Constructed features would likely need to create flow conditions with velocities as slow or slower than these values.

The DTS measurements reported in this chapter allowed for a comprehensive survey for cold patches over 7.2 kilometers of the Middle Fork John Day River. The results suggest that cold patches, where they exist, are not more than 2.31°C cooler than ambient stream temperatures, suggesting that the habitat benefit from existing cold patches is minimal. Further research would be needed to assess whether historical thermal conditions were different, and, if so, whether restoration options are feasible.

Chapter 3 – Interpretation of Remotely Sensed Temperature Datasets

3.1 Introduction

Stream temperature has been identified as an important fish habitat variable (Brett, 1956; Kaya et al., 1977; Baltz et al., 1987; Nielsen et al., 1994; Torgersen et al., 1999; Ebersole et al., 2003). Measurement of stream temperature has traditionally been accomplished by point temperature measurements (Baltz et al., 1987; Nielsen et al., 1994; Ebersole et al., 2003), continuous point temperature loggers (Sinokrot and Stefan, 1993; Johnson and Jones, 2000; Bayley and Li, 2008), and more recently, airborne remote sensing techniques such as Forward-Looking Infrared Radar (FLIR) (Torgersen et al., 1995; Loheide and Gorelick, 2006) or Thermal Infrared Radiometry (TIR) (Torgersen et al., 2001).

TIR and FLIR datasets have been used for regulatory (TDML) development (WSI, 2005; DEQ, 2010), for large-scale stream temperature monitoring (Faux et al., 2001), for restoration planning (Bouwes, 2005), and for fish habitat research (Torgersen, 1997; Torgersen et al., 1999, 2007). An example of FLIR datasets collected on two forks of the John Day River (the Middle Fork and North Fork) is displayed in Figure 3.1.

Airborne remotely sensed temperature datasets represent “snapshot” temperature measurements; an airborne survey can cover 50 kilometers of stream distance in

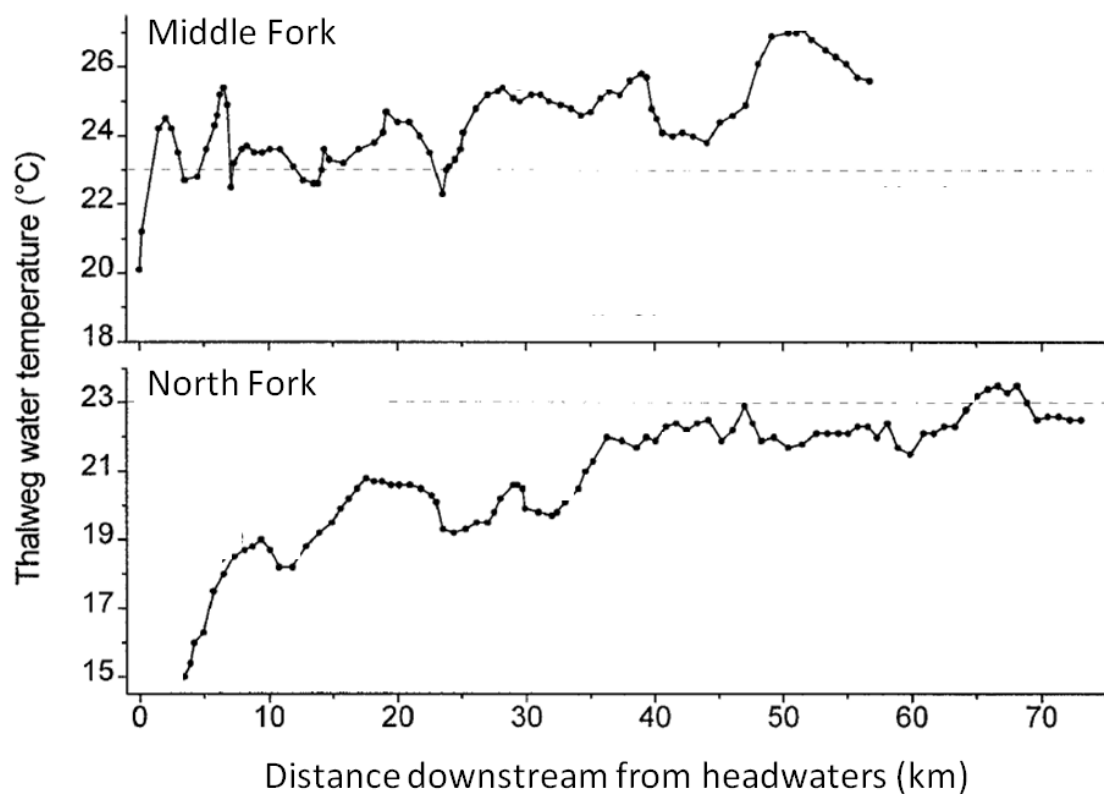


Figure 3.1: Longitudinal stream temperature in the Middle Fork John Day River (top) and the North Fork John Day River (bottom), as measured by Forward-Looking Infrared Radar during 14:30-16:00 August 5 and 8, 1994 (Torgersen et al., 1999)

under an hour. Because stream temperature maximums are of greatest interest for many fish habitat and temperature monitoring programs, most FLIR and TIR temperature surveys are conducted during the summertime and during the afternoon period when stream temperatures peak, generally between 11:00 and 18:00.

The temporal limitation of FLIR and TIR datasets is typically addressed by continuously-recording point temperature loggers deployed before and during the airborne survey (Torgersen et al., 2001). However, these loggers lack the continuous spatial data coverage for adequate characterization of spatially and temporally varying temperature patterns.

Distributed Temperature Sensing (DTS), a relatively new temperature measurement technology for hydrologic applications (Selker et al., 2006b), can provide high-resolution stream temperature information in both the spatial and temporal domains. DTS employs fiber optic technology, measuring temperature along a fiber optic cable by the backscattering of laser light pulses. Commonly-available DTS systems can measure temperature to a resolution of 0.1°C at 1 meter spatial intervals and 1 minute time intervals, over a cable length of 5 kilometers (van de Giesen et al., 2012).

This chapter describes an anomalous stream temperature pattern observed in FLIR and TIR datasets collected in the Middle Fork John Day River (MFJDR) in northeastern Oregon. Co-located with that anomalous reach, a DTS dataset collected between August 12-25, 2011 allowed for a close examination of spatial and temporal stream temperature variation. An analysis diagnosed the observed temperature anomaly with an unexpected cause, and the results have significance for interpretation of FLIR and TIR datasets in this and other fluvial systems.

3.2 Anomaly in TIR and FLIR datasets

Figure 3.2 depicts four TIR or FLIR datasets collected in the MFJDR. All measurements were collected during the month of August, between the hours of 11:00 and 17:00. Specific collection times, where available, are displayed in the figure. The red and green lines in those graphs highlight an area of decreasing stream temperature. The red line in each graph indicates the upstream end of the reach of interest, Oxbow2, and approximately corresponds to point *2 in Figures reffig:Oxbow2day - reffig:Oxbow2night. The green line approximately corresponds to point *1 in those figures. Two additional FLIR datasets, collected on August 9, 1995 and August 26, 1996, are not depicted here but also exhibited temperature decreases of similar magnitude at the indicated location. The reach in which the decrease is located will be referred to as “Oxbow2”.

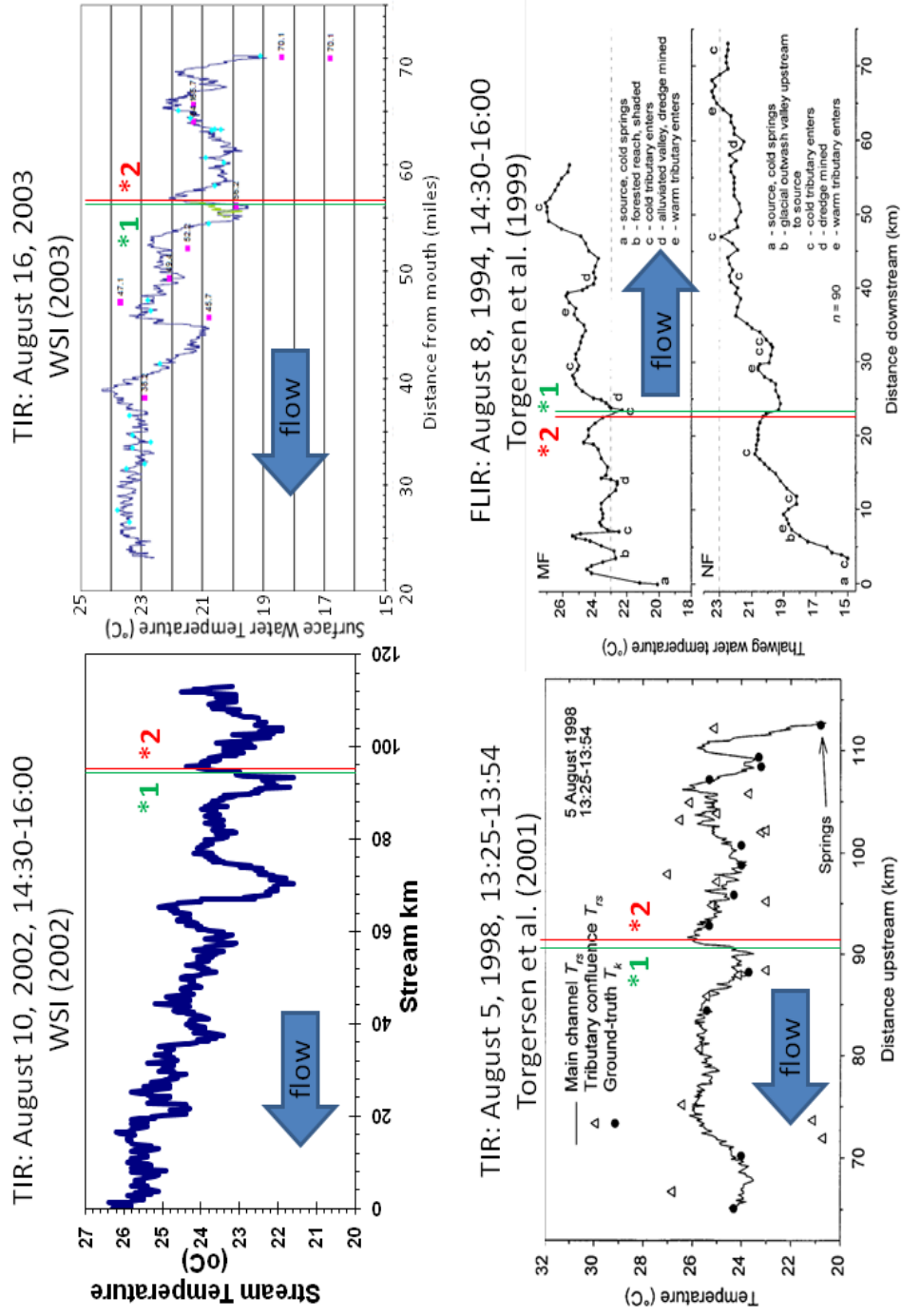


Figure 3.2: Thermal Infrared Radiometry (TIR) and Forward-Looking Infrared Radiometry (FLIR) datasets collected on the Middle Fork John Day River. The red line in each graph indicates the upstream end of the reach of interest, Oxbow2, and corresponds to point *2 in Figures reffig:Oxbow2day - reffig:Oxbow2night.

The Oxbow2 reach is near the upstream end of a wide, alluvial valley. Two tributaries, Butte Creek and Granite Boulder Creek, enter the mainstem within the reach, and the reach intercepts the alluvial fans of both creeks. Just downstream of the first tributary, Butte Creek, approximately 25% of the flow is lost to a side channel (the South Channel). This flow is not regained until downstream of the Oxbow2 reach. The upstream end of the reach has a riffle-run morphology typical for the Middle Fork John Day River. The downstream end of the reach is a man-made channel, remnant from historic mining operations, that is both deep and slow-flowing.

Initial observation of these channel characteristics suggested some hypotheses for the cause of the temperature decrease in Oxbow2. First, subsurface inflows (groundwater or hyporheic water) are likely suspects for causing longitudinal stream temperature decreases, particularly where streams intercept alluvial fans. Second, the presence of tributaries within the reach suggested that some or all of the decrease might be attributable to cool tributary inflows. Third, decreases in stream temperature down a reach might be caused by a negative net heat flux, such as might result from increased shading, evaporation, or differences in bed conduction. The loss of 25% of flow from the reach at the side channel is unusual, but flow losses typically increase daytime stream temperature, rather than decrease it. Fourth, advection in fluvial systems may influence stream temperature patterns, and the observed differences in channel morphology between the upstream and downstream portions of Oxbow2 might influence temperature.

3.3 Methods

To test the hypotheses proposed to cause the observed temperature decrease, three forms of data were collected. First, a DTS stream temperature dataset was collected in the Oxbow2 reach between August 12 and August 25, 2011. The dataset, which had 1-meter spatial resolution and ten-minute temporal resolution, provided higher spatial resolution and better temporal data coverage than the TIR and FLIR datasets. Second, synoptic discharge measurements were made over the Oxbow2 reach and the upstream reach (“Oxbow3”) to test for flow increases due to subsurface inflows on the reach. Third, visual observations of reach shading and bed material type both within Oxbow2 and upstream were made in an attempt to detect possible causes of longitudinal heat flux variation. Fourth, a simple temperature model was constructed for the Oxbow2 reach, allowing assessment of advection and heat flux effects on stream temperature.

3.4 Results

3.4.1 Comparison of TIR and FLIR with DTS

One day (August 23-24, 2011) from the DTS dataset collected on the Oxbow2 reach (point *2 to point *3) is displayed in Figures 3.3 - 3.4. The immediately upstream Oxbow3 reach (point *1 to point *2) is additionally displayed.

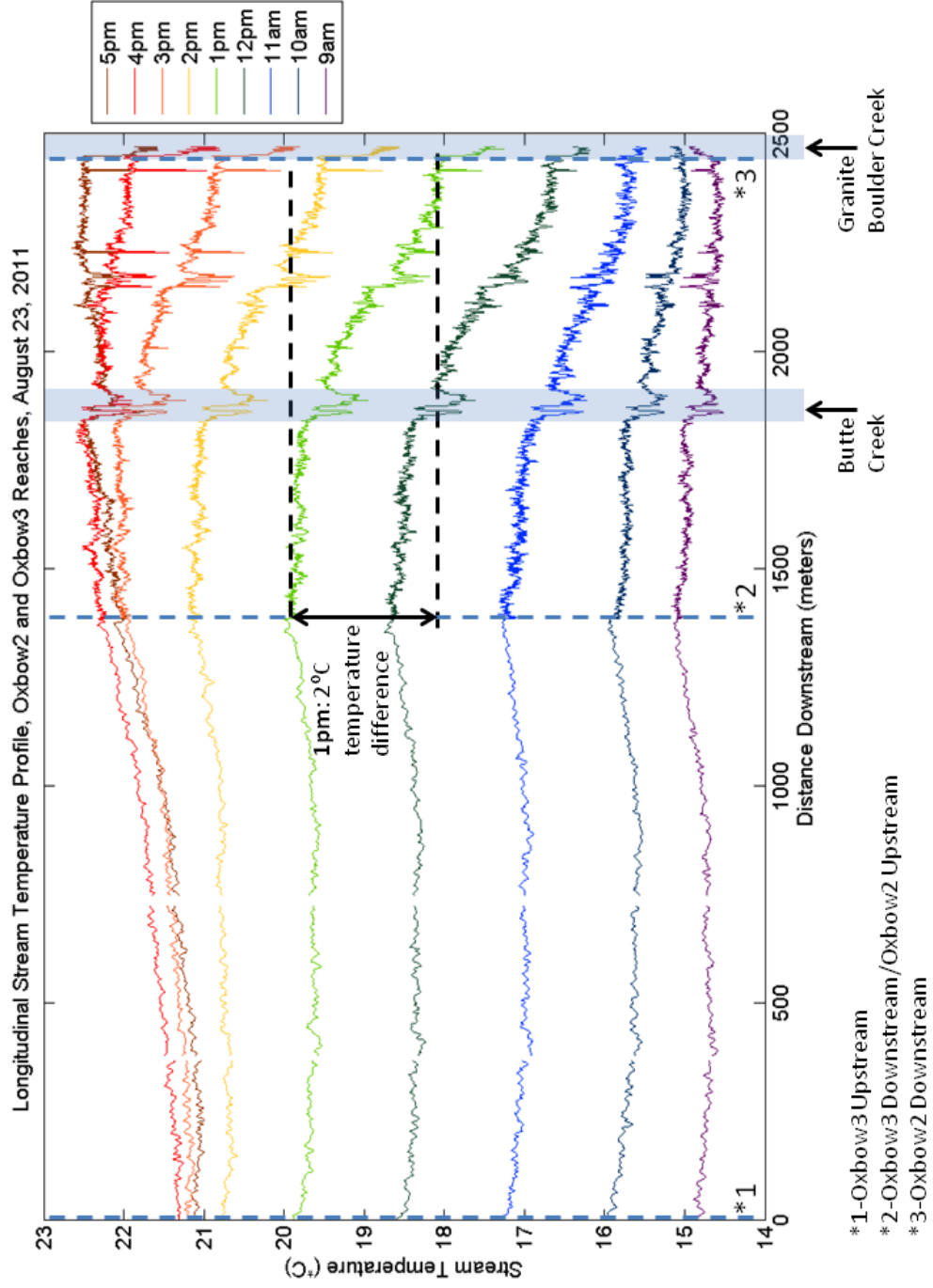


Figure 3.3: Daytime longitudinal stream temperature profiles of the Oxbow3 and Oxbow2 reaches on August 23, 2011. Each profile represents a 10-minute average centered on the hours 9:00-17:00.

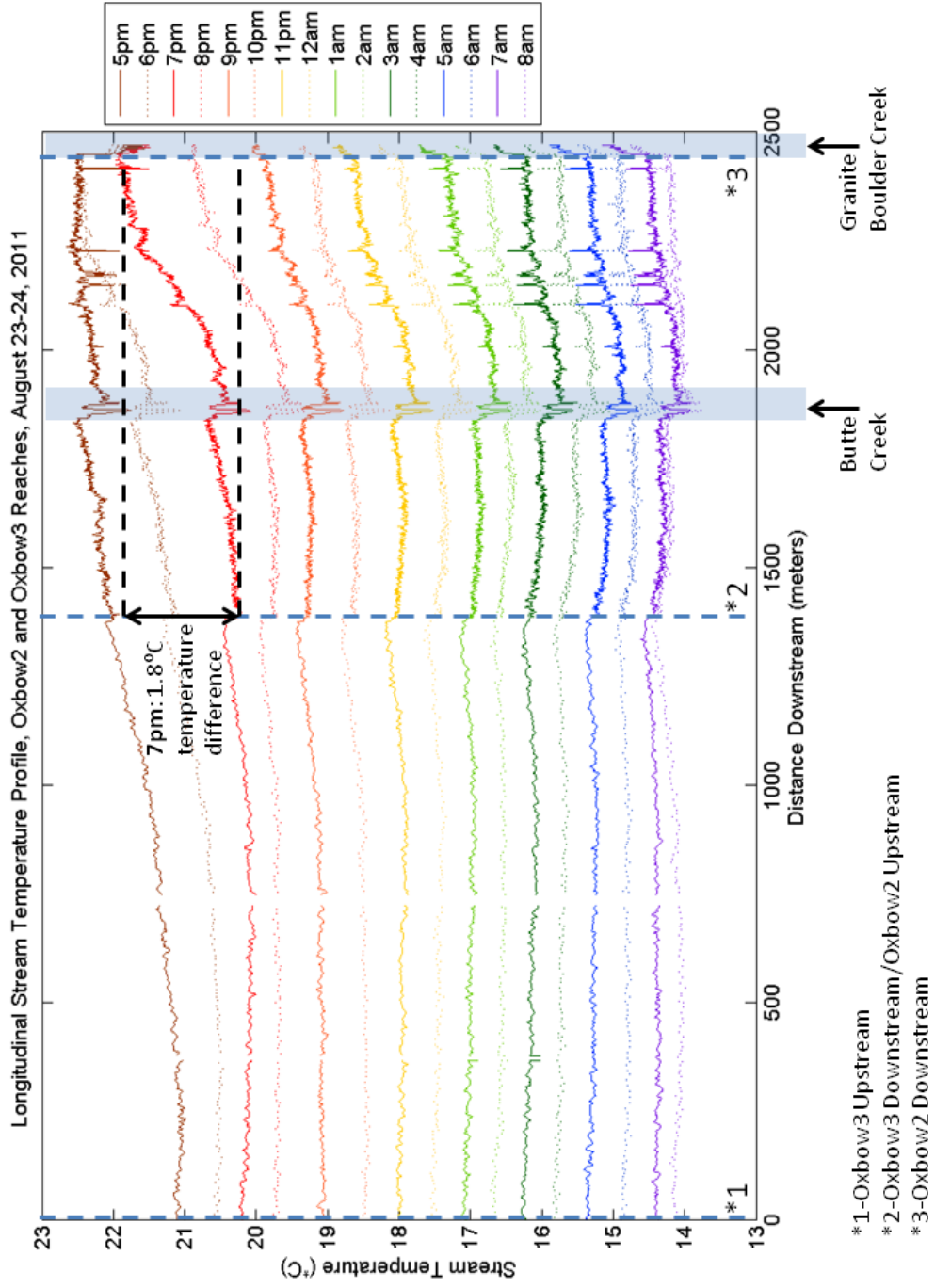


Figure 3.4: Nighttime longitudinal stream temperature profiles of the Oxbow3 and Oxbow2 reaches on August 23-24, 2011. Each profile represents a 10-minute average centered on the hours 17:00-8:00.

As can be seen in the figures, stream temperature on this day ranged between 14°C and 23°C. Furthermore, the shape of the diurnal temperature profiles varied throughout the day and night. At 12:00 and 13:00, stream temperature at the downstream end of Oxbow2 (point *3) was 2°C cooler than that at the upstream end of the reach (point *2). This longitudinal decrease corresponded to the location of the decrease observed in the TIR and FLIR datasets. The DTS dataset provided some additional temporal information about the decrease. It was transient, developing in the morning to early afternoon (9:00-13:00), and slowly dissipating throughout the later afternoon. By 17:00, temperatures at the two ends of the reach were about equal. In the early evening, temperature at the upstream end of Oxbow2 dropped more quickly than that at its downstream end. By 19:00, the downstream end was 1.8°C warmer than the upstream end.

The temperature profile behavior described above was observed on every day of the monitoring period August 12-25, 2011. Figure 3.5 demonstrates that the diurnal stream temperature signal at the downstream end of the Oxbow2 reach (point *3 in Figures 3.3 - 3.4) lagged the signal at its upstream end (point *2). The magnitudes of the two signals are approximately equal. A minimization of square differences between the two curves revealed that the time lag was 70 minutes.

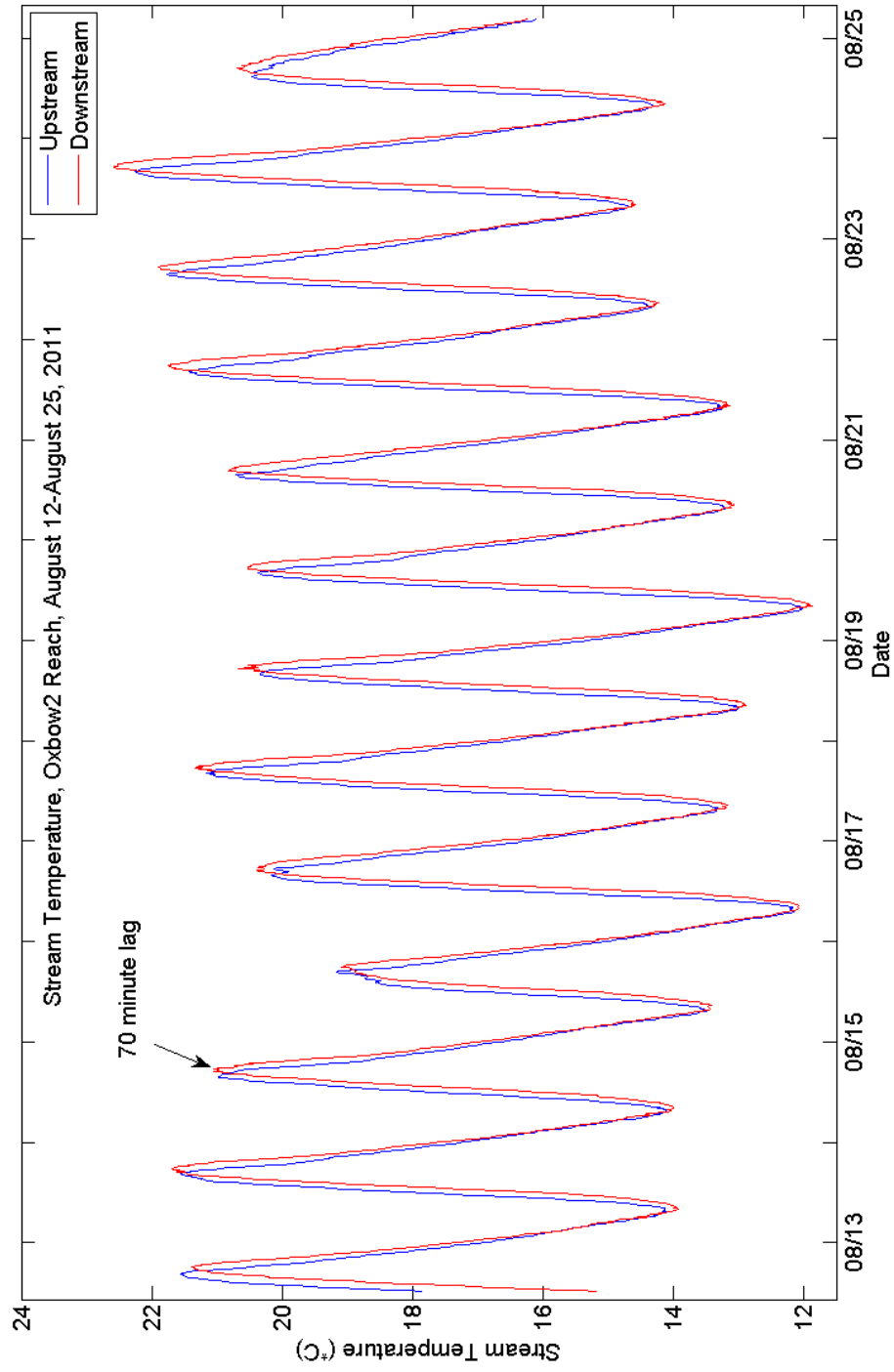


Figure 3.5: Diurnal stream temperature signal at the upstream and downstream ends of the Oxbow2 reach, August 12-25, 2011.

During the DTS monitoring period, the temperature of shallow groundwater in the vicinity of the Oxbow2 reach was measured at location 44°38'41.96"N, 118°39'33.81"W. At a depth of two meters below ground surface, the groundwater temperature ranged between 9.6°C and 9.7°C. Because the shallow groundwater temperature was well below the nighttime low stream temperatures in the Oxbow2 reach (approximately 12°C), groundwater inflows to the reach would be expected to lower stream temperature at all times of day.

Two features of the DTS dataset provided evidence that groundwater inflows were not the cause of the upstream-downstream temperature difference observed in Oxbow2. First, Figure 3.5 reveals that the downstream signal is not offset lower than the upstream signal, as would be expected if cool groundwater inflows, which lower both daytime and nighttime temperatures, were prominent along the reach. Second, the highest magnitude of upstream-downstream difference in temperature occurred at approximately 13:00 each day during the monitoring period, while the highest stream temperatures occurred around 16:00. If groundwater inflows did cause the observed difference, then the largest difference would be expected during the hour of warmest stream temperature, when groundwater temperature and stream temperature were most differentiated.

Although the DTS dataset provided preliminary evidence against groundwater inflows causing the observed temperature decrease, synoptic discharge measurements were made along the Oxbow2 and Oxbow3 reaches to test for the presence of subsurface inflows.

3.4.2 Synoptic Discharge Measurements

To test whether subsurface inflows might be augmenting flow in the Oxbow2 reach, synoptic discharge measurements were made on August 1, 13, and 24, 2011. Because of a cold, wet summer, discharge levels and groundwater levels were relatively high during the month of August, and especially on August 1. All measurements were made with a Marsh-McBirney flow meter. Figure 3.6 displays measurement locations and Table 3.1 displays measurement results. Over one section of Oxbow2 (point B to point D) the flow gain down the reach exceeded the expected difference accuracy of ($\pm 10\%$) (USGS, 2010), an indicator that diffuse inflows may be significant in this segment. However, an irrigation ditch (Figure 3.6) was inadvertently omitted from the synoptic measurement, and much of the gain is expected to be due to this unmeasured inflow. Additionally, even if diffuse flows were significant, this section corresponded to the upstream end of Oxbow2, not to the downstream end where most of the 13:00 upstream-downstream temperature difference was observed.



Figure 3.6: Locations of synoptic discharge measurements made on the Oxbow2 and Oxbow3 reaches in August 2011. The Oxbow2 reach extends from point A to point B, and the Oxbow3 reach extends from point B to point F.

Table 3.1: Synoptic discharge measurements made over the Oxbow2 and Oxbow3 reaches in August 2011. Measurement locations are indicated in Figure 3.6

Date	A		B		C		D		E		F		
	Oxbow3 Upstream	Oxbow2 Upstream	Oxbow3 Downstream/ Oxbow2 Upstream	Percent Gain: (B-A)/A	Tributary: Butte Creek	Oxbow2 Midstream	Oxbow2 Upstream	Oxbow2 Downstream	Oxbow2 Side Channel Upstream	Oxbow2 Side Channel Downstream	Percent Gain: (C+D-B)/B	Oxbow2 Side Channel Downstream	Percent Gain: (F-E)/E
	(m ³ /s)		%		(m ³ /s)		(m ³ /s)		(m ³ /s)		%		
8/1/2011													
9:30-12:00	n.m.	0.852	n/a		0.043	0.967	0.673	0.687	0.673	0.687	0.19	0.687	0.02
8/13/2011													
14:00-15:00	0.671	0.688	0.02		0.035 (est.)	0.709	0.521	0.514	0.521	0.514	0.08	0.514	-0.01
8/24/2011													
13:00-13:30	0.628	0.627	0.00		0.030 (est.)	0.627	0.470	0.467	0.470	0.467	0.05	0.467	-0.01

n.m. - not measured
n/a - not applicable
est. - estimated

South Channel
divergence, 25% of flow
leaves the Oxbow2 Reach

The Granite Boulder Creek alluvial fan borders the Oxbow2 reach on its northern bank. Tributary alluvial fans typically contain coarse sediments and have high groundwater levels fed by the adjacent tributary. A reasonable conceptual model consists of the tributary losing flow to its alluvial fan aquifer, which subsequently loses water to the hydraulic lowest point, the mainstem channel. To test whether Granite Boulder Creek might fit this conceptual model, the tributary discharge was measured at the top (44°39'23.91"N, 118°38'50.55"W) and at the bottom of the alluvial fan on August 1, 2011. A slight flow gain of +0.6% was detected over this reach. This result indicates that Granite Boulder Creek, at least on that date, was not losing groundwater to its alluvial fan at a significant rate, suggesting that flow from the alluvial fan aquifer to the Oxbow2 reach was low.

3.4.3 Visual Channel Condition Observations

Visual observation of channel conditions and streamside vegetation were made in the Oxbow2 and Oxbow3 reaches. The upstream end of Oxbow3 flowed through an alluvial canyon and had slightly taller streamside vegetation than downstream areas. Otherwise, no longitudinal differences in stream shading were noted. Oxbow3 and the upstream end of Oxbow2 had riffle-run morphology typical for the MFJDR. Streambed in these areas was cobble. The downstream end of Oxbow2 was a man-made channel, remnant from historic mining operations, that was both deep and slow-flowing. The streambed in this portion of the reach was largely silt-covered.

Visual observations suggested no obvious differences in solar heat flux between

the downstream and upstream ends of Oxbow2. On the other hand, differences in bed material between these two areas had the potential to cause differing streambed heat flux terms. Additionally, the observation of deep, slowly-flowing water at the downstream end of Oxbow2 suggested advection effects on temperature.

The influence of heat flux variation or advection velocity on the stream temperature patterns observed in the Oxbow2 reach were assessed by use of a simple stream temperature model.

3.4.4 Simple Stream Temperature Model

The lagged temperature behavior of the downstream end of the Oxbow2 reach, relative to its upstream end, suggested that streamflow velocity might play a role in the observed temperature profile behavior. Deep, slowly-flowing pools were observed in the midstream to downstream portion of the Oxbow2 reach. Those pools were part of a manmade channel remnant from mining operations of the 1940's.

To examine the possibility that advection velocity and flow depth largely explained the observed temperature pattern, a simple stream temperature model was constructed. As the upstream boundary condition, the DTS-measured stream temperature at the upstream end of Oxbow2 was used. No heat fluxes were added to the water in the model reach, and water moved in the model reach at the average advection velocity, which was computed by use of a HEC-RAS hydraulics model. Flow conditions on August 24, 2011 ($0.63 \frac{m^3}{s}$ measured at the upstream end of Oxbow2, and $0.47 \frac{m^3}{s}$ measured in the North Channel, just downstream of the South Channel divergence), thirty-

six channel cross sections defined by a LiDAR DEM (WSI, 2008), and water depth field estimates made in August 2011 were inputs to the model. Details of the HEC-RAS model are discussed in *Appendix C*. The uncertainty of the modeled velocities were not computed.

The performance of the simple stream temperature model was evaluated by assessing the correspondence between the modeled stream temperature and the DTS-measured stream temperature. Figure 3.7 depicts the model results superimposed on the stream temperature measurements. Average advection velocity, as computed by the HEC-RAS model, is plotted below the model output graph. Sharp transitions between low-velocity cross sections and high-velocity cross sections indicate that a greater number of model cross sections would have been beneficial. Despite this shortcoming, the model captures the 2°C longitudinal stream temperature decrease observed in the 12:00 and 13:00 DTS stream temperature traces.

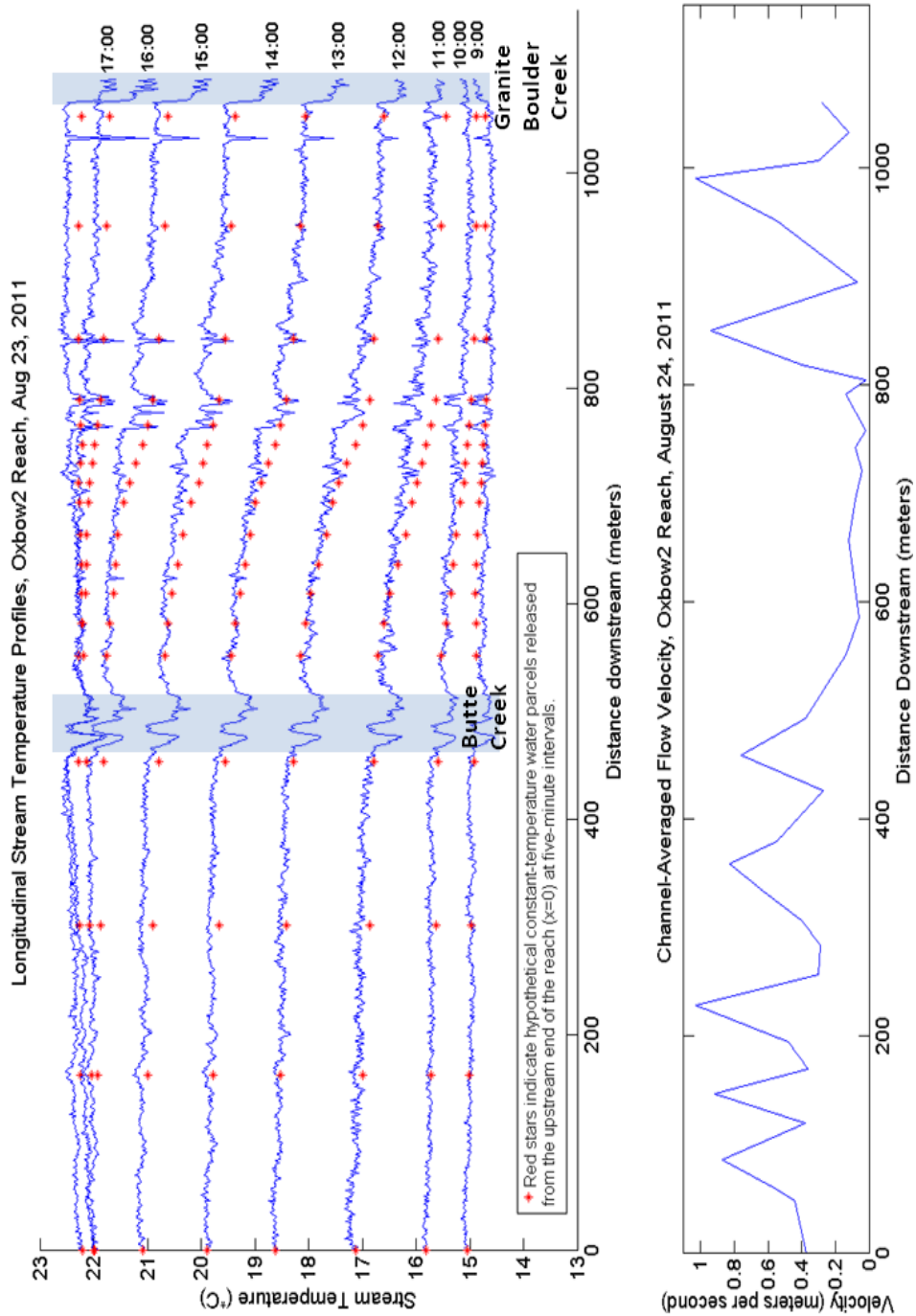


Figure 3.7: The upper graph depicts the Oxbow2 simple stream temperature model results (red dots) overlain on the Oxbow2 DTS stream temperature measurements. Average flow velocity is depicted in the lower graph. High-velocity areas correspond to riffles.

An alternate way of conceiving this simple stream temperature model is to consider a hypothetical experiment. The experiment entails releasing imaginary parcels of water at five-minute intervals from the upstream end of the Oxbow2 reach. As a rule, each parcel retains the temperature it had at the moment of its release and floats downstream at the average flow velocity. Because the temperature of each imaginary parcel is constant as it floats down the reach, it is effectively exposed to no heat fluxes or groundwater inflows within the reach. Each parcel spends one hour and twenty-five minutes within the reach. If the parcel temperatures match the temperature of the stream water immediately surrounding them (i.e. modeled temperature matches measured temperature), then evidence exists that the stream water and the imaginary parcels may have been exposed to similar thermal influences (i.e. an upstream boundary condition with an absence of heat flux or groundwater inflows).

The simple stream temperature model (or imaginary water parcels) replicated the measured stream temperature profiles at 12:00 and 13:00, suggesting that the 2°C stream temperature decrease observed at this time of day might have been the result of flow velocities over the reach. The ability of the model to reproduce this temperature decrease without the inclusion of spatially-varying heat fluxes or groundwater inflows suggests that these factors did not cause the observed decrease. The presence of Butte Creek within the reach also influenced mainstem temperature, suppressing downstream temperatures slightly during most hours of the day.

An advection and depth-related process was proposed to cause the longitudinal temperature decrease that peaked at 12:00 and 13:00. Over the downstream half of Oxbow2, the temperature impact of heat fluxes to the deep pools was dampened by a

lower surface area to volume ratio. The relatively shallow water at the upstream end of Oxbow2 heated more quickly than the deep water downstream. In the morning, the deep pools at the downstream end of Oxbow2 warmed not because of solar heat fluxes (at that time of day, the cumulative heat flux received per unit volume of water was small), but rather because of warmer water advecting into the pools from upstream areas. That advection process explained the correspondence between longitudinal stream temperature and the simple stream temperature model in the morning and early afternoon hours. As the afternoon progressed, the cumulative impact of positive solar heat fluxes began to overcome the thermal inertia of the deep pools, and to increase pool temperatures. Meanwhile, the solar maximum was passed, and temperature in the shallow upstream areas stopped rising. An equalizing of upstream and downstream temperatures occurred around 17:00 on August 23.

3.5 Conclusions

The results of DTS dataset analysis and synoptic discharge measurements described in this chapter indicate that the temperature decrease observed along the Oxbow2 reach in the MFJDR airborne remotely sensed temperature datasets was unlikely to be due to groundwater inflows. Rather, it appeared that the decrease was an early-afternoon phenomenon caused by slow flow velocities in a deep, pool-filled reach. Tributary inflows from Butte Creek and Granite Boulder Creek also contributed to the observed decrease.

These findings indicate that the time of day of TIR and FLIR dataset collection is important. Like the blind men describing an elephant, spatially and temporally limited

stream temperature measurements sometimes fail to capture the full picture of stream temperature dynamics. An understanding that deep, slow-moving sections of stream can exhibit lagged temperature behavior and that temperature patterns can vary temporally is helpful for accurate interpretation of TIR and FLIR river temperature datasets.

Chapter 4 – Data Artifacts in DTS Stream Temperature Measurements

4.1 Introduction

Distributed Temperature Sensing (DTS) is a relatively new temperature measurement technique for hydrologic sensing applications (Selker et al., 2006b). It employs fiber optic technology to make spatially and temporally continuous temperature measurements at distance intervals as narrowly spaced as 0.25 meters and time intervals as small as one second. Selker et al. (2006b) explored uses of the technology in a variety of hydrologic systems, including fluvial, lacustrine, glacial, and manmade.

For stream temperature applications, DTS has been deployed in the Maisbich, a first-order stream in Luxembourg (Selker et al., 2006a), Allequash Creek in northern Wisconsin (Lowry et al., 2007), a forested stream in the H.J. Andrews Experimental Forest in Oregon (Roth et al., 2010), the Walla Walla River in northeastern Oregon (Gryczkowski, awaiting publication), and select reaches of the Middle Fork John Day River (MFJDR) in northeastern Oregon (Huff, 2009; Arik, 2011).

The spatial continuity of DTS is based on use of fiber optic cable as the temperature sensor. In theory, the temperature of the cable equilibrates with the temperature of the medium with which it is in contact, allowing for thermal sensing of the medium. In practice, temperature measurement may be biased because equilibration of the cable temperature with the medium of interest is prevented by external heat fluxes to the cable.

Nielson et al. (2010) investigated the biasing of DTS water temperature measurements by the solar heating of a submersed fiber optic cable. Krause et al. (2012) investigated temperature patterns of streambed sediments and found that measurement accuracy was greatly improved by full burial of the fiber optic cable within the sediment. Without burial, cable contact with turbulent water would have introduced an external heat flux that would have reduced the quality of sediment temperature measurements.

In the summers of 2009 to 2011, fifteen DTS stream temperature datasets were collected on six 1-3 kilometer-long reaches of the MFJDR. The present study draws from experience gained during those deployments to explore techniques and challenges of DTS deployment in streams. Two types of potential data artifacts in stream temperature DTS measurements are discussed: streambed influence on DTS measurements and data artifacts due to solar radiative heating of the fiber optic cable.

4.2 DTS Deployment in Fluvial Systems

DTS employs the principle that the back scattered light within an optical fiber has a temperature-dependent component. A pulse of laser light directed down a glass optical fiber weakens with distance, due to interactions with the glass. These interactions result in the backscattering of a portion of the incident light. The backscattered signal consists of a spectrum of wavelengths, with certain wavelength bands arriving at greater intensities than others. Two sets of these bands, the Stokes and anti-Stokes Brillouin bands and the Stokes and anti-Stokes Raman bands, can be separately used to calculate temperature. Because it provides superior performance for cables shorter than 10 kilometers in

length, most DTS systems marketed for environmental sensing applications are based on the Raman band data (Selker et al., 2006b; Tyler et al., 2009), with the ratio of the intensity of the anti-Stokes Raman band to that of the Stokes Raman band exponentially related to fiber temperature.

Stream temperature typically varies subtly in the spatial dimension, so DTS deployments in stream settings require high accuracy. DTS data accuracy is positively related to length of measurement time, with integration of the backscatter data from more laser pulses allowing for higher-accuracy statistical representation of cable temperature. For Raman-based instruments, measurement error ($^{\circ}\text{C}$) is proportional to cable length, spatial resolution, and length of measurement time as follows

$$E \propto \sqrt{\frac{D * N}{T}} \quad (4.1)$$

where the error (E) is proportional to linear cable distance from the DTS instrument (D), the number of resolved spatial intervals over that distance (N), and the time length over which the measurement is integrated (T) (Selker et al., 2006b).

Temperature patterns of interest in rivers occur on a variety of scales. Because deployment of fiber optic cable in rivers is typically labor-intensive, and because data accuracy is dependent on cable length, feasible distances for stream DTS installations are typically four kilometers or less. Maximum fiber optic cable length and minimum measurement spatial resolution are also subject to certain DTS instrument constraints. A researcher selecting a cable length, spatial resolution, and integration time for a measurement must balance data precision needs with the instrument capability, the variation

in time and space of the thermal system being measured, and the feasibility of the cable installation.

Cable for river installations may be exposed to high-velocity flow, moving rocks, and human/animal disturbance. As a result, the cable must be durable, and stainless steel is often used as the structurally protective layer. This layer imposes a minimum feasible cable weight and reel size. For a 2000-meter cable reel, a weight of 25 kilograms and a reel diameter of 0.5 meter is minimum, with 40 kilograms and 0.75 meters more typical. Larger, heavier cable reels pose some challenges for maneuverability, although use of a boat or pontoon can facilitate installation under most conditions. High flow velocity, shallow or deep water, and presence of in-stream obstructions can all pose a challenge for cable installation, and a well-designed manual or boat-mounted deployment system is crucial for success.

DTS data must be calibrated to at least three independent temperature measurements per section of cable in order to accurately compute temperature from the raw Stokes/ anti-Stokes backscatter data. Accuracy of the calibrated dataset is related to the accuracy of these independent measurements. Instrument precision and the uniformity of temperature conditions at each reference measurement location are key for ensuring absolute accuracy of DTS measurements. For summertime stream installations, it is recommended that one independent measurement be made within a 0°C ice bath. The large temperature difference between ice bath and stream provides a high-quality correction factor for temperature-varying data error. At least two independent temperature measurements should be made within the stream itself. Choosing well-mixed and shaded stream locations for these measurements can improve their accuracy. Co-locating each

measurement with 15-50 meters of coiled cable also improves calibration quality. Calibration techniques and the biases they address are discussed at length in other work (Smolen and van der Spek, 2003; Tyler et al., 2009; Huff, 2009; Arik, 2011; van de Giesen et al., 2012; Hausner et al., 2011).

Post-calibration, DTS data often requires a quality control review. Measurement accuracy can be assessed by comparison of the data with the independently measured temperatures. To identify areas where cable misplacement may have caused measurement artifacts, inspection for anomalous datapoints and review of cable placement field notes is beneficial. For stream temperature datasets, any location where the cable contacts air, rather than water, should be flagged. Riffles, shallow water, and cross-stream obstructions are often associated with cable exposure to air, so field documentation of stream conditions can assist in the quality control process. Additionally, shallow water increases exposure of the cable to more intense solar radiation, possibly biasing DTS measurements higher than the surrounding water temperature (Nielson et al., 2010). However, because water temperature in shallow areas also may increase due to higher insolation per unit volume, the biasing effect of direct cable exposure is difficult to reliably identify during the data inspection process.

4.3 Data Artifacts in DTS Stream Temperature Measurements

4.3.1 Streambed influence on DTS measurements

Cable contact with the streambed has the potential to influence DTS temperature measurements under certain conditions. Cobble-dominated streambeds do not strongly influence DTS measurements because they contact the cable minimally, allow turbulent flow above the cable, and equilibrate quickly with water temperature. However, soft silt streambeds have the potential to envelop the cable in material that is not in thermal equilibrium with the flowing water. An example of a silt streambed impacting DTS measurements is shown in Figure 4.2. This DTS measurement was made in a slow-flowing stream channel containing a series of soft, silt beds formed where milfoil plants trapped fine sediments (Figure 4.1). The dense fiber optic cable sank into the silt beds and the resulting contact reduced excursions in both minimum and maximum stream temperatures. Temperature measurements made within and above a soft silt bed with Onset HOBO Water Temp Pro v2 temperature loggers revealed that the beds had a lagged and dampened diurnal temperature signature relative to the surrounding water temperature (Figure 4.3). The diurnal temperature range within the beds was a third of the range of the ambient stream temperature.



Figure 4.1: A milfoil bed within the MFJDR trapped fine sediments, creating a soft silt streambed feature.

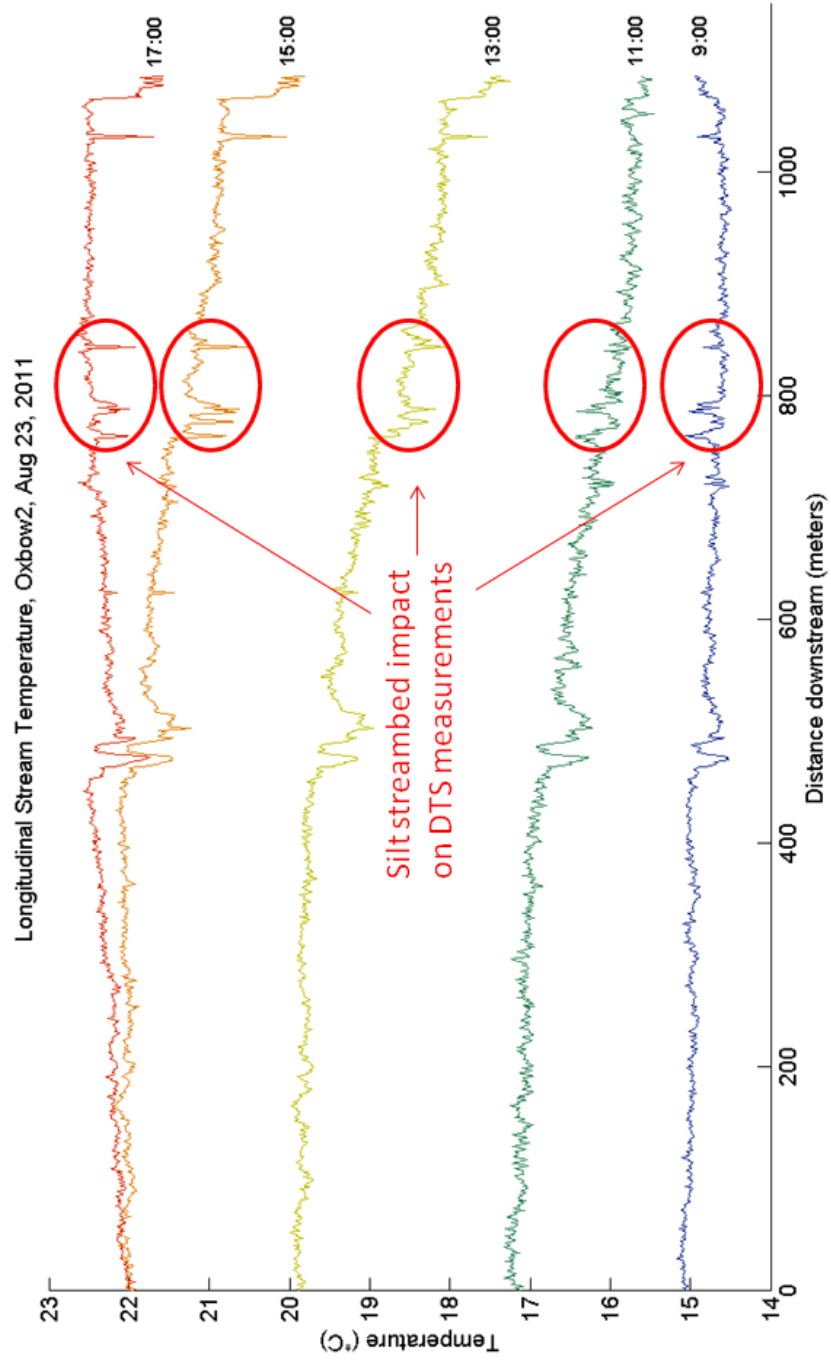


Figure 4.2: DTS stream temperature measurements made in the MFJDR that were impacted by temperature of a silt streambed.

Conveniently, fiber optic cable used in DTS installations is typically denser than water. This feature limits cable floating and exposure to air, which is beneficial for stream temperature dataset quality. Additionally, the cable position on the channel bottom is useful in some river applications for assessing pool-bottom temperature or subsurface inflows. However, because the dense cable is almost always in contact with the streambed, measures must be taken to identify data features that are due to streambed contact, rather than to temperature conditions in the ambient streamflow. For stream temperature datasets, streambed influences constitute data artifacts, and proper documentation of cable location and stream conditions can help to identify those artifacts and prevent data misinterpretation.

4.3.2 Influence of solar radiative heating on DTS measurements

Fiber optic cable used for river temperature monitoring typically is protected by a dark, UV light-resistant outer jacket. Because of its color, the cable jacket enhances the cable's absorption of solar radiative heat. Nielson et al. (2010) investigated the biasing effect of this cable heating on DTS water temperature measurements. They determined that the biasing effect is significant for DTS measurements made at shallow depths in clear, low-velocity water bodies. They predicted a temperature increase of 0.1°C to be caused by cable insolation at depths of 0.1, 0.3, and 0.5 meters with axial water flow at 0.57, 0.47, and $0.32 \frac{m}{s}$, respectively.

The depth-velocity combinations for which Nielson et al. (2010) predicted significant effects of cable insolation are present in many locations of the MFJDR. Dis-

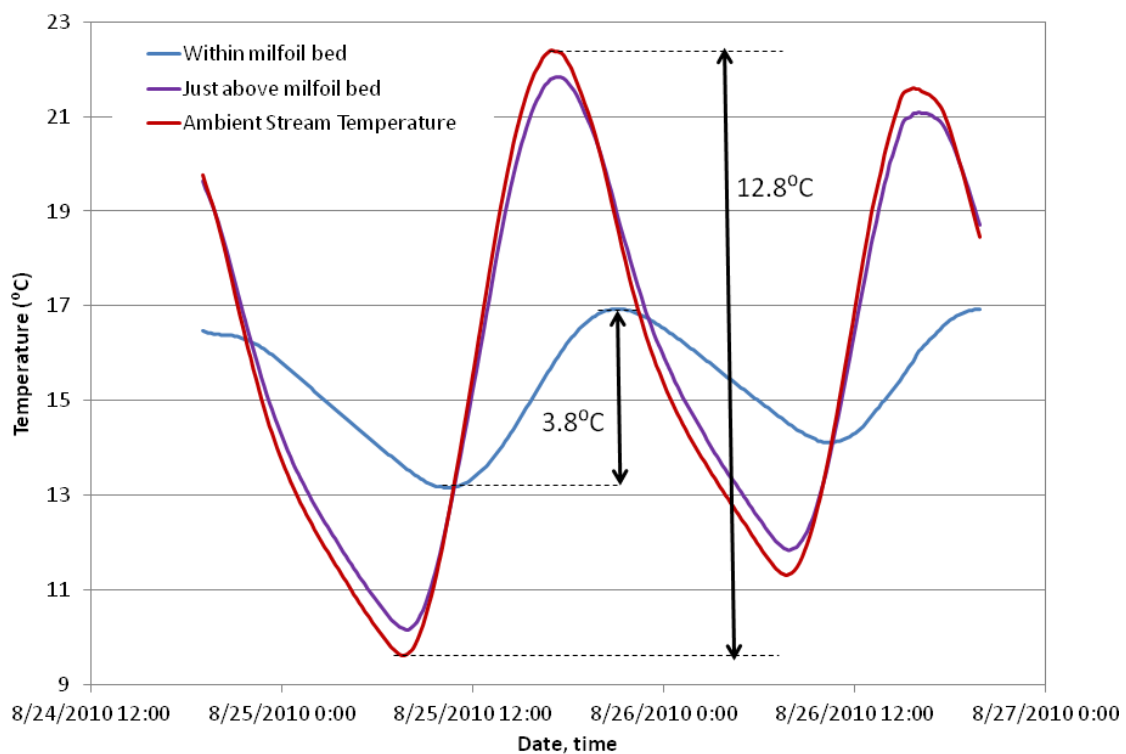


Figure 4.3: Diurnal temperature signal measured by point temperature loggers within and at two locations above a soft silt streambed.

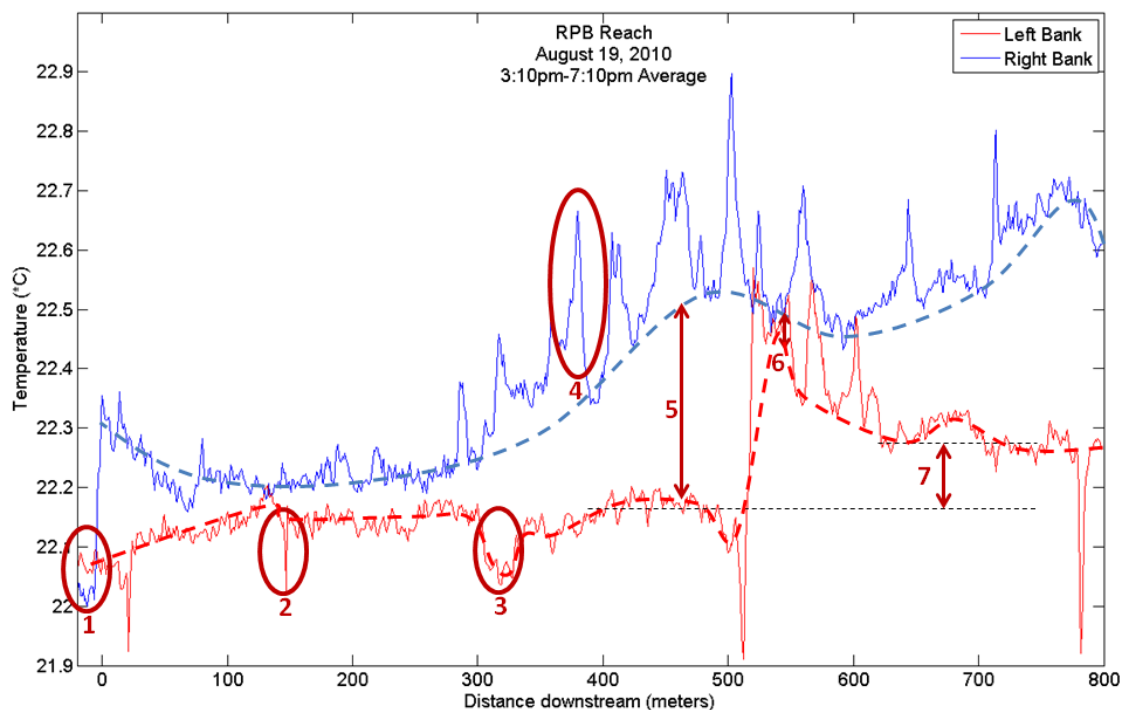


Figure 4.4: Longitudinal stream temperature as measured by DTS along two banks of the RPB reach. Left bank and right bank are defined for a viewer looking downstream. The displayed measurements are averages of four hours of data between 15:10-19:10, the hottest four hours of the day on August 19, 2010. Circled features are described in text.

section of a DTS stream temperature dataset heavily influenced by cable heating can highlight associated data artifacts and data interpretation techniques. For the following dataset, detailed documentation of cable placement helped to identify those areas where cable insolation, or lack of insolation, affected water temperature measurements. The following discussion presents an analysis of a late afternoon DTS dataset collected on the MFJDR (Figure 4.4).

The displayed dataset is a four-hour average of water temperatures (15:10-19:10). This time period (late afternoon) and the time-averaging procedure itself are significant

for data interpretation, as will be discussed below. Time-averaging improves the accuracy of DTS data, and is commonly used for dataset analysis (Huff, 2009; Arik, 2011).

A prominent feature of Figure 4.4 is the consistently higher temperatures recorded on the right bank of the stream, as compared to the left bank. This difference was caused by sun exposure: this northern-flowing reach received the afternoon sun on its eastern (right) bank, while the left bank remained mostly shaded. Because depth-velocity combinations within the reach match those identified to allow insolation-caused biasing effects in DTS data (Nielson et al., 2010), it is possible that some of the observed temperature difference measured between the right and left banks is a data artifact.

In Figure 4.4, Circle No. 1 highlights a low point in measured right bank temperature at the upstream end of the reach. At this location, right bank and left bank cables were co-located and coiled together, shaded beneath cobbles and a bridge. Because these features provided more shading than was available downstream, the right bank temperature at this location was cooler than the downstream temperatures. As was mentioned above, it is possible that downstream measured temperatures were biased higher due to radiative heating of the cable.

Circle No. 2 identifies a sharp negative deviation of temperature on the right bank at a distance of 140 meters. Similar negative spikes were also observed at distances of 20, 510, and 785 meters. These negative spikes are attributed to locations where the cable came near the water surface, slightly contacting air. The diurnal air temperature signal near the MFJDR at this time of year has a larger magnitude (approximately 5°C to 30°C (*Tara O'Donnell, unpublished field data*) than does the diurnal stream temperature signal (approximately 12°C to 24°C). Additionally, water temperatures lag air

temperatures by several hours. Thus, a sharp temperature gradient exists at the air-water interface, particularly in the evening and morning. Because the four-hour DTS data averages depicted in Figure 4.4 included the early evening, when air temperatures were much cooler than water temperatures, locations where the cable slightly contacted air exhibited cooler temperatures. It is assumed that these negative spikes were only identified on the left bank of the channel because that area was shaded in the late afternoon. It is possible that early evening air temperature over the sunny right bank was significantly warmer than that over the shaded left bank.

Circle No. 3 highlights a cable location with depressed temperature. This was a calibration point, where 20 meters of cable were coiled and placed beneath stream cobbles. It is possible that the cobbles provided shade which lowered the measured temperature, or that the presence of the cobbles influenced the measured temperature by shading and limiting turbulent flow around the cable.

A sharp, positive temperature spike is highlighted in Circle No. 4. This spike is one of many along the reach associated with solar radiative heating of the cable. It represents a data artifact that appears to bias the temperature measurement upward 0.2°C - 0.3°C . Characteristic of this type of artifact, the spike is sharp, and measured temperatures before and after the spike are approximately equal. The spike was likely associated with one of many riffles observed along the reach. A technique to estimate unbiased water temperature in the region of the spikes is to connect the temperatures upstream and downstream of the spikes. The dashed blue and red lines in Figure 4.4 represent an estimate of stream temperature less biased by cable heating.

While the right bank temperature was consistently higher than the left bank tem-

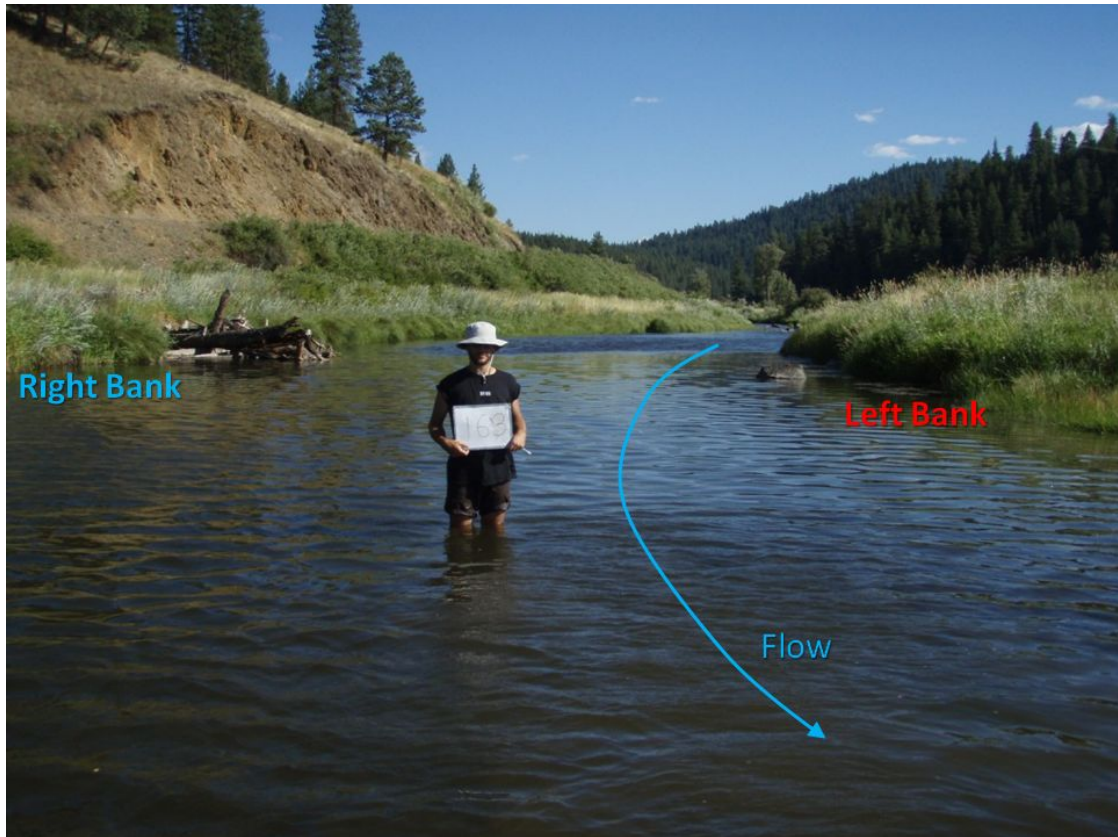


Figure 4.5: A wide, slow-flowing section of the RPB reach. Flow conditions here inhibited channel mixing and caused the temperature difference indicated by Circle No. 3 in Figure 4.4

perature, this difference became greatest between 300 and 500 meters downstream (Arrow No. 5). Over this section, the channel was both slowly-flowing and wide, minimizing cross-channel mixing. (Figure 4.5).

Arrow No. 6 identifies an area where left bank and right bank temperatures are approximately the same. This area corresponds to a channel-spanning riffle. This riffle redirected flow briefly towards the west, playing the dual role of mixing water and exposing the left bank of the channel to direct sunlight.

The left bank temperature downstream of the channel-spanning riffle was higher than that upstream of the riffle (Arrow No. 7). This step-like temperature increase was likely due to the channel-wide mixing that occurred within the riffle.

The DTS dataset features described in this section highlight the importance of a sound quality control procedure to identify stream temperature data artifacts. Field documentation of cable location and consideration of the impact of cable heating on daytime stream temperatures can help eliminate data misinterpretation.

4.4 Conclusions

Stream temperature patterns change in both space and time, and DTS can be a useful technology for monitoring stream temperature. The impacts of data artifacts in DTS datasets can be minimized by the following measures:

- External heat fluxes to the cable, such as those resulting from direct solar radiation, should be avoided where possible, or properly identified where not possible
- Detailed documentation of cable placement can help identify areas where the cable temperature may not have equilibrated with water temperature, such as might happen if the cable contacts air or if turbulent water flow around the cable is prevented.
- Preventing data artifacts at calibration locations and ensuring that an adequate length of cable (10-50 meters) is included at each calibration location can help improve calibration quality.

The application of DTS should be chosen carefully, to ensure that the value of the data is worth the cost of its deployment. Arik (2011) estimated that the cost to collect and analyze two days of DTS data on a one kilometer river reach was \$10,000-\$12,000. DTS is well-suited to river reaches of one to four kilometers in length, where flow conditions permit safe cable deployment. Spatial temperature variation in streams is often subtle, and it is necessary to verify that DTS instrumentation and set-up are adequate to detect the thermal features of interest. A quality control process can help to identify data artifacts such as those caused by streambed temperature or cable heating. Under the proper conditions, DTS is capable of providing valuable temporal and spatial stream temperature information.

Chapter 5 – DTS Analysis of Longitudinal Stream Temperature Patterns

5.1 Introduction

In the Pacific Northwest, regulation of stream temperature is increasingly enforced under the U.S. EPA Clean Water Act and state-specific Total Maximum Daily Load (TDML) standards. River-specific temperature TDMLs define the level of thermal pollution each river can withstand without exceeding water quality standards. The development of TDMLs requires a detailed understanding of how stream temperature varies longitudinally, and models designed during standard development must accurately capture longitudinal temperature patterns (ORDEQ, 2012). In Oregon, a not-for-profit water conservancy, The Freshwater Trust, has created a temperature credit program, designed to offset thermal pollution in one part of a basin with temperature mitigation in another. The design of thermal offset programs, like the design of TDML standards, requires a detailed understanding of longitudinal temperature patterns in streams.

DTS datasets, which provide stream temperature data in both the spatial and temporal domains, can shed light on reach-scale stream thermal processes that may have an impact on the larger-scale longitudinal trends of interest for regulatory and temperature credit development. This section presents an analysis of the longitudinal temperature trends observed in four DTS stream temperature datasets collected on the Middle Fork John Day River.

The Middle Fork John Day River is a fourth to sixth (6+) order stream (BOR, 2010) located in the Columbia Basin in northeastern Oregon. During the summers of 2010 and 2011, DTS temperature measurements were collected over three 1-3 kilometer long reaches of the MFJDR. One of the reaches (Forrest) was monitored during both summers, two reaches (Oxbow1 and Oxbow3) were monitored in 2011. The monitored reaches were chosen based on access permission and relevance to ongoing stream restoration projects and planning. These reaches were monitored for temperature in the stream thalweg, the portion of the stream that carries the majority of the flow. Other reaches in the MFJDR basin were monitored for temperature near their right and left banks. These bank measurements were not as appropriate for longitudinal trend analysis as the thalweg measurements were. Table 2.1 displays dataset properties for each of the four DTS installations.

Table 5.1: Summary of DTS installations used to assess longitudinal temperature patterns.

<p>Forrest Reach, 2011 <i>Monitoring Period: Jul26-Aug4, Aug6-Aug8</i> Thalweg installation Length: 1643 meters Upstream Coord.: 44°35'45.15"N, 118°31'21.95"W Upstream Discharge: 0.50-0.41 cms Dataset accuracy: 0.11 °C</p>	<p>Oxbow1 Reach, 2011 <i>Monitoring Period: Jul30-Aug1, Aug4-Aug9</i> Thalweg installation Length: 2168 meters Upstream Coord.: 44°38'55.39"N, 118°40'0.11"W Upstream Discharge: 1.55-1.04 cms Dataset accuracy: 0.06 °C</p>
<p>Forrest Reach, 2010 <i>Monitoring Period: Aug19-Aug24</i> Thalweg installation Length: 1719 meters Upstream Coord.: 44°35'45.15"N, 118°31'21.95"W Upstream Discharge: 0.39-0.33 cms Dataset accuracy: 0.08 °C</p>	<p>Oxbow3 Reach, 2011 <i>Monitoring Period: Aug11-Aug21, Aug23-Aug24</i> Thalweg installation Length: 1384 meters Upstream Coord.: 44°38'37.43"N, 118°38'5.76"W Upstream Discharge: 0.67-0.63 cms Dataset accuracy: 0.04 °C</p>

5.2 Longitudinal Stream Temperature Trends

Figures 5.1 - 5.4 display longitudinal temperature profiles from the four DTS installations: Forrest reach on August 22, 2010 and on July 29, 2011, Oxbow3 reach on August 12, 2011, and Oxbow1 reach on August 6, 2011. Linear-like longitudinal temperature trends were observed in each of the four datasets. Some of these trends exhibited positive slopes (increasing temperature with downstream distance), some exhibited negative slopes (decreasing temperature with downstream distance), and some had diurnally varying slopes. The locations of slope breaks defined segments. While the slope of these segments varied diurnally, their locations did not. The slope breaks defining most segments were visually identifiable at all times of day.

Based on the slope break locations, segments were defined in each dataset. Segment boundaries (slope breaks) are indicated by vertical dotted lines in the top sections of Figures 5.1 - 5.4. First-order regression lines were fitted to each segment. The slopes of these regression lines were allowed to change through time, generating a time series of slope values for each segment. The slopes of most segments were observed to vary on a diurnal cycle throughout each monitoring period. Four days of the segment slope time series from each dataset are displayed on the bottoms of Figures 5.1 - 5.4.

It was noted that the segment slopes from Forrest during the 2010 monitoring period were twice as large as most segment slopes from the other reaches. This feature may relate to flow volume. The upstream discharge during the Forrest 2010 monitoring period receded from 0.39 to $0.33 \frac{m^3}{s}$ (between August 14 and August 26, 2010), which were lower flow rates than those during the 2011 monitoring period, when discharge receded from 0.55 to $0.41 \frac{m^3}{s}$ (between July 27 and August 7, 2011). Also, the Forrest 2010 flow rates were much lower than the upstream flow volume in the Oxbow1 and Oxbow3 reaches, which were as high as $1.55 \frac{m^3}{s}$ and $0.67 \frac{m^3}{s}$, respectively. It is reasonable to expect a river with low flow volume to heat and cool more quickly than a river with high flow volume, under the influence of the same heat fluxes. Higher surface area to volume ratio in a low-flow river allows for greater impact of heat fluxes, per unit volume.

The significance of linear-like longitudinal temperature increases and decreases (henceforth referred to as “temperature slopes”) is manifold. Temperature slopes on the order of 1°C change per kilometer were observed, and this magnitude has implications for downstream temperature potentials. Spatial temperature variation in a stream channel also suggests spatially varying heat flux, or a temporally changing upstream boundary condition. Understanding these processes would be useful for improving stream temperature modeling. Finally, all other factors equal, a steeper decreasing slope in one segment than in another might suggest a higher volume of cool groundwater or hyporheic water inflow, which could be useful information for river restoration planning. The following analysis aims to determine causal mechanisms for the observed temperature slopes and for the time-varying behavior of the segments.

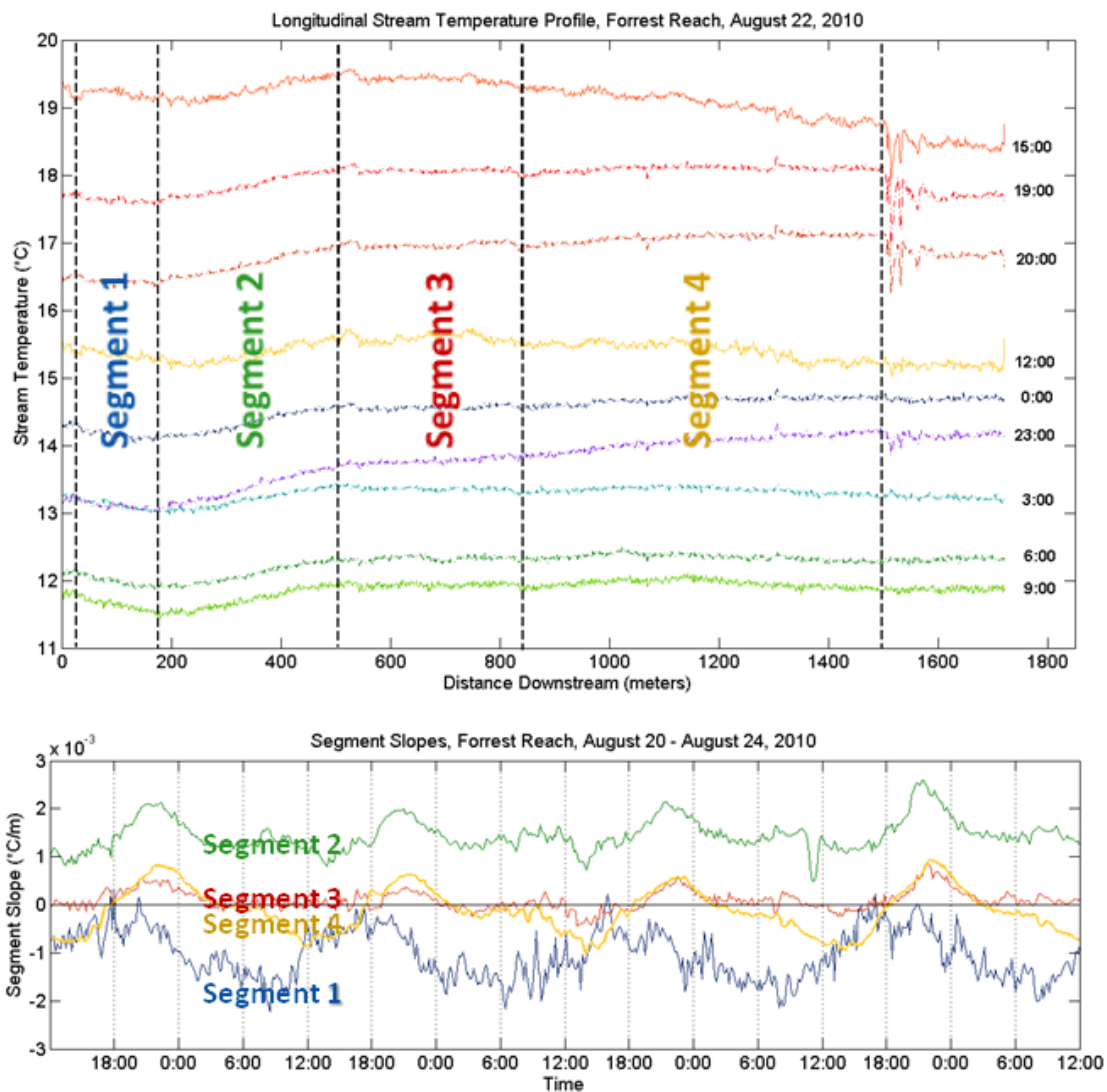


Figure 5.1: Forrest reach longitudinal temperature profiles from August 22, 2010 and segment slopes from August 20-24, 2010

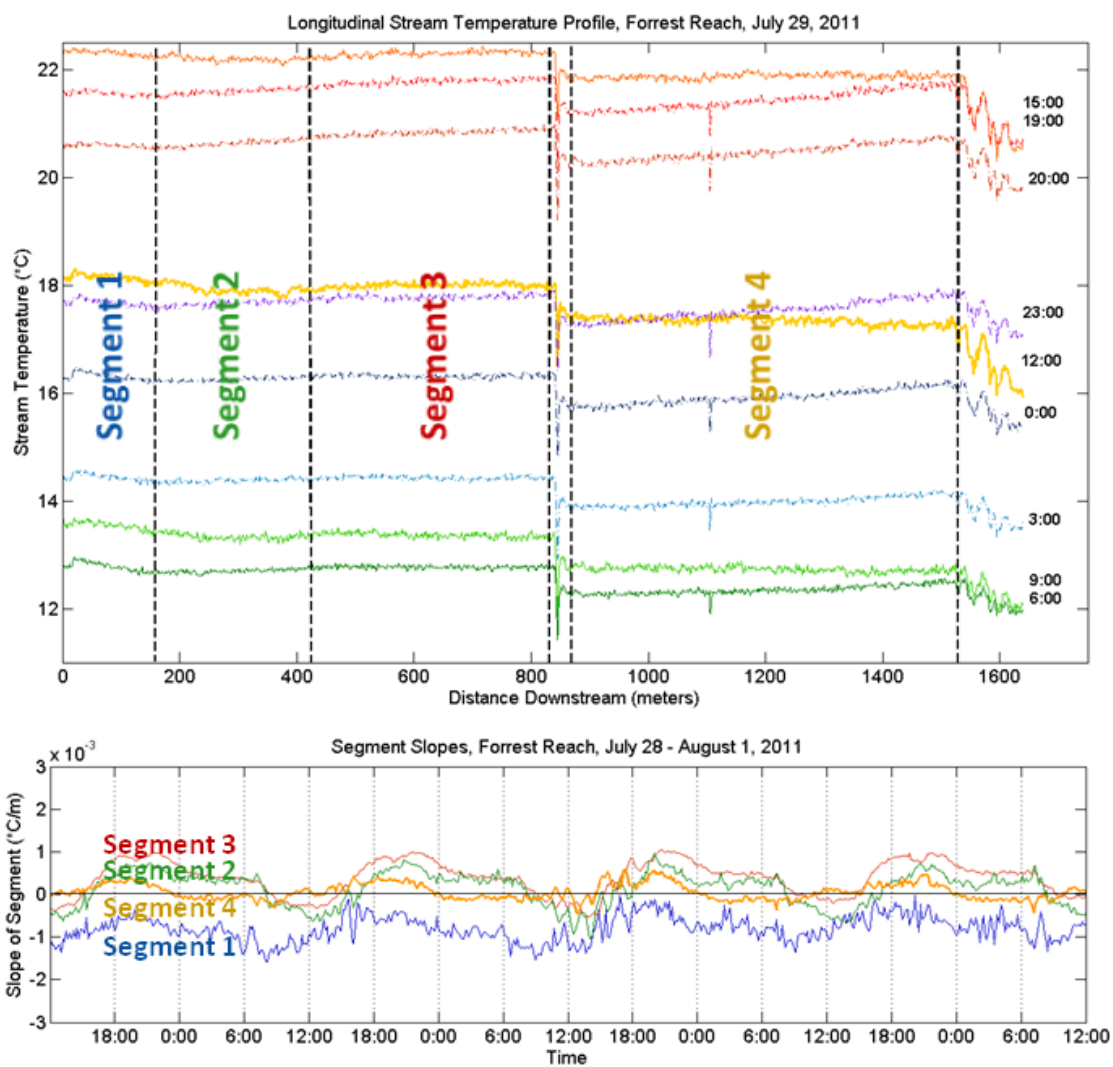


Figure 5.2: Forrest reach longitudinal temperature profiles from July 29, 2011 and segment slopes from July 28-August 1, 2011

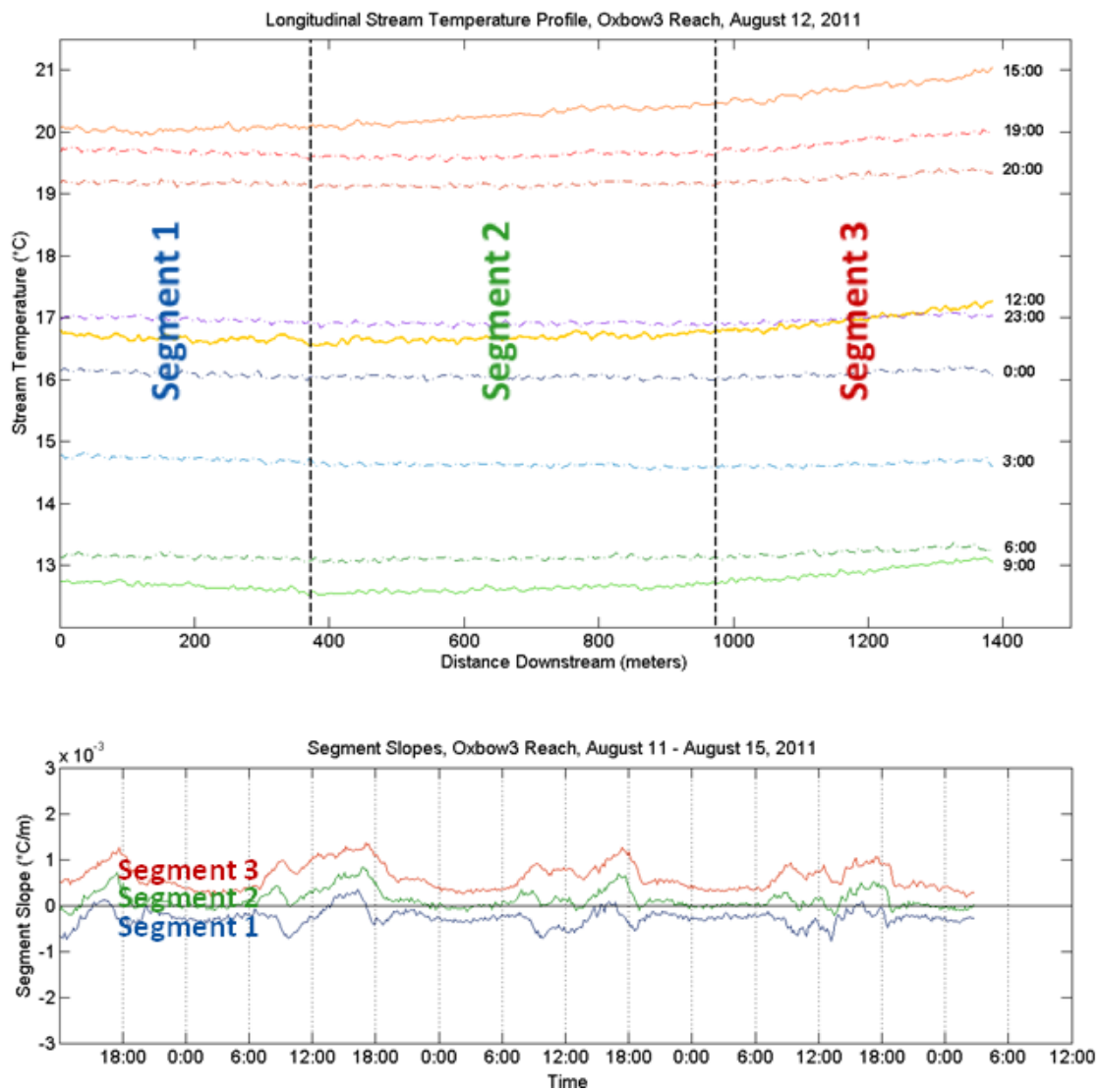


Figure 5.3: Oxbow3 reach longitudinal temperature profiles from August 12, 2011 and segment slopes from August 11-15, 2011

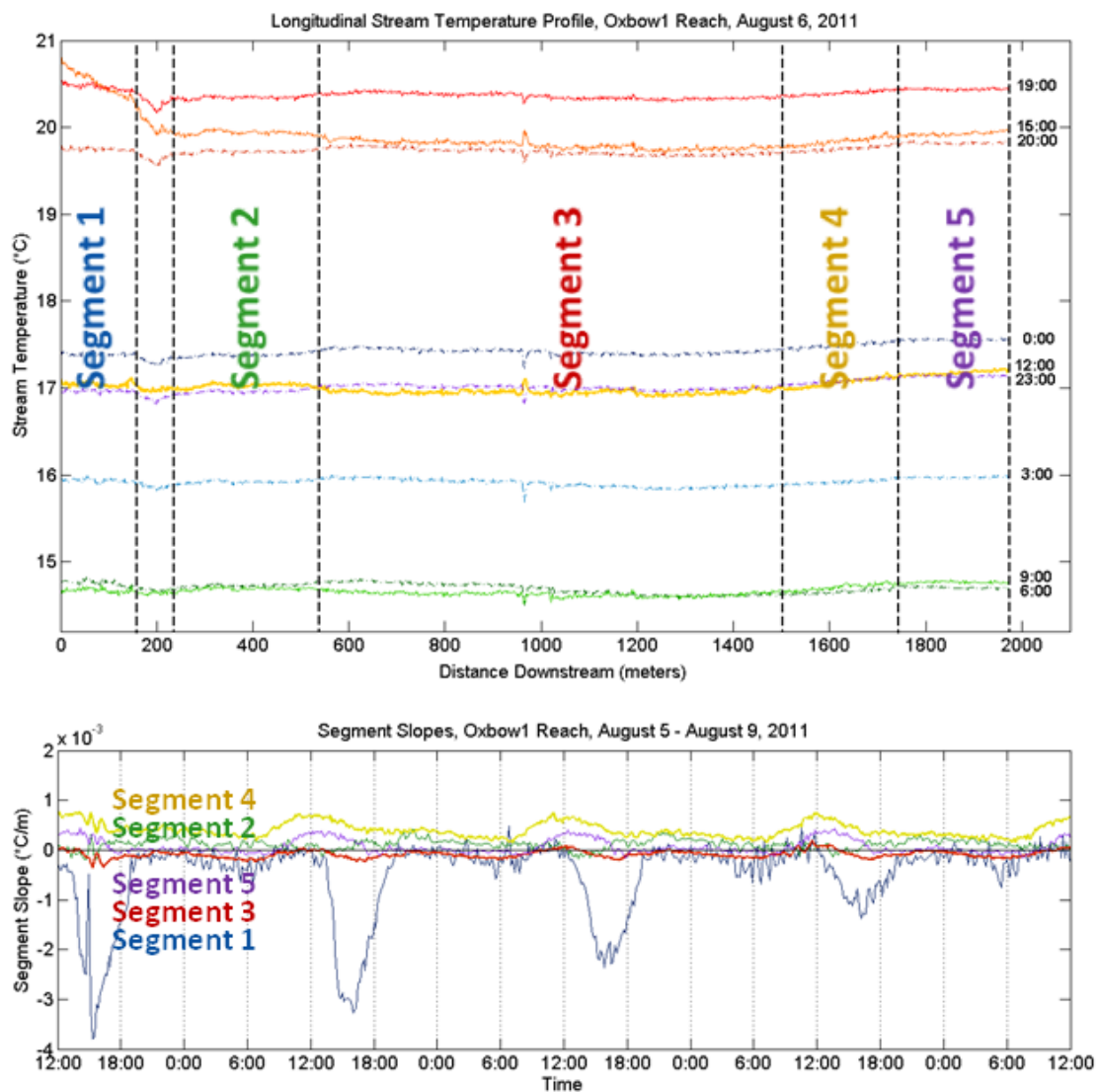


Figure 5.4: Oxbow1 reach longitudinal temperature profiles from August 6, 2011 and segment slopes from August 5 - 9, 2011

5.3 Potential Drivers of Temperature Slopes

While it is likely that no one process was responsible for inter-segment slope differences or the temporal slope variation, the diurnal periodicity of the slope values suggested one or more diurnally-changing processes as drivers. An exploratory list of potential explanations was considered, including tributary inflows, groundwater inflows, large-scale, advection-transported heat waves, and spatial heat flux variations. The likelihood of each of these drivers causing the observed slope periodicity was assessed.

5.3.1 Tributary Inflows

Tributary water temperatures vary on diurnal cycles, with those cycles rarely matching the diurnal temperature cycle of the mainstem. Time lags in temperature maximums or differences in magnitude or offset are common. Tributaries that descend from high elevations, that are well-shaded, or that transport significant volumes of groundwater or snowmelt tend to have a lower maximum temperature than the mainstem. Unshaded tributaries are more likely to exceed mainstem temperatures in the hottest part of the day. In the MFJDR, nighttime tributary temperatures are typically cooler than those of the mainstem, due to the smaller flow volumes and higher elevations of tributaries. To make any determination of tributary influences on temperature slopes, some information about tributary temperature must be known.

Segment 1 of Oxbow1 (Figure 5.4), exhibited a slope behavior out of phase with the other segments in the reach. It was known that the Ruby Creek/ South Channel Irrigation Ditch tributary joined the mainstem 50 meters upstream of Segment 1. This

tributary flowed slowly over hundreds of meters of unshaded meadow and mine tailings before confluence with the mainstem. High solar exposure and slow flow speed gave this tributary the potential to be warmer than the main channel, especially during the warmest hours of the day (12:00 to 18:00). It was hypothesized that this warm inflow could raise stream temperature in the main channel, and the negative slope observed in Segment 1 could be driven by that upstream warm temperature influence. If this were true, the slope should be most negative during the hours of the day when the difference between tributary and mainstem temperature was greatest. An examination of Figure 5.4 reveals that the slope of Segment 1 is indeed most negative during the hours of 12:00 to 18:00, which is the time of day when that maximum difference would be expected. Additionally, the maximum negative magnitude of the Segment 1 slope decreased steadily between August 5 and August 9. This decrease might have been related to a concurrent decrease in tributary flow levels observed in that period. Finally, it should be noted that a cool, subsurface inflow was suspected to enter the channel near the downstream end of Segment 1. This inflow was discussed further in Section 2.4.2.1.

Segment 1 of the Forrest reach, in both 2010 and 2011, also exhibited a consistently negative slope and periodicity out of phase with the other segments in the reach. It seemed possible that an upstream tributary was also responsible for this behavior; Placer Gulch joins the mainstem 25 meters upstream of Segment 1. However, no information was known about the diurnal temperature behavior of Placer Gulch. The slope of Segment 1 was most negative during the hours when stream temperatures were coolest (0:00 to 12:00), and this seemed an unlikely time for Placer Gulch temperatures to be warmer than those of the mainstem.

5.3.2 Groundwater Inflows

Groundwater temperature remains relatively constant diurnally. Deep groundwater temperature varies little even seasonally, and its temperature is often assumed constant, equal to the average annual air temperature (Huff, 2009) (approximately 8°C in the MFJDR (Agrimet, 2012)). Shallow groundwater temperature varies seasonally and is slightly warmer than deep groundwater temperature in the summer months. In August 2011, groundwater temperatures measured in the Forrest and Oxbow Conservation Areas ranged between 9°C and 14°C (*Appendix D*). Because typical MFJDR stream temperature range in the month of August is between 12°C and 24°C, groundwater temperature is cooler than stream temperature throughout most of the day. Thus, groundwater inflows lower daytime stream temperature, and may slightly raise nighttime stream temperature in some locations. If the quantity of groundwater inflow remains constant through time, then stream temperature would be most impacted by groundwater inflows when the temperature difference between the stream and groundwater is the greatest. In the MFJDR, this period corresponds to stream temperature maximums between 12:00 and 18:00. Thus, any temperature slope influenced by groundwater inflows would be most negative during this time of the day. The only segment that exhibited this behavior was Segment 1 of Oxbow1. However, as described previously, the behavior of this segment appeared to be related to an upstream warm inflow.

5.3.3 Thermal and Hydrodynamic Waves

Thermal waves and hydrodynamic waves have been studied in fluvial settings in the context of the outflows from dams and hydropower facilities (Khangaonkar and Yang, 2008; Toffolon et al., 2010). A fluvial thermal wave is caused by a discrete outflow of a certain temperature suddenly released into a river of a different temperature. The outflow water moves down the channel at the river advection velocity, and downstream thermometers would detect the passage of the outflow water as a thermal wave. Hydrodynamic waves travel not at the advection velocity, but rather at the wave celerity, which depends on river depth. They arise when constant temperature water is released continuously from an upstream source. The combination of the upstream constant-temperature boundary condition, advection, and diurnal thermal forcing impacts the magnitude of the diurnal temperature range at regular distances from the constant-temperature source. For example, at a distance of 5 kilometers from the source, the daily range of stream temperatures might be dampened, while the daily temperature range at a distance 10 kilometers from the source might be amplified. While there are no dams on the Middle Fork John Day River, the possibility exists that thermal or hydrodynamic waves might develop through other forcing mechanisms (such as tributary or spring inflows).

No definite determination could be made as to whether hydrodynamic waves were present in the MFJDR. However, a few aspects of Figures 5.1 - 5.4 were examined to assess the likelihood that thermal waves might be present and might have been the cause of the slope periodicity observed.

Most of the reach segments observed in this analysis (Segments 2-4 of Forrest,

Segments 1-3 of Oxbow3 and Segments 4-5 of Oxbow1) displayed periodicity in phase with the other segments in their reach. At the advection velocity typical in the MFJDR ($0.3 \frac{m}{s}$ to $0.6 \frac{m}{s}$), the crest of a thermal wave would be expected to pass through a 2000-meter reach in 55 to 110 minutes. Within any given reach, all segments would be expected to exhibit a slope response from a thermal wave within a relatively short time period. This was indeed the behavior observed in the slope periodicity graphs. During both the 2010 and 2011 monitoring periods in the Forrest reach, the segment slopes were most positive between 18:00 and 0:00. In Oxbow3 and for Segments 4-5 of Oxbow1, the slopes are most positive between 6:00 and 18:00. Furthermore, in Oxbow3, the slope vs. time curves mirrored each other closely, suggesting a single process driving temporal slope variation, at least in that reach. It was hypothesized that thermal waves were responsible for the synchronous slope behavior.

To test the hypothesis, predicted thermal wave propagation time was compared to the difference in response time between the Forrest reach and the Oxbow3 reach. Thermal waves advect at the average flow velocity (Toffolon et al., 2010), between $0.3 \frac{m}{s}$ and $0.6 \frac{m}{s}$ for the MFJDR. According to DEQ (2010), the center of the Oxbow3 reach is located 12 kilometers downstream of the Forrest reach. However, the distance scale of the DEQ (2010) study was biased shorter than the actual channel distance (compare DEQ (2010) stream kilometer distances to field-measured reach lengths in Table 2.1). Therefore, it is likely that Oxbow3 is actually located 15-20 kilometers downstream of Forrest. Over that distance range and the estimated advection velocity range, a thermal wave would travel from Forrest to Oxbow3 in 6.9 to 18.5 hours. The observed lag time between the rising limb of the slope vs. time curve for the Forrest reach (16:00)

and the rising limb of the curve for the Oxbow3 reach (7:00, the next day) was 15 hours, which is within that predicted range. While this analysis was cursory, it provides some support for the possibility that a thermal wave advecting down the MFJDR channel might help explain the slope periodicity in the Forrest and Oxbow3 reaches.

Contradicting the finding described above, some evidence against thermal waves causing the slope periodicity was seen in the shape of the slope versus time curves. If a heat wave were advecting down the channel, the top halves of the curves would represent the leading limb of the wave, and the bottom halves would represent the falling limb. Symmetry between these two halves should be expected for a thermal wave of regular waveform. Instead, the slope versus time curves in Figures 5.1 - 5.4 had only distinct top halves. The bottom halves were poorly defined and not matching in shape. There is a possibility that dispersion could weaken the trailing limbs of such large-scale “heat waves”, similarly to how dispersion affects the trailing limbs of flood waves.

5.3.4 Heat Flux Variation

Even if the diurnal periodicity of the slopes is explained by an upstream forcing mechanism such as a thermal wave, within-reach processes must also be present to cause slope differences between segments. Specifically, the net heat flux received by the stream must vary between segments. To test this possibility, heat fluxes were computed at five-meter intervals along the Forrest reach between July 28 - August 1, 2011. Ttools, a spatial data analysis tool, was applied to a LiDAR DEM (WSI, 2008) to measure stream topography and shading. This information, along with meteorologic and hydrologic data measured

during the 2011 Forrest monitoring period, was input to Heat Source, a stream temperature modeling software that employs the algorithms described in Boyd and Kasper (2004). Spatial variation in net heat to the stream was assessed by comparing the 11:00 to 17:00 averages of net heat flux for every five-meter increment along the reach. The period 11:00 to 17:00 was chosen because it encompasses the late morning/ early afternoon solar conditions, which influence afternoon stream temperature, as well as the late afternoon conditions, when some parts of the stream become shaded. Figure 5.5 depicts along-reach and inter-segment variation in the 11:00 to 17:00 average heat flux.

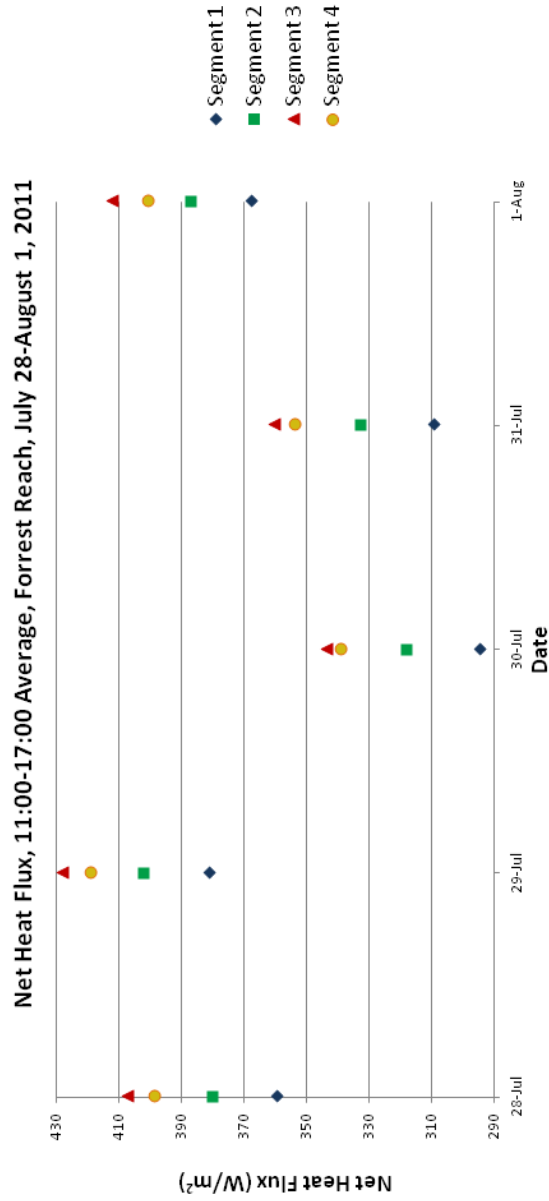
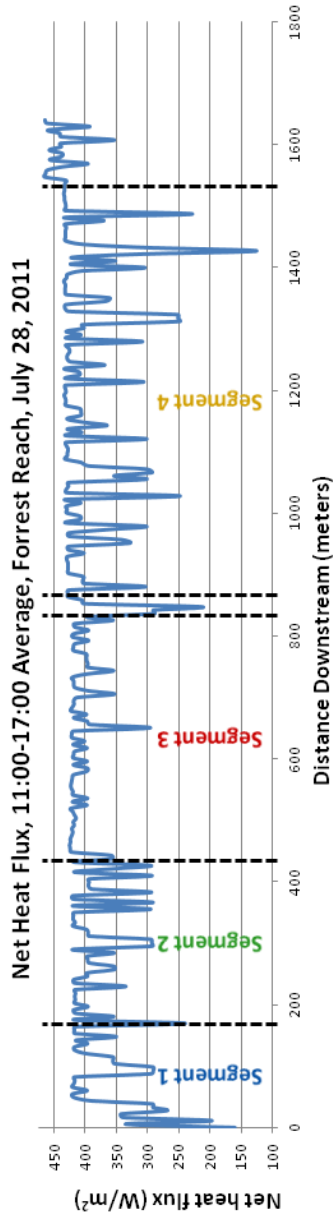


Figure 5.5: The top graph displays the 11:00 to 17:00 average of net heat flux on July 28, 2011 in the Forrest reach, as a function of stream distance. The net heat flux was estimated based on the sum of shortwave, longwave, bed conduction, convection, and evaporation heat flux terms estimated by a Heat Source stream temperature model. The bottom graph depicts the 11:00 to 17:00 average on each of the four slope segments of the 2011 Forrest reach.

According to heat flux computations, Segment 1 consistently received the lowest net heat flux during the 11:00 to 17:00 time period, and Segment 3 consistently received the highest flux. The difference between these highest and lowest heat fluxes was approximately 12% - 18%, a difference likely attributable to water surface top width, channel aspect, and shading. As can be seen in Figure 5.2, the difference between the slopes of Segment 1 and Segment 3 was 0.002°C per meter during most of the day, but approximately 0.0005°C per meter (0.5°C per kilometer) during the afternoon time period (12:00-18:00).

To translate the 12% - 18% difference between Segment 1 and Segment 3 average heat fluxes into a temperature gain differential, an idealized heat transfer model was used. The largest difference in average net heat flux between Segment 1 and Segment 3 was approximately 50 watts per square meter ($\frac{W}{m^2}$). The outputs of the Heat Source computations indicated that 90% of the net heat flux difference between segments was attributable to the direct solar radiation heat flux term. Because direct solar radiation is received on the water's top surface (not through the streambed), the heat transfer model was simplified by assuming that all the $50 \frac{W}{m^2}$ inter-segment heat flux differential was received through the top surface. One cubic meter of water, if assumed to have a uniform depth of 0.3 meters, has a top surface area of 3.33 m^2 . This cubic meter parcel of water could be expected to receive a differential heat flux (H) of 167 W , or 167 joules (J) over the time period (Δt) of one second. Assuming water at 20°C , the water parcel has a mass (m) of 998 kilograms and a specific heat capacity coefficient (c_p) of 4182 joules per kilogram-degree Celcius ($\frac{J}{kg * ^{\circ}C}$). According to the idealized heat transfer model

$\frac{\Delta T}{\Delta t} = \frac{H}{c_p * m}$, the parcel of water would experience a temperature increase of 4×10^{-5} °C per second. For typical flow speeds in the MFJDR of $0.3 \frac{m}{s}$ - $0.6 \frac{m}{s}$, the water parcel would travel 200 meters in 333-667 seconds. During this time, its temperature would increase by 0.013°C - 0.027°C. This longitudinal rate of temperature change (0.065°C - 0.135°C per kilometer) is less than a third of the difference in segment slopes between Segment 1 and Segment 3 (0.5°C per kilometer) during the 12:00 to 18:00 period.

The idealized heat transfer model described above indicated that the Heat Source-computed heat fluxes failed to fully explain the observed inter-segment slope differences. This failure may be due to the time of day for which the comparison was made (12:00 to 18:00), when the difference in slopes between Segment 1 and Segment 3 was least pronounced. It may relate to the model quality: the model assumed constant streambed thermal conductivity, thermal diffusivity, and porosity over the entire reach. Although unlikely to affect results significantly, bed conduction from deep alluvium was not included in the model.

5.4 Conclusions

The analysis described in this section reached no certain conclusions for the causes of the observed segment slope differences among these four DTS datasets. However, a tributary inflow was identified as a likely driving mechanism for the slope behavior of Segment 1 of the Oxbow 1 reach. The periodicity of segment slopes suggested that the passage of a thermal wave might be a driving mechanism for the slope behavior. The phase shift between slope periodicity of the Forrest reach and slope periodicity of the

Oxbow3 reach (15 hours) fell within a range of predicted lag times based on thermal wave advection velocity and downstream distance. An effort was made to quantify the differences in heat fluxes between two segments and to compare that difference to observed differences in slope. The model-predicted heat fluxes did not fully explain the observed slope differences. The results of this analysis may provide the basis for future investigation.

Chapter 6 – Conclusion

This research has explored features of the spatial and temporal patterns of stream temperature variation, and described the use of DTS for monitoring and analyzing those patterns.

A cold patch survey in the Middle Fork John Day River (MFJDR) in northeastern Oregon found no cold patch exceeding 2.31°C cooler than ambient stream temperature and that tributary inflows provided some of the most temperature-differentiated cold patches. These findings are significant for fish habitat assessment, and agree with the speculation of some river restoration practitioners that disturbances to the channel have reduced the number of off-channel and in-channel thermal refugia in the MFJDR system (RDG, 2007; BOR, 2008).

The theoretical potential for cold patch formation in the MFJDR was estimated by applying a Richardson number computation and cavity flow mixing predictions to field measurements made in that system. The results of those computations generally supported the lack of observed stratified pools seen in the temperature data collected during the study. The highest Richardson number value computed during this study was 29.7, and it was based on thermal conditions that have yet to be measured in the MFJDR or any other fluvial system (13°C pool top-to-bottom temperature difference). Additionally, that Richardson number was much lower than those computed in northern California streams by Nielsen et al. (1994) (>500,000), suggesting that the potential for

thermal stratification in MFJDR pools is lower than in those streams. The estimation of cavity purging rate (Q), possibly applicable to transport from a cool water pool in the MFJDR, resulted in a purge rate lower than available estimates of groundwater flux to the MFJDR, suggesting that portions of the MFJDR receive groundwater influx adequate to sustain a cold water “cavity” in the streambed. However, it is possible that the experimental conditions upon which the cavity purge rate equation was based do not match natural flow conditions, resulting in an underestimate of actual stream mixing processes.

Restoring thermal heterogeneity in the MFJDR system would likely require channel modification that protects cool-water areas from mainstem flow. The cool stream pools described by (Nielsen et al., 1994) were channel backwater areas, were partially separated from mainstem flow by gravel bars and fed by tributaries, or had long pool residence times (large pool volume-to-discharge ratios). Few such areas exist in the MFJDR system. The questions of whether they existed historically or whether constructed versions could be stable in the current system are up for debate. Temperature within an off-channel pond near one of the MFJDR study reaches (Oxbow1) was at least 4°C cooler than mainstem temperatures in August 2011. However it is unknown whether that pond would retain its thermal and physical character if connected to the main channel and whether dissolved oxygen conditions within the pool would be suitable for fish habitat.

DTS dataset analysis and synoptic streamflow measurements indicated that a temperature anomaly observed in TIR and FLIR datasets collected on the MFJDR was not caused by groundwater inflow. Rather, low advection velocity in a deep, slowly-

flowing reach appeared to cause a time lag of the diurnal temperature signal within the reach. This finding, and the fact that TIR and FLIR datasets are generally collected during summertime afternoons when the effect is potentially greatest, recommends caution for interpreting FLIR and TIR stream temperature datasets. Knowledge of hydraulic flow conditions could be useful for preventing data misinterpretation.

Techniques and challenges of DTS deployment in streams was explored. The potential for DTS data artifacts due to external heat fluxes on the fiber optic cable sensor were discussed. Conditions under which streambed contact with the fiber optic cable could impact stream temperature measurements were described. Dissection of a DTS stream temperature dataset heavily influenced by solar radiative heating of the fiber optic cable pointed out associated data artifacts and data interpretation techniques.

Longitudinal stream temperature trends in the MFJDR exhibited slopes on the order of 1°C change per kilometer. This magnitude of longitudinal temperature evolution has implications for downstream temperature potentials. Temporal variation of these slopes was also measured, and the variation exhibited a diurnal periodicity in most monitored river segments. Analysis of this periodic behavior was unsuccessful in convincingly identifying causal mechanisms, but the likelihoods of various mechanisms were explored.

Stream temperature patterns change in both space and time, and DTS can be a useful technology for monitoring stream temperature. Its application should be chosen carefully, to ensure that the value of the data is worth the cost of its deployment. Arik (2011) estimated that the cost to collect and analyze two days of DTS data on a one kilometer reach was \$10,000-\$12,000. DTS is well-suited to river reaches of one to

four kilometers in length, where flow conditions permit safe cable deployment. Spatial temperature variation in streams is often subtle, and it is necessary to verify that DTS instrumentation and set-up are adequate to detect the thermal features of interest. Under the proper conditions, DTS is capable of providing valuable information about fluvial thermal features.

Bibliography

- Agrimet (2012). Bureau of reclamation agrimet system: Prairie city agrimet station (pcyo)1989-2012 air temperature data. Technical report, Bureau of Reclamation. <http://www.usbr.gov/pn/agrimet/wxdata.html>.
- Arik, A. D. (2011). A study of stream temperature using distributed temperature sensing fiber optics technology in big boulder creek, a tributary to the middle fork john day river in eastern oregon. Master of science, Water Resources Engineering, Oregon State University.
- Armfield, S. and Debler, W. (1993). Purging of density stablized basins. *International Journal of Heat and Mass Transfer*, 36(2):519–530.
- Baltz, D. M., Vondracek, B., Brown, L. R., and Moyle, P. B. (1987). Influence of temperature on microhabitat choice by fishes in a california stream. *Transactions of the American Fisheries Society*, 116:12–20.
- Bayley, P. B. and Li, H. W. (2008). Stream fish responses to grazing enclosures. *North American Journal of Fisheries Management*, 28:35–147.
- Bilby, R. E. (1984). Characteristics and frequency of cool-water areas in a western washington stream. *Journal of Freshwater Ecology*, 2:593–602.
- BOR (2008). Middle fork and upper john day river tributary assessments, grant county, oregon. Technical report, Bureau of Reclamation. Technical Service Center, Denver, CO and Pacific NW Regional Office, Boise, ID.
- BOR (2010). Oxbow conservation area reach assessment, middle fork john day river, grant county, oregon. Technical report, Bureau of Reclamation. Pacific NW Regional Office, Boise, ID.
- Bormans, M. and Condie, S. (1997). Modelling the distribution of anabaena and melosira in a stratified river weir pool. *Hydrobiologia*, 364(1):3–13.
- Bouwes, N. (2005). Integrated status and effectiveness monitoring john day pilot program. Technical report, Eco Logical Research, Inc. Prepared for NOAA Fisheries and Bonneville Power Administration and funded by Bonneville Power Administration.

- Boyd, M. and Kasper, B. (2004). *Analytical methods for dynamic open channel heat and mass transfer: methodology for Heat Source Model Version 7.0*. <http://www.deq.state.or.us/WQ/TMDLs/tools.htm>.
- Brett, J. R. (1956). Some principles in the thermal requirements of fishes. *The Quarterly Review of Biology*, 31(2):75–87.
- Briggs, G., Thompson, R., and Snyder, W. (1990). Dense gas removal from a valley by crosswinds. *Journal of Hazardous Materials*, 24(1):1–38.
- Brown, G. and Krygier, J. (1970). Effects of clear-cutting on stream temperature. *Water Resources Research*, 6(4):1133–1139.
- Caissie, D., Satish, M. G., and El-Jabi, N. (2007). Predicting water temperatures using a deterministic model: Application on miramichi river catchments (new brunswick, canada). *Journal of Hydrology*, (306):303–315.
- Constantz, J., Thomas, C., and Zellweger, G. (1994). Influence of diurnal variations in stream temperature on streamflow loss and groundwater recharge. *Water Resources Research*, 30(12):3253–3264.
- Debler, W. (1996). Flushing criteria in estuarine and laboratory experiments. *Journal of Hydraulic Engineering*, 122(12):728–734.
- Debler, W. and Armfield, S. (1997). The purging of saline water from rectangular and trapezoidal cavities by an overflow of turbulent sweet water. *Journal of Hydraulic Research*, 35(1):43–62.
- DEQ (2010). John day river basin tdml, appendix a: Temperature model calibration report. Technical report, Oregon Department of Environmental Quality. Prepared by Julia Crown.
- Ebersole, J. L., Liss, W. J., and Frissell, C. A. (2001). Relationship between stream temperature, thermal refugia and rainbow trout *oncorhynchus mykiss* abundance in arid-land streams in the northwestern united states. *Ecology of Freshwater Fish*, 10(1):1–10.
- Ebersole, J. L., Liss, W. J., and Frissell, C. A. (2003). Thermal heterogeneity, stream channel morphology, and salmonid abundance in northeastern oregon streams. *Canadian Journal of Fisheries and Aquatic Sciences*, (60):1266–1280.

- Faux, R. N., Maus, P., Lachowski, H., Torgersen, C. E., and Boyd, M. S. (2001). New approaches for monitoring stream temperature: Airborne thermal infrared remote sensing. Technical report, United States Department of Agriculture, Forest Service, Engineering. Remote Sensing Applications Center.
- Hausner, M. B., Suarez, F., Glander, K. E., van de Giesen, N., Selker, J. S., and Tyler, S. W. (2011). Calibrating single-ended fiber-optic raman spectra distributed temperature sensing data. *Sensors*, 11:10859–10879.
- Hopson, R. (1997). Shallow aquifer characteristics adjacent to the upper middle fork john day river, eastern oregon. Master of science, Oregon State University.
- Huff, J. A. (2009). Monitoring river restoration using fiber optic temperature measurements in a modeling framework. Master of science, Water Resources Engineering, Oregon State University.
- Johnson, S. L. and Jones, J. A. (2000). Stream temperature responses to forest harvest and debris flows in western cascades and oregon. *Canadian Journal of Fisheries and Aquatic Sciences*, 57(2):30–39.
- Kaya, C. M., Kaeding, L. R., and Burkhalter, D. E. (1977). Use of a cold-water refuge by rainbow and brown trout in a geothermally heated stream. *The Progressive fish-culturalist*, 39(1):37–39.
- Keller, E. A., Kondolf, G. M., and Hagerty, D. J. (1990). Groundwater and fluvial processes: selected observations. In Higgins, C. G. and Cotes, D. R., editors, *Groundwater geomorphology: the role of subsurface water in Earth-surface processes and landforms*, pages 319–340, Boulder, CO. Geological Society of America Special Paper.
- Khangaonkar, T. and Yang, Z. (2008). Dynamic response of stream temperatures to boundary and inflow perturbation due to reservoir operations. *River Research and Applications*, 24:420–433.
- Krause, S., Blume, T., and Cassidy, N. J. (2012). Investigating patterns and controls of groundwater up-welling in a lowland river by combining fibre-optic distributed temperature sensing with observations of vertical head gradients. *Hydrology and Earth System Sciences*, 9:337–378.

- Loheide, S. P. and Gorelick, S. M. (2006). Quantifying stream-aquifer interactions through the analysis of remotely sensed thermographic profiles and in situ temperature histories. *Environmental Science and Technology*, 40(10):3336–3341.
- Lowry, C. S., Walker, J. F., Hunt, R. J., and Anderson, M. P. (2007). Identifying spatial/variability of groundwater discharge in a wetland stream using a distributed temperature sensor. *Water Resources Research*, 43(10).
- McAllister, L. S. (2008). Reconstructing historical riparian conditions of two river basins in eastern oregon, usa. *Environmental Management*, (42):412–425.
- McDowell, P. F. (2000). Human impacts and river channel adjustment, northeastern oregon: implications for restoration. In Wigington, P. J. and Beschta, R. L., editors, *Riparian ecology and management in multi-land use watersheds*, pages 257–261. American Water Resources Association.
- Nielsen, J. L., Lisle, T. E., and Ozaki, V. (1994). Thermally stratified pools and their use by steelhead in northern california streams. *Transactions of the American Fisheries Society*, 23(4):613–626.
- Nielson, B. T., Hatch, C. E., and Tyler, S. W. (2010). Effects of solar radiative heating on fiber optic cables used in aquatic settings. *Water Resources Research*, 46.
- ORDEQ (2012). Total maximum daily loads (tmdls) program, basin modeling reports. Various Basins. Reports can be accessed at <http://www.deq.state.or.us/wq/tmdls/basinlist.htm>.
- Ozaki, V. (1988). Geomorphic and hydrologic conditions for cold pool formation on redwood creek, california. Technical report, National Park Tech. Report. Rep. No. 24.
- Poole, G. C. and Berman, C. H. (2001). An ecological perspective on in-stream temperature: Natural heat dynamics and mechanisms of human-caused thermal degradation. *Environmental Management*, 27(6):787–802.
- RDG (2007). Reach assessment and restoration design report, the middle fork john day river near galena. Technical report, River Design Group, Inc. Prepared on behalf of Oregon Trout, Portland, OR.

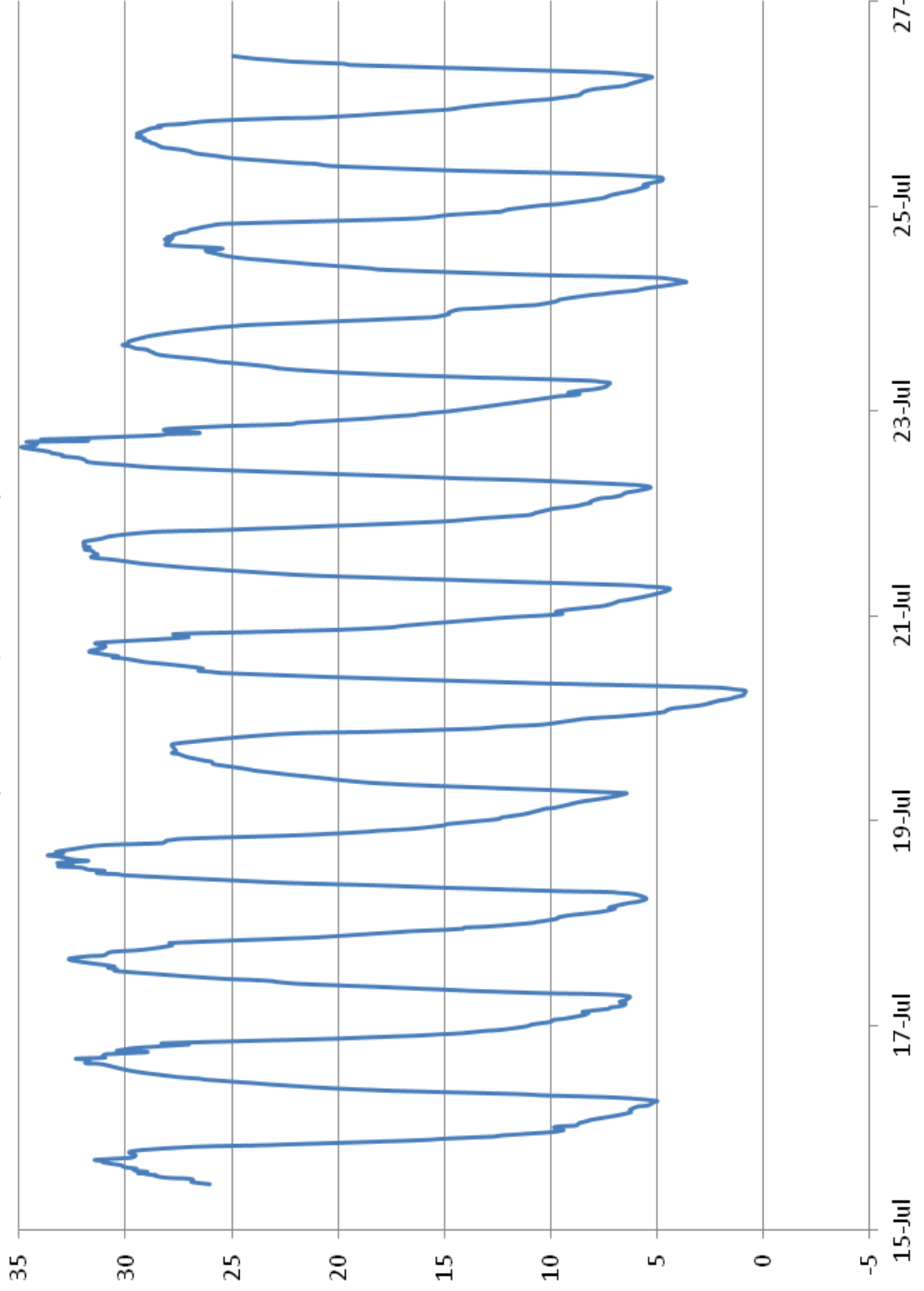
- Roth, T. R., Westhoff, M. C., Huwald, H., Huff, J. A., Rubin, J. F., Barrenetxea, G., Vetterli, M., Parriaux, A., Selker, J. S., and Parlange, M. B. (2010). Stream temperature response to three riparian vegetation scenarios by use of a distributed temperature validated model. *Environmental Science Technology*, 44:2072–2078.
- Schmidt, C., Bayer-Raich, M., and Schirmer, M. (2006). Characterization of spatial heterogeneity of groundwater-stream water interactions using multiple depth streambed temperature measurements at the reach scale. *Hydrology and Earth System Sciences Discussions*, 3(4):1419–1446.
- Selker, J., Thvenaz, L., Huwald, H., Mallet, A., Luxemburg, W., van de Giesen, N., Stejskal, M., Zeman, J., Westhoff, M., and Parlange, M. B. (2006a). Distributed fiber-optic temperature sensing for hydrologic systems. *Water Resources Research*, 42(W12202):8.
- Selker, J., van de Giesen, N., Westhoff, M., Luxemburg, W., and Parlange, M. B. (2006b). Fiber optics opens window on stream dynamics. *Geophysical Research Letters*, 33(L24401):4.
- Sinokrot, B. A. and Stefan, H. G. (1993). Stream temperature dynamics: Measurements and modeling. *Water Resource Research*, 29(7):2299–2312.
- Smolen, J. and van der Spek, A. (2003). A dts primer for oil and gas production. Technical report, Shell. Report EP 2003-7100 May 2003.
- Storey, R. G., Howard, K. W. F., and Williams, D. D. (2003). Factors controlling riffle-scale hyporheic exchange flows and their seasonal changes in a gaining stream: A three-dimensional groundwater flow model. *Water Resource Research*, 39(2):1034–1051.
- Strang, E. and Fernando, H. (2004). Shear-induced mixing and transport from a rectangular cavity. *Journal of Fluid Mechanics*, 520:23–49.
- Toffolon, M., Siviglia, A., and Zolezzi, G. (2010). Thermal wave dynamics in rivers affected by hydropeaking. *Water Resources Research*. doi:10.1029/2009WR008234.
- Torgersen, C. E. (1997). Multiscale assessment of thermal patterns and the distribution of chinook salmon in the john day river basin, oregon. Master of science, Department of Fisheries and Wildlife, Oregon State University.

- Torgersen, C. E., Faux, R. N., McIntosh, B. A., Poage, N. J., and Norton, D. J. (2001). Airborne thermal remote sensing for water temperature assessment in rivers and streams. *Remote Sensing of Environment*, 76:386–398.
- Torgersen, C. E., Hockman-Wert, D. P., Bateman, D. S., Leer, D. W., and Gresswel, R. E. (2007). Longitudinal patterns of fish assemblages, aquatic habitat, and water temperature in the lower crooked river, oregon. Technical report, United States Geological Survey. Open-File Report 20071125.
- Torgersen, C. E., Price, D. M., Li, H. W., and McIntosh, B. A. (1995). Thermal refugia and chinook salmon habitat in oregon: Applications of airborne thermal videography. In *15th Biennial Workshop on Videography and Color Photography in Resource Assessment*, pages 161–171. American Society for Photogrammetry and Remote Sensing.
- Torgersen, C. E., Price, D. M., Li, H. W., and McIntosh, B. A. (1999). Multiscale thermal refugia and stream habitat associations of chinook salmon in northeastern oregon. *Ecological Applications*, 9(1):301–320.
- Tyler, S. W., Selker, J. S., Hausner, M. B., Hatch, C. E., Torgersen, T., Thodal, C. E., and Schladow, S. G. (2009). Environmental temperature sensing using raman spectra dts fiber-optic methods. *Water Resources Research*, 45.
- USGS (2010). Discharge measurements at gaging stations. Technical report, United States Geological Survey. "Techniques and Methods", Book 3, Section 8, Page 79 "Accuracy of Current-Meter Discharge Measurements".
- USGS (2012). Monthly streamflow statistics, ritter, or. Technical report, United States Geological Survey. <http://waterdata.usgs.gov>.
- van de Giesen, N., Steele-Dunne, S., Jansen, J., Hatch, O., Hausner, M. B., Tyler, S., and Selker, J. (2012). Double-ended calibration of fiber-optic raman spectra distributed temperature sensing data. *Sensors*, 12.
- WSI (2005). Aerial thermal infrared remote sensing, eel river, ca. Technical report, Watershed Sciences, Inc. Draft Report Date: October 15, 2005.
- WSI (2008). Lidar dem, middle fork john day river watershed. Technical report, Watershed Sciences, Inc. Collected August 19-27, 2008.

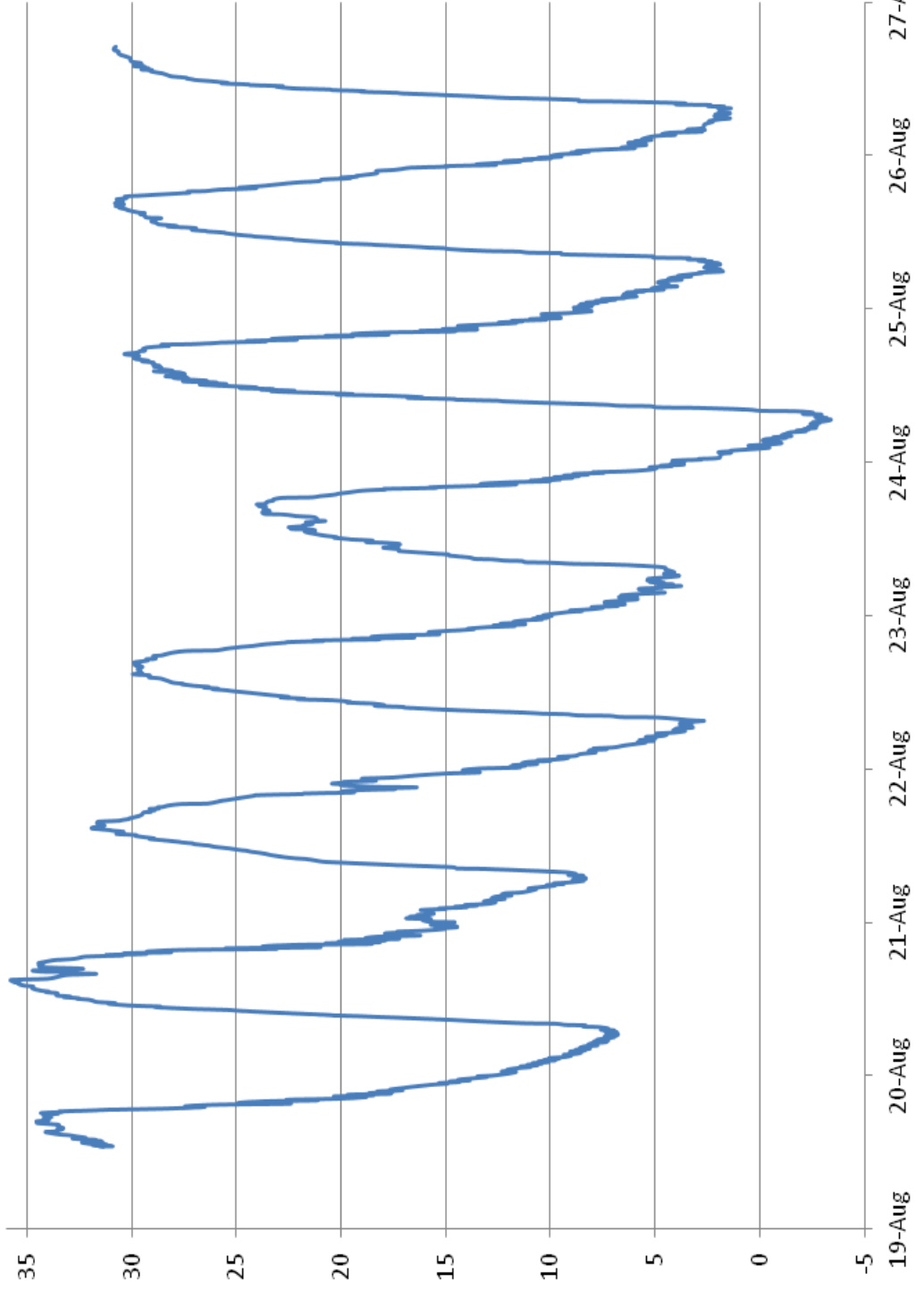
APPENDICES

Appendix A – Air temperature data summary, 2009-2011

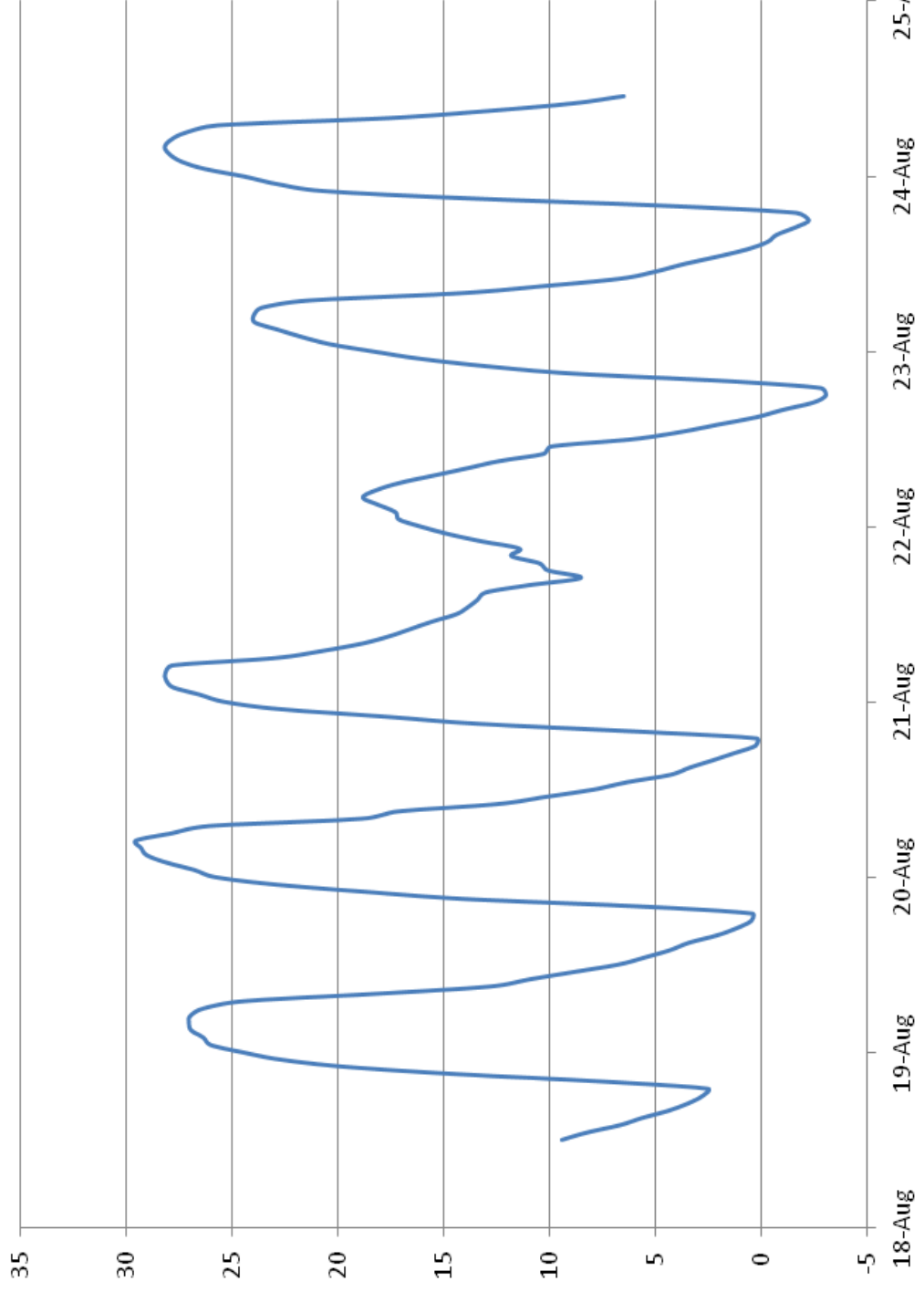
Air Temperature, July 15 - 27, 2009, Forrest Conservation Area
(44°35'45.61"N, 118°31'22.50"W)



Air Temperature, August 19 - 26, 2009, Forrest Conservation Area
(44°35'45.61"N, 118°31'22.50"W)

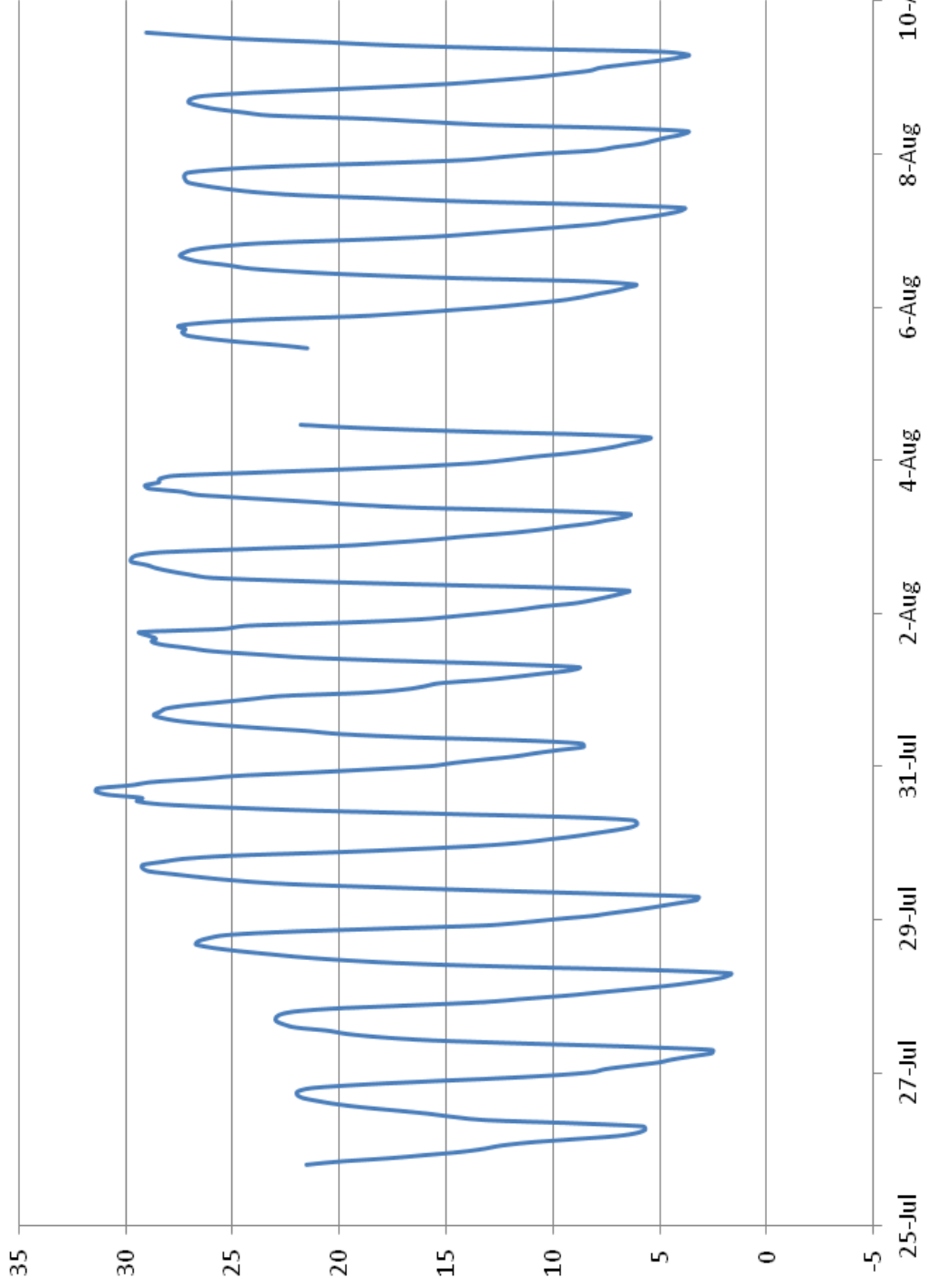


Air Temperature, August 18 - 24, 2010, Forrest Conservation Area
(44°36'3.14"N, 118°32'2.94"W)

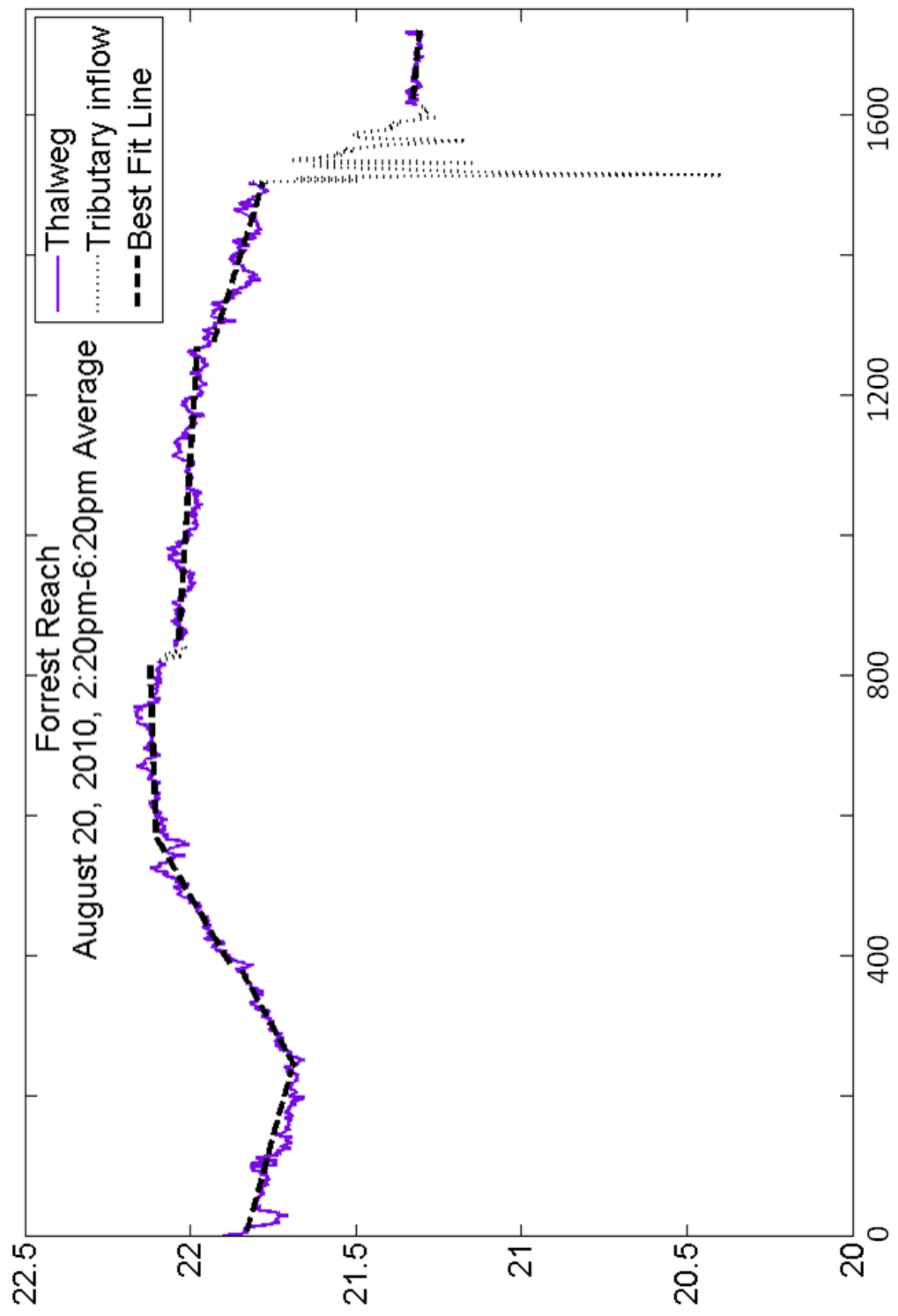


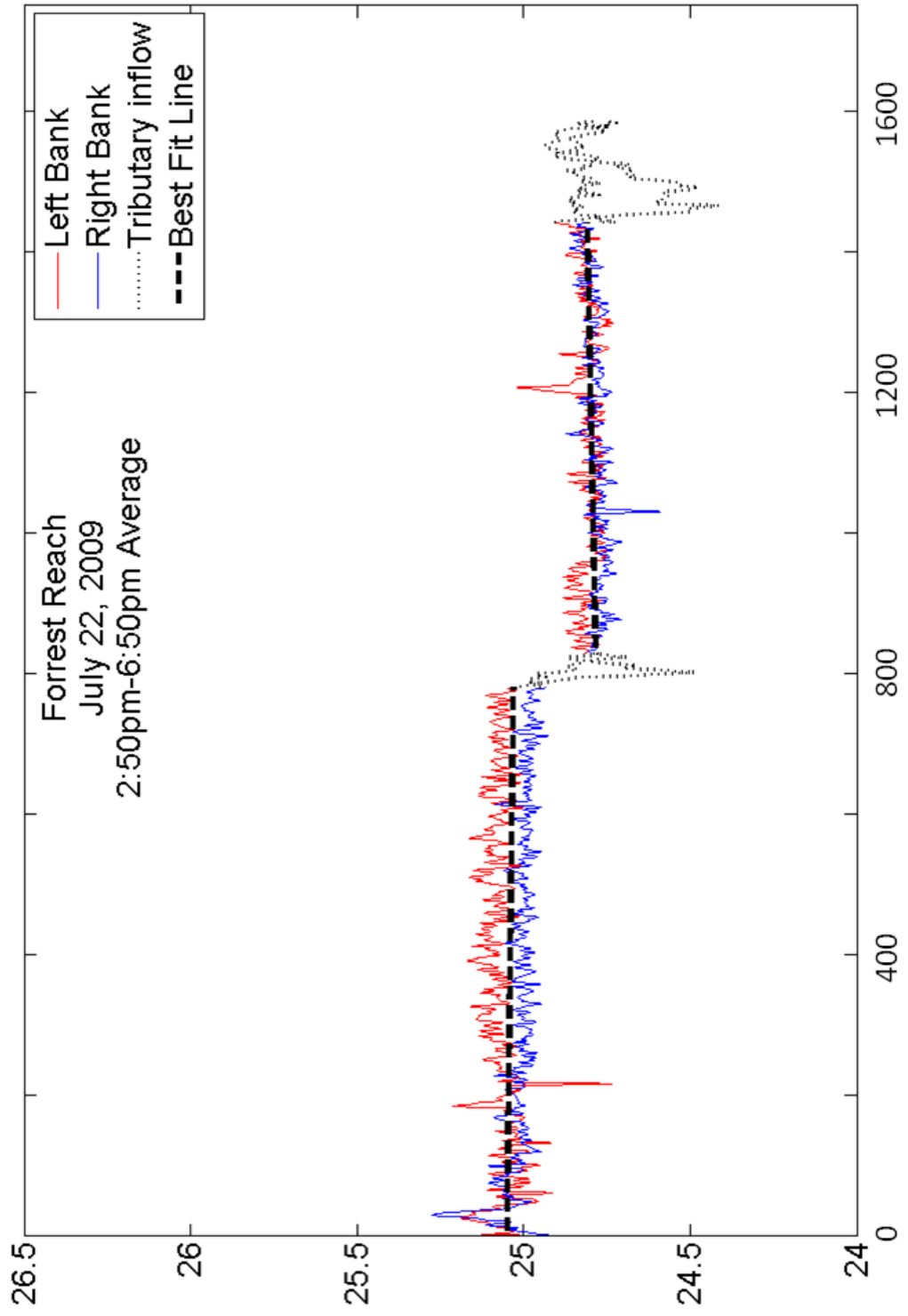
Air Temperature, July 25 - August 9, 2011, Forrest Conservation Area

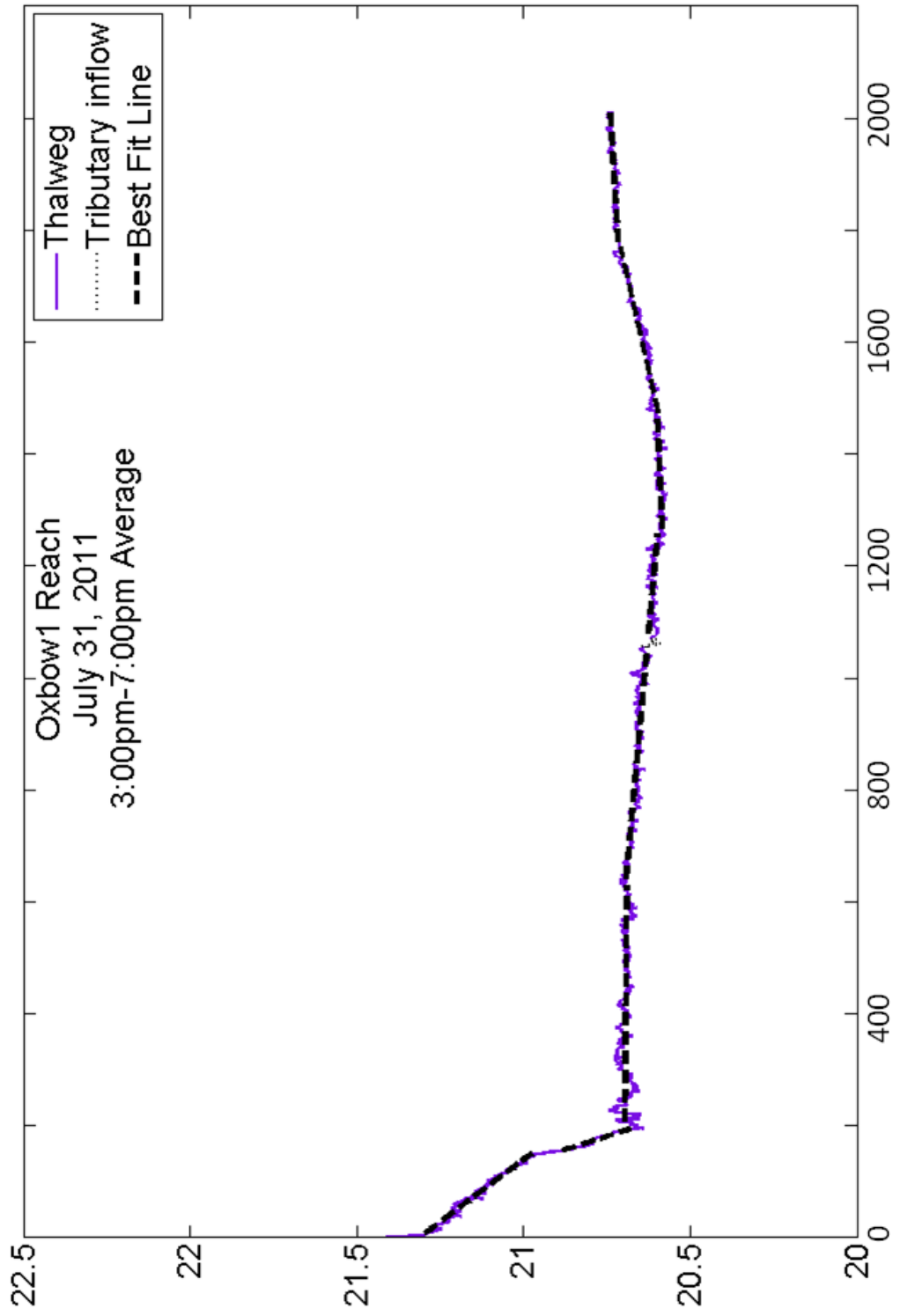
(44°35'45.61"N, 118°31'22.50"W)

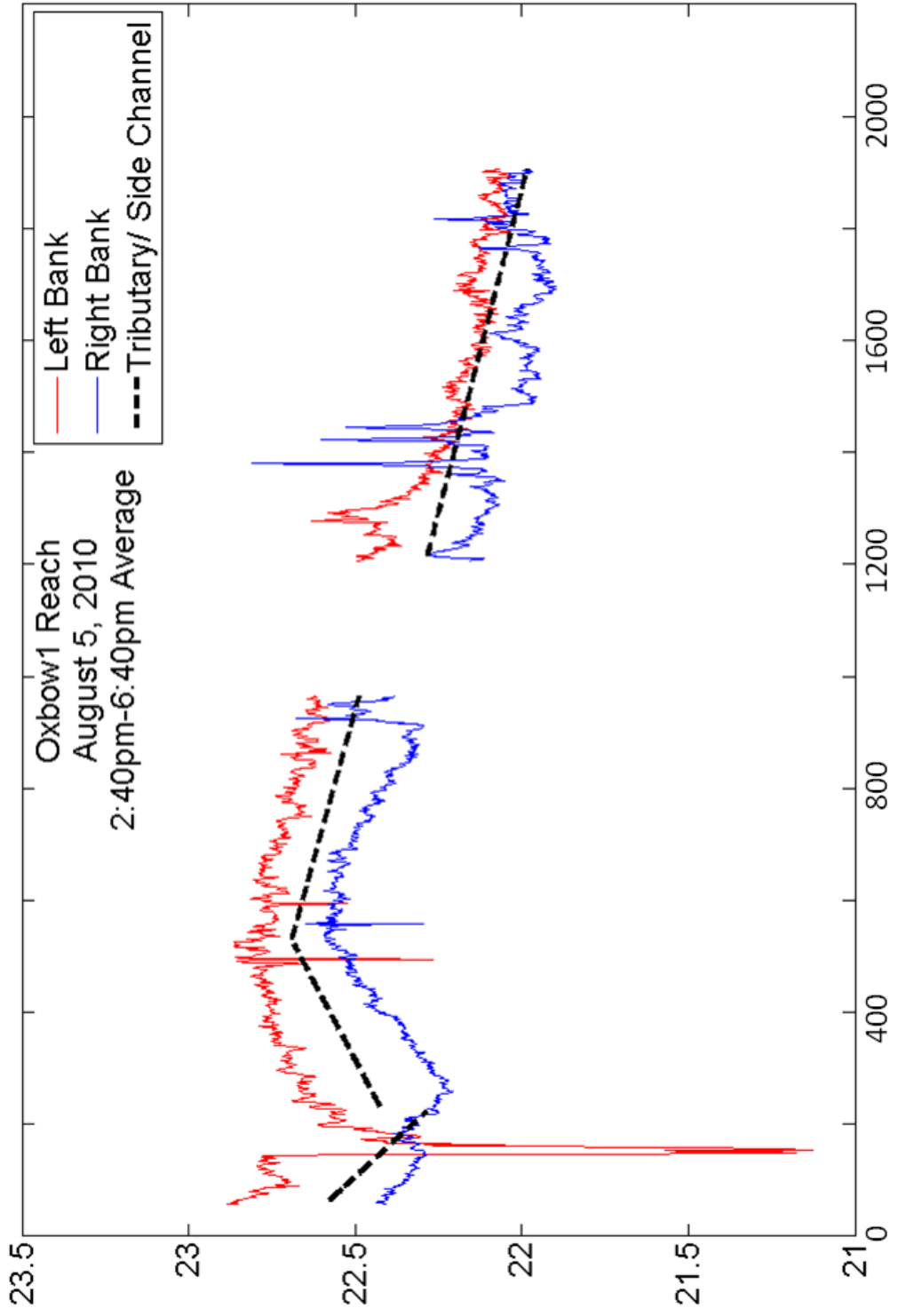


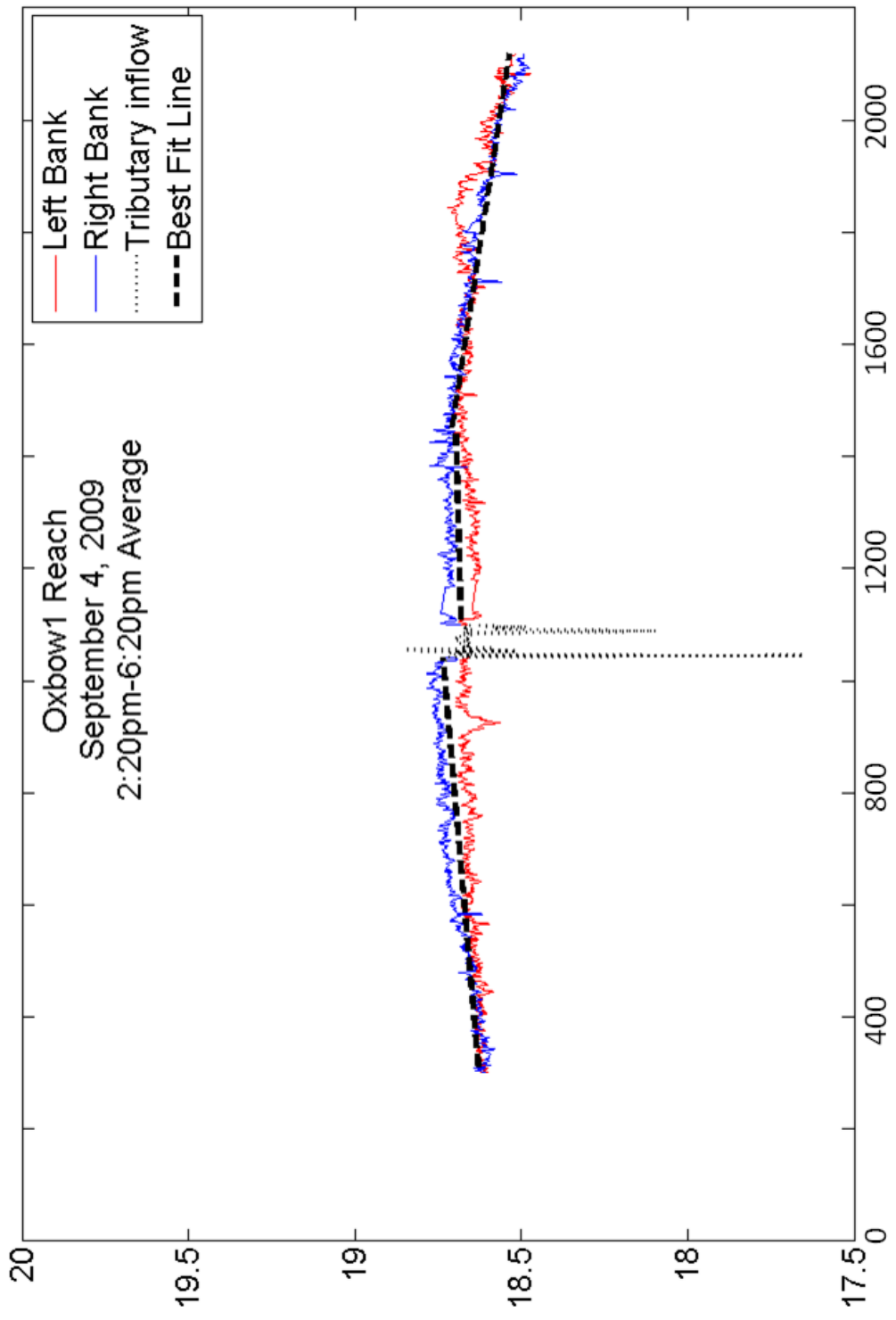
Appendix B – Large-scale versions of the graphs in Figure 2.6

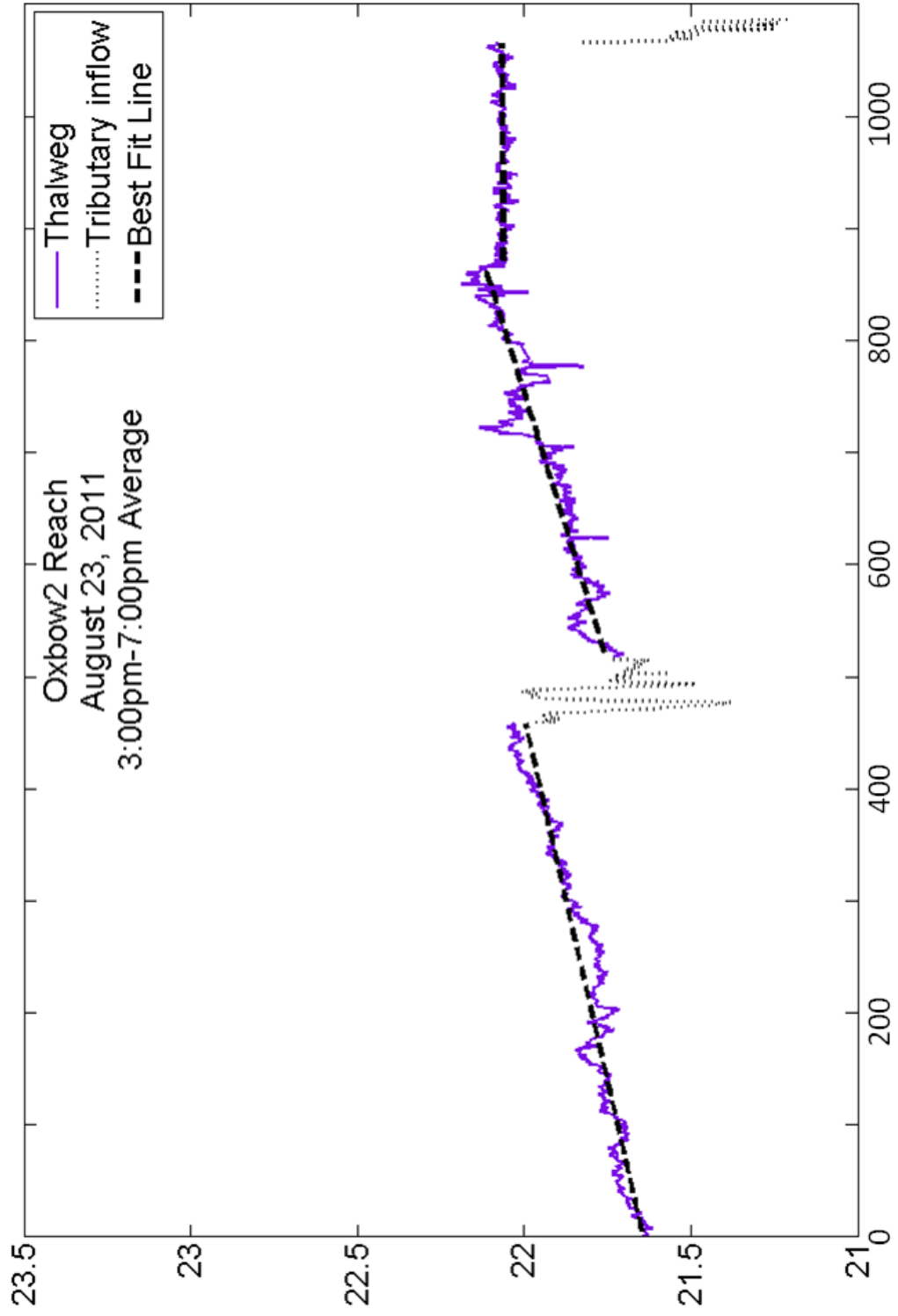


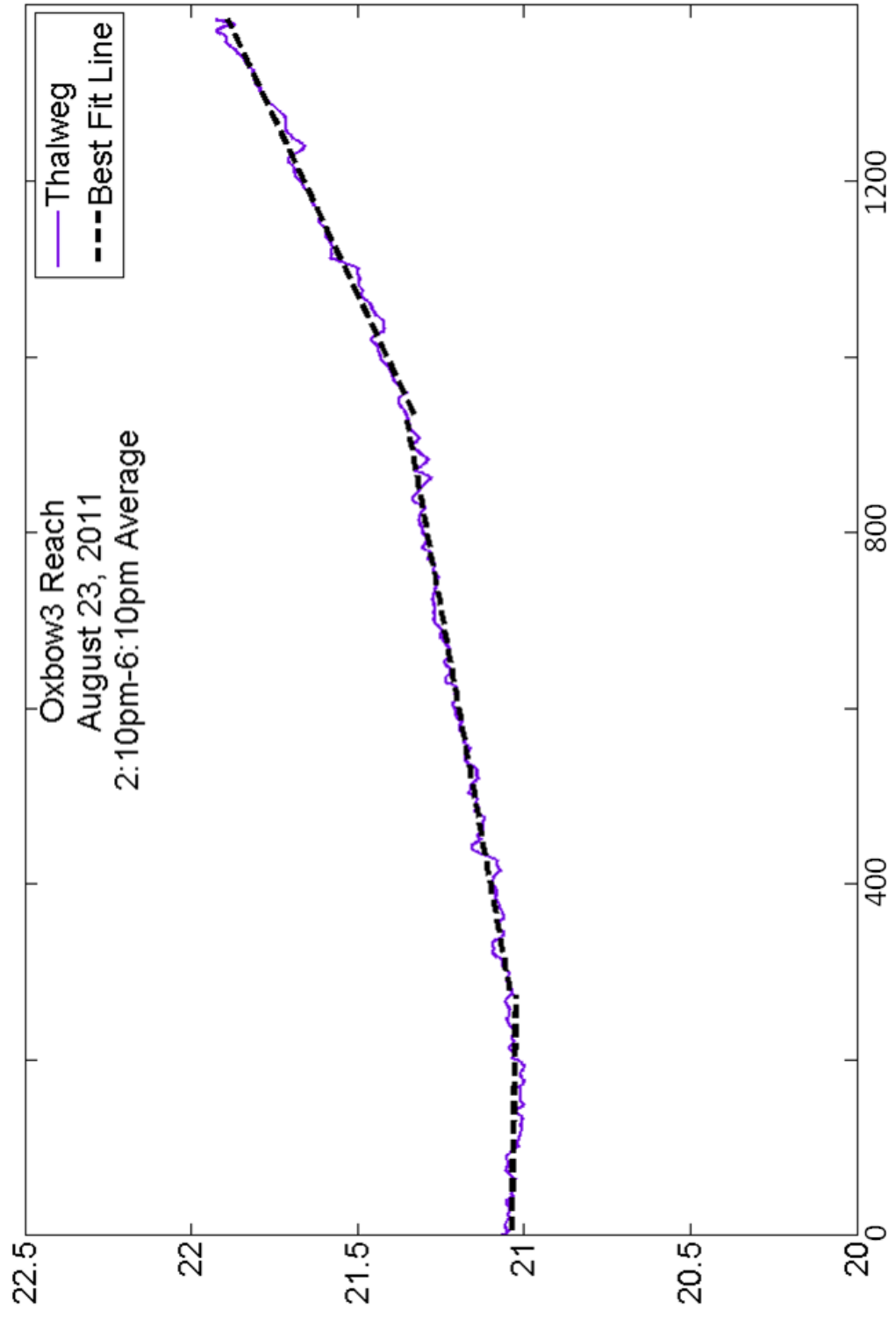


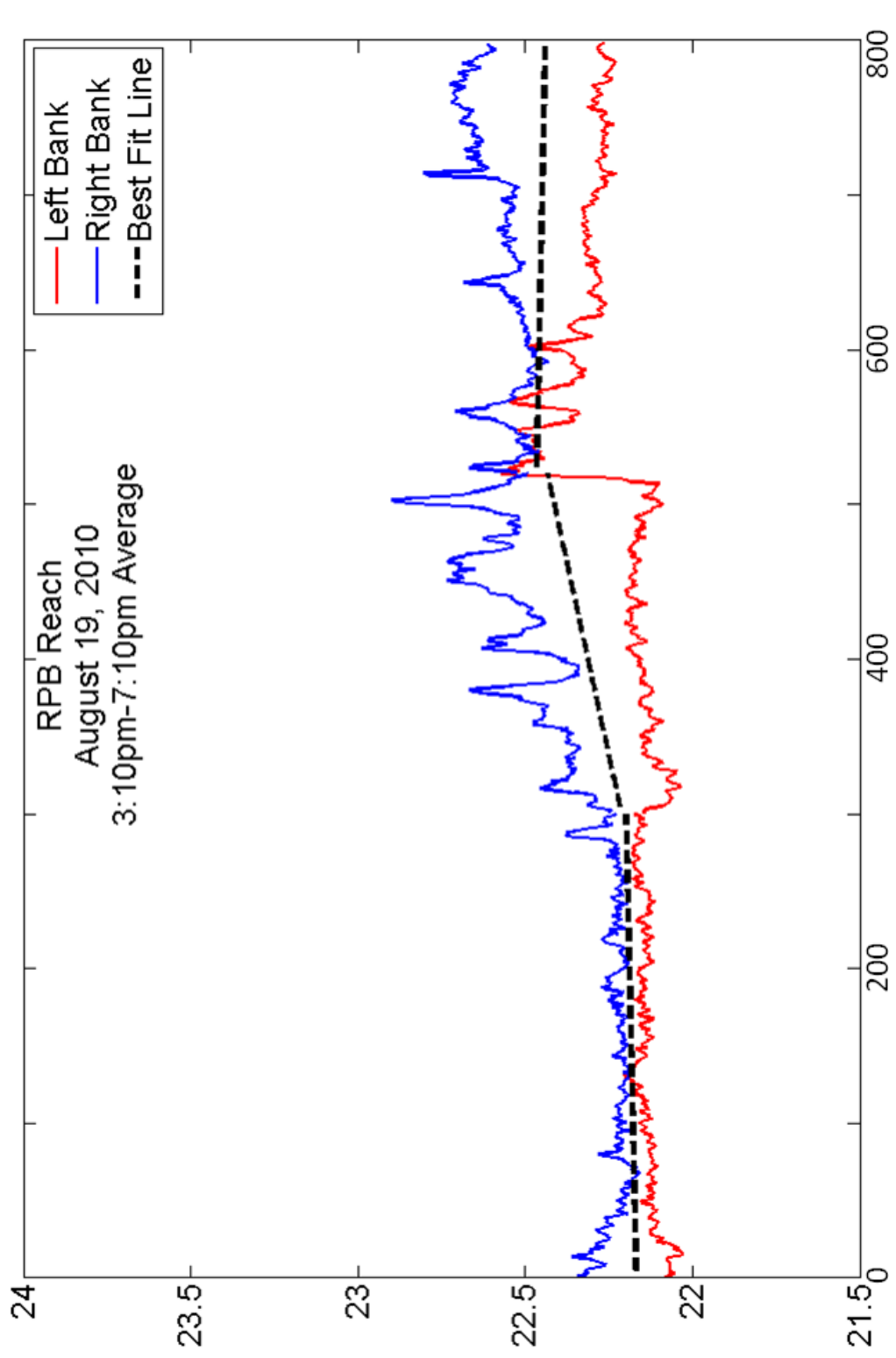








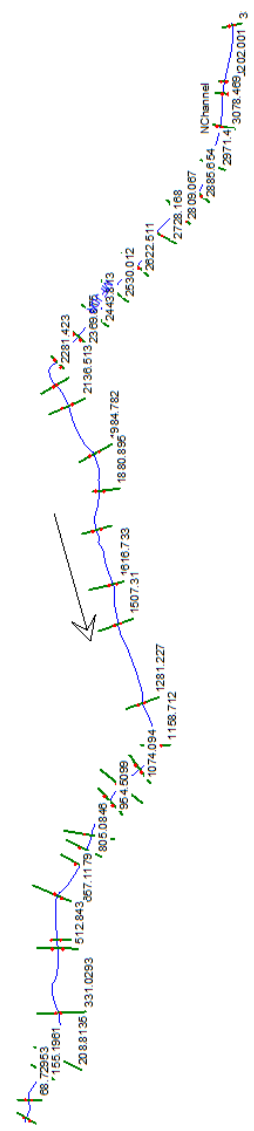




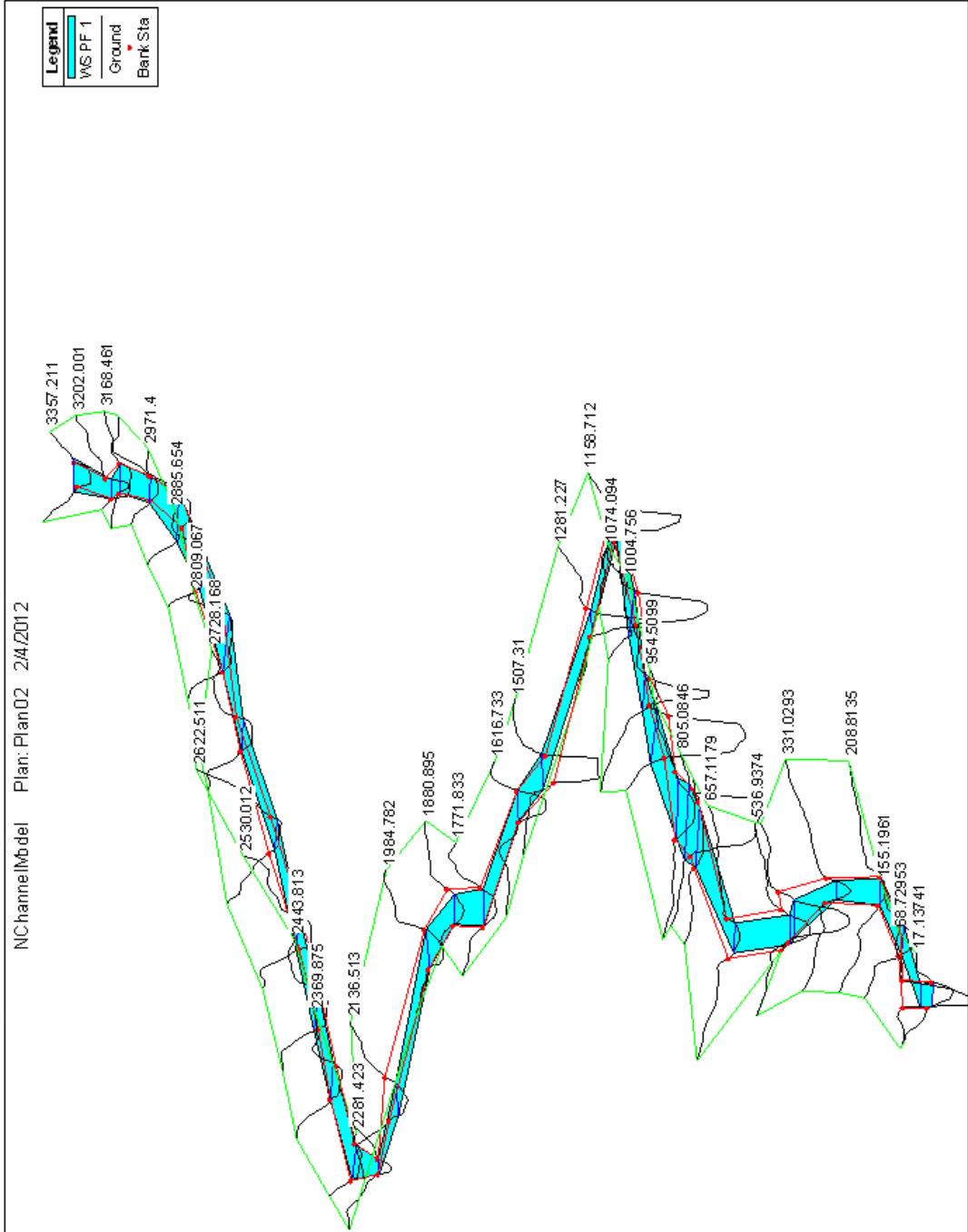
Appendix C – Oxbow2 HEC-RAS hydraulic model

HEC-RAS Hydraulic Model Oxbow2 Reach

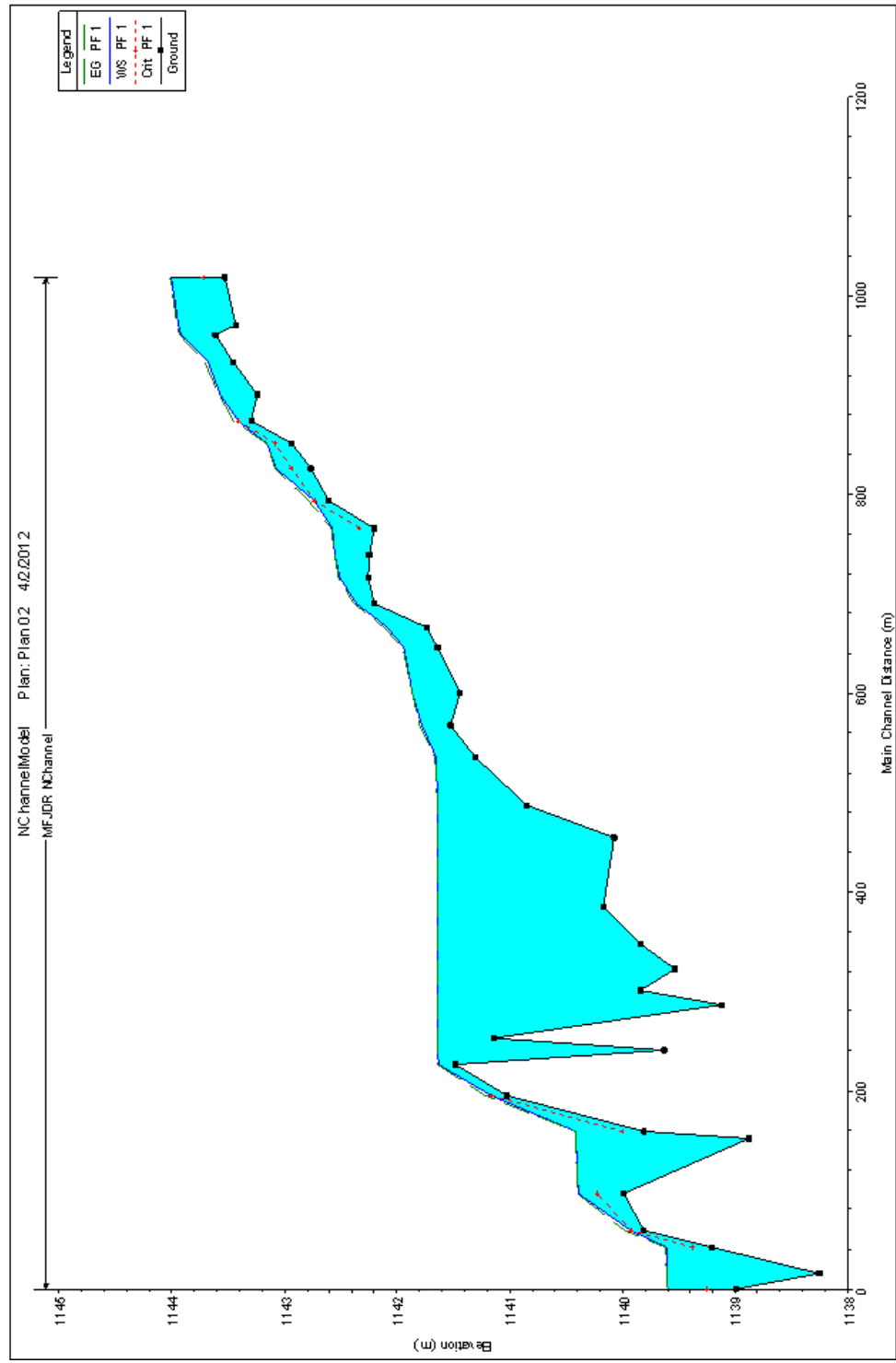
- Channel morphology data was taken from a LiDAR DEM (WSI, 2008) and modified to appropriate channel depth by a visual channel depth survey
- Upstream flow boundary condition data collected by a Marsh McBirney flow meter on August 13, 2011.
- A detailed model evaluation was not made. However, modeled water depths at Cross Sections 3357.211 and 17.137 were within 20% of measured depths, and modeled velocities were within 40% of measured velocities.
- Model planar geometry:



- Model output with multiple cross section 3D plot:

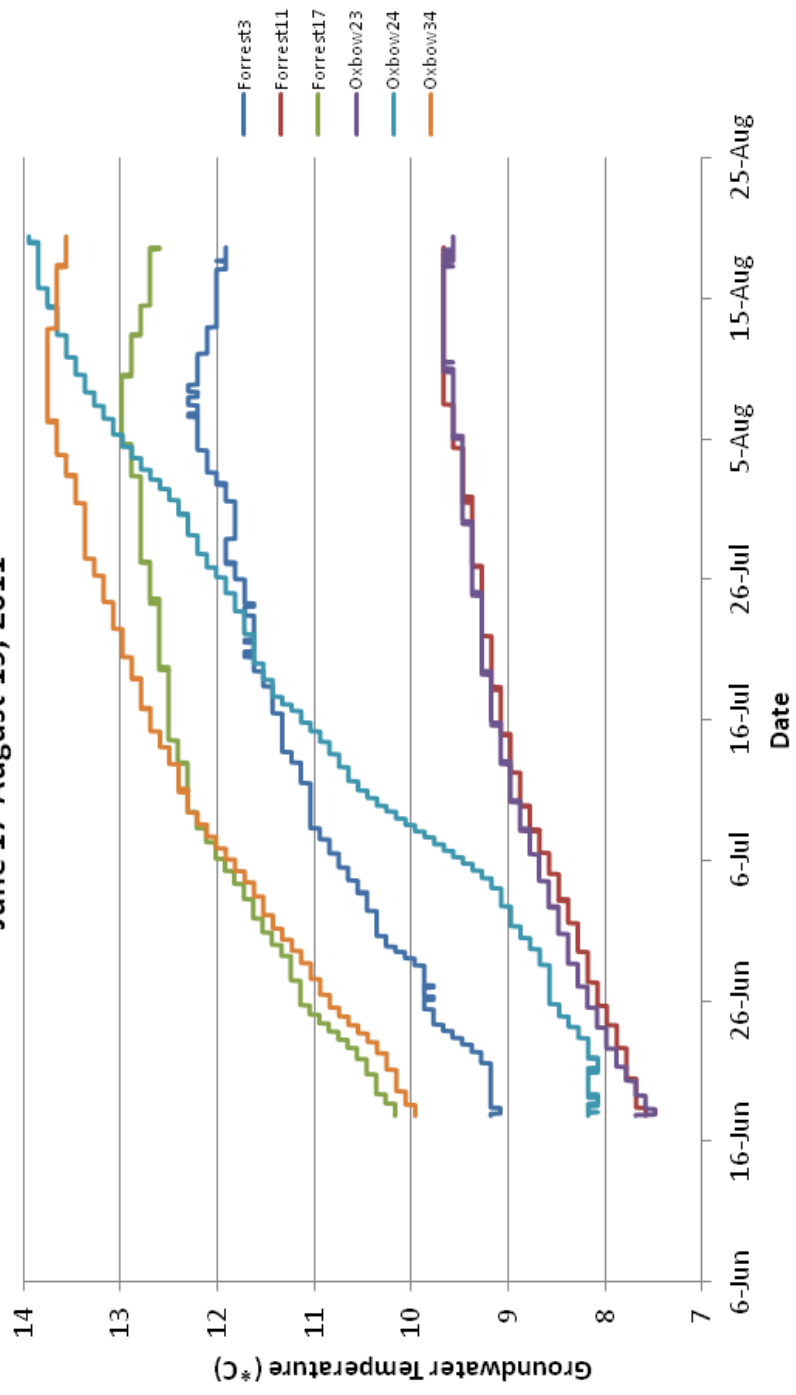


- Model output with water level profile plot:



Appendix D – Groundwater temperature data summary, June-August, 2011

Shallow Groundwater Temperature Forrest Conservation Area and Oxbow Conservation Area June 17-August 19, 2011



	Forrest3	Forrest11	Forrest17	Oxbow23	Oxbow24	Oxbow34
Latitude	44°35'53.30"N	44°36'9.09"N	44°36'49.97"N	44°38'41.96"N	44°38'38.24"N	44°39'18.67"N
Longitude	118°31'44.81"W	118°32'20.68"W	118°33'29.07"W	118°39'33.81"W	118°39'38.67"W	118°40'57.01"W

